

**Battery energy storage for maturing markets: performance, cost, perceptions, and
environmental impacts**

Submitted in partial fulfillment of the requirements for
the degree of
Doctor of Philosophy
in
Engineering and Public Policy

Rebecca E. Ciez
B.S., Mechanical Engineering, Columbia University

Carnegie Mellon University
Pittsburgh, PA
May 2018

Abstract

As the use of renewable energy technologies and electric vehicles continues to expand in our electricity generation and transportation sectors, demand for energy storage technologies will only grow. Meeting this increased demand will require both technology innovations, but also new ways of thinking about the costs of implementing these technologies. This dissertation examines electrochemical energy storage technologies at multiple phases of the product cycle to assess how to meet some of the challenges associated with widespread adoption of electrochemical energy storage. Using a process-based cost model to identify the factors that contribute most to battery manufacturing cost, I find that economies of scale cost reductions have largely already been achieved. However, changes in cell design parameters can help to lower the per kWh cost of lithium-ion cells. Looking at a use case for energy storage in a hybrid microgrid, I find that both battery chemistry characteristics and technology costs impact the overall performance of hybrid microgrids and the cost of delivering electricity. As more batteries are produced to meet growing demand, the greenhouse gas emissions associated with battery manufacturing and waste disposal will become increasingly important. Using an attributional life cycle analysis, I compare the emissions associated with two different recycling processes: pyrometallurgical recycling and direct cathode recycling. While pyrometallurgical recycling does not offer emissions reductions, direct cathode recycling does have the potential to reduce greenhouse gas emissions, even if the cathode recovery process has relatively low yield rates. Using these recovered cathode materials is contingent on a market that will accept these recycled materials. A survey of current electric vehicle owners shows that consumer preferences about battery materials differ depending on whether consumers purchased a plug-in hybrid or an all electric vehicle. Overall, plug-in hybrid vehicle owners seem to have a slightly negative perception of recycled battery materials. For electric vehicle owners that have an all-electric vehicle, there are more diverse preferences, with groups that have positive, negative, and indifferent preferences about the type of battery material used in their vehicle. The heterogeneous preferences of different electric vehicle owners could enable different trends in material recovery and reuse as the number of electric vehicles on the road, and the battery energy storage used for transportation, increase.

Acknowledgments

First, I would like to thank the members of my committee: Jay Whitacre, my advisor and committee chair, for supporting me throughout my time in EPP and allowing me the freedom to shape my own research path. To my committee members: Meagan Mauter for her mentorship and practical advice; Jeremy Michalek for the thoughtful discussions that helped to shape several chapters of this thesis; and Costa Samaras for his encouragement and enthusiasm for my work. Additionally, I would like to thank all the administrative staff in the Engineering and Public Policy department for their help over the years.

A huge thanks to my friends and family for their constant support and encouragement. Special thanks to my parents, Al and Brenda, and brother, Matthew for their love, support, and patience throughout this and all my previous journeys. Thanks to all my friends in EPP and at CMU for their support, insight, and collaboration over the years.

I must also thank the sources of financial support over the course of my doctoral research. These sources include a National Science Foundation Graduate Research Fellowship under Grant No. DGE 1252522, the Department of Engineering and Public Policy, the Bushnell Fellowship in Engineering, the Friedman Fellowship, Aquion Energy, and a Carnegie Mellon GSA/Provost Office Graduate Small project Help Grant.

Contents

1	Introduction	1
2	Manufacturing costs of lithium-ion batteries: impacts of form factor, material inputs, and economies of scale	5
2.1	Introduction	5
2.2	Methods	8
2.2.1	Battery Cell Model	8
2.2.2	Cost model	9
2.3	Results & Discussion	16
2.3.1	Cathode Material Costs	16
2.3.2	Unit Costs	16
2.3.3	Sensitivity Analysis	17
2.3.4	Cost Breakdown	18
2.4	Conclusions	22
3	Comparative techno-economic analysis of hybrid microgrid systems utilizing different battery types	25
3.1	Introduction	25
3.2	Methods	28
3.2.1	System Operational Model	28
3.2.2	Economic Model	34
3.3	Results	35
3.3.1	Battery operational lifetime	35
3.3.2	Levelized cost of electricity	36
3.3.3	Sensitivity to discount rate	38

3.3.4	Renewable energy requirement	40
3.4	Discussion	41
3.4.1	Price changes	42
3.4.2	Feed-in tariffs	42
3.4.3	Carbon tax	43
3.4.4	Other policy recommendations	44
3.5	Conclusions	44
4	Prospects for reducing battery manufacturing emissions from direct material recovery	47
4.1	Introduction	47
4.2	Methods	50
4.2.1	LCA Assumptions	50
4.2.2	Cost Model	53
4.3	Results	53
4.3.1	Cell Manufacturing Emissions	53
4.3.2	Cell Recycling Emissions	55
4.3.3	Impact of Transportation	58
4.3.4	Breakeven Recovery Cost	59
4.4	Discussion	60
4.4.1	Recycling and future market demand for metals	61
5	Evaluating Consumer Risk Perceptions of Recycled Batteries in the Electric Vehicle Market	63
5.1	Introduction	63
5.1.1	Literature review	64
5.2	Theory: Revealed and Stated Preference Studies	65
5.3	Methods	66
5.3.1	Survey Design	66
5.3.2	Data Collection	69
5.3.3	Model Specification	70
5.4	Results	73
5.5	Discussion	76

5.5.1	Limitations and Future Work	77
6	Conclusions	81
6.1	Summary of Results	81
6.2	Policy Recommendations	82
A	Electric Vehicle Market Information and Process Based Cost Model Assumptions	85
A.1	Electric vehicle battery analysis	85
A.2	Uncertainty Analysis	91
A.2.1	Equipment Assumptions	91
A.2.2	Operating Time	91
A.2.3	Formation Cycle	91
A.2.4	Labor Cost	92
A.2.5	Cell dimensions	92
A.2.6	Cell Yield rates	92
A.2.7	Material Cost	92
A.2.8	Maintenance and overhead	93
A.2.9	Building cost	93
A.2.10	Cathode Cost	93
A.3	Cost drivers by process step	94
A.4	Assumptions for prismatic cells	94
A.5	Cascading Unplanned Downtime in Sequenced Processes	95
B	Calculation Details for Battery Model Calculations	97
B.1	Carbon Tax Calculations	97
B.2	Generation Subsidy Calculations	97
B.3	Power Flow Optimization	98
B.4	Battery Degradation Models & Manufacturer Data	99
B.5	Matlab Solvers	100
C	Recycling Model Assumptions and Detailed Results	101
D	Survey Design Data	123
D.1	Market Data for Survey Levels	123

D.2 Number of Classes Selection Criteria 124

D.3 Alternative Model Specifications and Results 124

List of Figures

2.1	Historical prices and future cost predictions for lithium ion batteries. Estimates include both cell- and pack-level cost assessments, which is reflected in the significant variability in the cost estimates.	6
2.2	Estimate of storage capacity (by GWh), broken out by chemistry, format, and vehicle type. BEVs account for 79% of total capacity.	7
2.3	Historical prices and future cost predictions for lithium ion batteries. Estimates include both cell- and pack-level cost assessments, which is reflected in the significant variability in the cost estimates.	11
2.4	Cost per cell and per kWh for NCA, LMO, and NMC batteries, assuming 18650 cells, 70 μm electrodes, and 2GWh of annual production	17
2.5	Cost per kWh of NCA, NMC, and LMO batteries generally reach economies of scale at 1GWh of annual production, and remain stable as the annual production volumes increases. Production volumes used in later sensitivity analyses (2 GWh, 4 GWh, and 8 GWh) are highlighted.	18
2.6	Change in cost per kWh for NCA and NMC batteries as production volumes, cell dimensions, and electrode thicknesses vary (50 μm to 100 μm)	19
2.7	Per kWh baseline and optimistic cost breakdowns for NCA and NMC cells. Materials account for roughly 40% of the total cost.	19
2.8	Per kWh material cost breakdown for NCA and NMC cells	21
2.9	per kWh cost breakdown comparison for baseline 18650 cylindrical cells, optimistic 20720 cylindrical cells, and BatPaC prismatic cells	22
2.10	Material costs per kWh of 18650 cylindrical and prismatic NCA cells	23

2.11 Additional cost per kWh for batteries made with purchased cathode materials (in green), relative to the cost per kWh for in-house manufacturing of active material for baseline 18650 cylindrical cells, optimistic 20720 cylindrical cells, and BatPaC prismatic cells	24
3.1 Model overview diagram	27
3.2 Relationships between the number of cycles and SOC swing for lead acid, high energy density Lithium ion, and high power density Lithium-ion batteries.	32
3.3 Nameplate storage capacity for different battery operational lifetimes as maximum state of charge swing varies with a 75% renewable requirement for a) lead-acid, b) high power density lithium-ion, and c) high energy density lithium-ion batteries. . . .	34
3.4 Median daily SOC swing (with 95% confidence interval) compared to the maximum cumulative SOC swing for high energy density lithium-ion batteries.	36
3.5 LCOE for different battery operational lifetimes with a 75% renewable requirement and 5% discount rate as maximum state of charge swing varies for (a) lead-acid, (b) high power density lithium-ion, and (c) high energy density lithium-ion.	37
3.6 Optimal number of battery sets over 20 year lifetime with 5% discount rate as maximum SOC swing varies for a) lead-acid, b) high power lithium ion, and c) high energy lithium ion batteries.	38
3.7 (a) Lowest LCOE envelope for each battery chemistry as maximum SOC swing varies with 75% renewable requirement at 5% discount rate and with a comparison to diesel-only generation and (b) how the Lowest LCOE for each chemistry varies with discount rate	39
3.8 Required storage capacity and corresponding percentage of energy from renewable sources as the renewable target and operational lifetime of the high energy density lithium-ion batteries vary (1, 5, and 20 years)	40
3.9 (a) Diesel prices required to switch to hybrid system depending on discount rate and assumed storage prices for each battery chemistry and (b) Battery price changes required to switch to a hybrid system as discount rate varies	41

3.10	Incentives policies to induce switch to a hybrid system with variation in discount rate. Feed in tariffs (a) required to reach LCOE parity between lowest-cost systems and diesel-only generation, with comparison to the highest and lowest US electricity provider Feed-In Tariff rates and (b) Carbon taxes required to switch to a hybrid system, with comparison to existing global tax rates.	43
4.1	Cathode materials are a substantial contributor to overall costs and CO _{2e} emissions for manufacturing NMC cylindrical cells.	48
4.2	Manufacturing (in blue), pyrometallurgical (in yellow), and direct cathode recycling (green) pathways for NCA and NMC cells. Ni, Co, and Mn inputs can be sourced from either sulfates or nitrates. Mn is only an input for NMC cells, Al(OH) ₃ is only for NCA cells. We do not consider the emissions for cell use.	49
4.3	kg CO _{2e} per kg of cell emitted during the manufacturing of NMC and NCA cylindrical batteries using US average, NWPP, and RFCM average grid emissions data. Manufacturing includes processing of cathode material preparation	54
4.4	CO _{2e} emissions per kg of battery for (a) manufacturing and recycling processes (pyrometallurgical and direct cathode recycling) less the emissions offsets from recovered materials, and the (b) net CO ₂ emissions avoided by using a recycling process for NMC and NCA cells and recovering material. All processes use the US average electricity grid.	56
4.5	net kg of CO _{2e} emissions avoided per kg battery when combining manufacturing with direct cathode recycling over using no recycling method after manufacturing. As the cathode yield rate from the direct recycling process decreases, so do emissions benefits. Pyrometallurgical recycling does not offer significant greenhouse gas emissions reductions.	57
4.6	Relithiation cost per kg of cathode material for NMC and NCA cells as production volumes vary. The process reaches economies of scale at roughly 1,500 tons of annual production.	59
5.1	Flow chart for survey version decision based on current vehicle owned	67
5.2	Sample discrete choice question	69

5.3	Partworth, Linear, and Logarithmic models of range for BEV and PHEV data. A logarithmic model is a better fit to the partworth data than a linear model for the vehicle range attribute.	72
5.4	PHEV owners willingness to pay for miles of range and final range (when percentage is 70%). There is decreasing willingness to pay as the miles of range available increases	77
5.5	Overall and latent class perceptions of recycled and refurbished batteries for BEV and PHEV owners. Error bars represent the 95% confidence interval. The environmentally-conscious group of BEV owners (class 2), and risk-averse PHEV owners (class 3) are the only groups that have a willingness to pay that is significantly different from zero.	79
5.6	Percentage reduction in pack costs for risk-averse PHEV owners to be willing to accept recycled and refurbished battery materials. Accounting for the uncertainty in their aversion to both types of battery packs, the cost reductions for recycled battery packs to be competitive for very short range vehicles are high relative to overall pack cost at nearly 50%. Additional work is necessary to determine if there are any segments of the overall PHEV owners group where range influences overall willingness to pay for recycled and refurbished materials.	80
A.1	Material costs per kWh of 18650 cylindrical and prismatic NCA cells	91
A.2	Per kWh costs by manufacturing step for baseline NCA and NMC cell production . .	94
C.1	kg CO _{2e} (with 95% confidence) per kg of cell emitted during the manufacturing process of NMC and NCA cylindrical cells for US average, NWPP, and RFCM average grid emissions.	108
C.2	MJ (with 95% CI) of input energy per kg of battery produced using a US average, NWPP, and RFCM grids	109
C.3	kg CO _{2e} emitted per kWh of battery produced on US average, NWPP, and RFCM grids	109
C.4	MJ of input energy per kWh of battery produced on US average, NWPP, and RFCM grids	110

C.5	Top: CO _{2e} emissions per kg of battery for battery manufacturing and pyrometallurgical recycling (blue) and for battery manufacturing and direct recycling (yellow) less the emissions offsets for product outputs for NCA and NMC cells on US average, NWPP, and RFCM grids. Bottom: Net CO _{2e} emissions avoided using a pyrometallurgical or direct recycling process. For NMC batteries, pyrometallurgical recycling has a median environmental cost (no CO _{2e} emissions avoided). For NCA cells, the emissions offsets of a pyrometallurgical process are not significantly different from zero.	112
C.6	Top: MJ of input energy per kg of battery for battery manufacturing and pyrometallurgical recycling (blue) and for battery manufacturing and direct recycling (yellow) less the emissions offsets for product outputs for NCA and NMC cells on US average, NWPP, and RFCM grids. Bottom: Net energy savings from using a pyrometallurgical or direct recycling process. For both chemistries, the median energy savings from pyrometallurgical recycling is positive, but not significantly different from zero. .	113
C.7	Top: CO _{2e} emissions per kWh of battery for battery manufacturing and pyrometallurgical recycling (blue) and for battery manufacturing and direct recycling (yellow) less the emissions offsets for product outputs for NCA and NMC cells on US average, NWPP, and RFCM grids. Bottom: Net CO _{2e} emissions avoided using a pyrometallurgical or direct recycling process. For NMC batteries, pyrometallurgical recycling has a median environmental cost (no CO _{2e} emissions avoided). For NCA cells, the savings of a pyrometallurgical process are not significantly different from zero.	114
C.8	Top: MJ of input energy per kg of battery for battery manufacturing and pyrometallurgical recycling (blue) and for battery manufacturing and direct recycling (yellow) less the emissions offsets for product outputs for NCA and NMC cells on US average, NWPP, and RFCM grids. Bottom: Net energy savings from using a pyrometallurgical or direct recycling process. For both chemistries, the median energy savings from pyrometallurgical recycling is positive, but not significantly different from zero. .	115
C.9	net kg CO _{2e} avoided per kg of battery when combining manufacturing with direct cathode recycling over using no recycling method after manufacturing. Yield rates of recovered cathode material vary from 0 to 100% for both NMC and NCA chemistries.	116

C.10 MJ of energy saved by using a direct recycling process over doing nothing after cell manufacturing. Yield rates of the recovered cathode material vary from 0 to 100% for both NMC and NCA chemistries.	116
C.11 net kg CO _{2e} avoided per kWh of battery by using a direct recycling process over doing nothing after cell manufacturing. Yield rates of recovered cathode material vary from 0 to 100% for both NMC and NCA chemistries.	117
C.12 MJ of energy saved by using a direct recycling process over doing nothing after cell manufacturing. Yield rates of the recovered cathode material vary from 0 to 100% for both NMC and NCA chemistries.	117
C.13 kg CO _{2e} avoided per kg of battery by using a direct recycling process over a pyrometallurgical process. Yield rates of recovered cathode material vary from 0 to 100% for both NMC and NCA chemistries. Because pyrometallurgical has more environmental benefits for NCA cells than NMC cells, the yield rate for cathode material recovered during the direct recycling process must be higher for direct recycling to be more beneficial than pyrometallurgical recycling.	118
C.14 MJ of input energy avoided per kg of battery by using a direct recycling process over a pyrometallurgical process. Yield rates of recovered cathode material vary from 0 to 100% for both NMC and NCA chemistries. Because pyrometallurgical has more environmental benefits for NCA cells than NMC cells, the yield rate for cathode material recovered during the direct recycling process must be higher for direct recycling to be more beneficial than pyrometallurgical recycling.	118
C.15 kg CO _{2e} avoided per kWh of battery by using a direct recycling process over a pyrometallurgical process. Yield rates of recovered cathode material vary from 0 to 100% for both NMC and NCA chemistries. Because pyrometallurgical has more environmental benefits for NCA cells than NMC cells, the yield rate for cathode material recovered during the direct recycling process must be higher for direct recycling to be more beneficial than pyrometallurgical recycling.	119

C.16 MJ of energy avoided per kWh of battery by using a direct recycling process over a pyrometallurgical process. Yield rates of recovered cathode material vary from 0 to 100% for both NMC and NCA chemistries. Because pyrometallurgical has more environmental benefits for NCA cells than NMC cells, the yield rate for cathode material recovered during the direct recycling process must be higher for direct recycling to be more beneficial than pyrometallurgical recycling. 119

C.17 Relithination costs and breakeven costs as the percentage of lithium added varies between 0 and 100%. For both cell chemistries, the lithination costs are nearly indistinguishable. In practice, no more than 60% of the lithium would need to be replaced, as the original cathode crystal structure collapses if more than 60% of the lithium is removed from the cathode (shaded in gray). 120

C.18 kg CO_{2e} emissions per kg of battery manufactured and recycled using a direct recycling process, less the emissions offset from recycling process outputs as the lithium recovered through direct recycling varies. In practice, no more than 60% of the lithium would need to be replaced, as the original cathode crystal structure collapses if more than 60% of the lithium is removed from the cathode (shaded in gray). 120

C.19 MJ of energy saved per kg of battery manufactured and recycled using a direct recycling process, less the emissions offset from recycling process outputs as the lithium recovered through direct recycling varies. In practice, no more than 60% of the lithium would need to be replaced, as the original cathode crystal structure collapses if more than 60% of the lithium is removed from the cathode (shaded in gray). 121

C.20 kg CO_{2e} emissions per kWh of battery manufactured and recycled using a direct recycling process, less the emissions offset from recycling process outputs as the lithium recovered through direct recycling varies. In practice, no more than 60% of the lithium would need to be replaced, as the original cathode crystal structure collapses if more than 60% of the lithium is removed from the cathode (shaded in gray). 121

C.21 MJ of energy saved per kWh of battery manufactured and recycled using a direct recycling process, less the emissions offset from recycling process outputs as the lithium recovered through direct recycling varies. In practice, no more than 60% of the lithium would need to be replaced, as the original cathode crystal structure collapses if more than 60% of the lithium is removed from the cathode (shaded in gray). 122

D.1 Electric Range and Manufacturer's Suggested Retail Price (MSRP) for BEVs and PHEVs available in 2017 124

D.2 Historical US sales of PHEVs by lowest model price (2010 - 2017) 125

List of Tables

2.1	Cell BOM Parameters examined	8
2.2	Facility wide model parameters and sensitivity ranges	10
2.3	Material yield rates and associated manufacturing steps. Uncertainty in the cell yield rate is italicized and included below the baseline estimate	10
2.4	Equipment, area, labor, and process rate assumptions for each manufacturing step. BatPaC point estimates are used for each of the steps common for all cell formats. Uncertainty bounds for the cylindrical cells and precursor preparation steps are italicized.	13
2.5	Precursor drying and calcining process assumptions	15
2.6	Cathode active material costs per kg with uncertainty bounds, 2015\$	16
2.7	Impact of lithium prices on NCA and NMC cells in baseline and optimistic scenarios	20
3.1	Fixed System Parameters	28
3.2	Fixed System Parameters	29
3.3	Battery chemistries and degradation models	31
3.4	System component cost assumptions	33
4.1	Comparison of greenhouse gas emissions and energy inputs to cell manufacturing between this and other studies	55
5.1	Attribute Descriptions	68
5.2	Respondent Demographic Data	73
5.3	BEV Willingness to pay results	74
5.4	PHEV Willingness to Pay Results	75

5.5	Latent classes for BEV owners in the willingness to pay space. Environmentally-conscious owners, with a positive opinion of refurbished materials, make up 35% of the sample population.	76
5.6	Latent classes for PHEV owners in the Willingness to pay space. Risk-averse owners make up 40% of those sampled.	78
A.1	U.S. BEV sales and storage capacity, 2010-2015. Blank cells indicate no vehicle sales	87
A.2	U.S PHEV sales and storage capacity, 2010-2015. Blank cells indicate no vehicle sales	89
A.3	Cell dimension parameter values	92
A.4	Material cost values (excluding cathode precursors)	92
A.5	Cathode precursor cost assumptions	93
A.6	Prismatic cell step assumptions	95
A.7	Prismatic cell physical parameters	95
A.8	Connected Manufacturing Steps and Cumulative Operating Time	96
A.9	Change in cost per kWh as a result of cascading unplanned downtime	96
B.1	Power Flow Optimization Parameters	99
B.2	Capacity Loss Calculations for different battery chemistries	100
B.3	Charging and Discharging Power Flow Limits	100
C.1	Cell Input Assumptions for NMC Cells. Baseline assumptions are listed along with upper and lower bounds (italicized)	102
C.2	Cell Input Assumptions for NCA Cells. Baseline assumptions are listed along with upper and lower bounds (italicized)	103
C.3	Material inputs and output for cathode precursor mixing step using nitrate precursor materials	103
C.4	Material inputs and output for cathode precursor mixing step using sulfate precursor materials	103
C.5	Material and energy inputs for manufacturing sulfate precursor materials	104
C.6	Material inputs for manufacturing nitrate precursor materials	104
C.7	Material inputs and output for lithination of NMC and NCA	104

C.8	Energy inputs for cathode drying and calcining	104
C.9	Emissions and heat input assumptions for electricity and natural gas inputs	104
C.10	Embodied emissions for cathode materials	105
C.11	Embodied Emissions for Cell Materials (excluding cathode)	105
C.12	Per ton-mile emissions for water, rail, and road transport	105
C.13	Transportation Distance Assumptions (in miles) by mode for RFCM, NWPP, and US average	106
C.14	Process inputs for pyrometallurgical Recycling. Emissions and Resource data sourced from GREET 2016.	106
C.15	Percentage of metal content that goes to Slag and Alloy in pyrometallurgical process [1]	106
C.16	Facility-wide parameter assumptions [2, 3]	107
C.17	Equipment, labor, and process rate assumptions for cathode manufacturing/ repro- cessing steps [2]	107
C.18	Material price assumptions for cathode precursor metals and lithium carbonate. Data is based on USGS data [4]	107
C.19	Comparison of greenhouse gas emissions and energy inputs to cell manufacturing between this and other studies per kWh of battery	111
D.1	Market Data - Battery Warranties	126
D.2	Survey versions and attribute levels	127
D.3	2- and 3- Latent Class Models for BEVs in the preference space	128
D.4	4 latent class model for BEVs in the preference space	129
D.5	5 latent class model for BEVs in the preference space	130
D.6	6 latent class model for BEVs in the preference space	131
D.7	2- and 3- Latent Class Models for PHEVs in the preference space	132
D.8	4 Latent Class Models for PHEVs in the preference space	133
D.9	Latent Class Selection Criteria for PHEVs	133

Chapter 1

Introduction

As electrochemical energy storage technologies have improved and become less expensive in recent years, the number of applications where these technologies are viable has only increased. Two such applications are for grid electricity storage, which can occur at many different scales and locations within an electricity system, and electric vehicles.

Between 2010 and the end of 2015, roughly 419,000 battery electric and plug-in hybrid vehicles were sold in the U.S., with a combined storage capacity of 11 GWh.¹ Similarly, according to the Department of Energy Global Energy Storage Database, there are nearly 1,000 grid-connected electrochemical energy storage projects that can provide over 3MW of power in the U.S. today, with most of the growth occurring since 2010 [5].

These two technology markets are also projected to increase as additional intermittent renewable electricity sources are brought online and fuel economy standards drive higher adoption rates of hybrid and battery electric vehicles. However, there are still outstanding questions about the technology cost, performance, emissions, and acceptance that have the potential to impact the size and scope of these future markets. My dissertation seeks to address some of these questions, with particular focus on lithium-ion and other established, widely available battery chemistries.

Despite recent technology improvements and cost reductions, there are still challenges to making energy storage technologies economically viable in many situations. The Department of Energy Vehicle Technology Office estimates that battery costs will have to fall to \$125/kWh or less to truly be cost competitive [6]. In Chapter 2, I investigate the potential for manufacturing cost reductions of the large-format cylindrical and prismatic lithium-ion batteries commonly found in today's

¹Additional detail provided in Appendix A.1

U.S. electric vehicle market. Using a process-based cost model, I compare the costs of several cell chemistries and variations at different production volumes. Although there is some potential for reducing costs by adjusting the cell parameters and format, additional savings from economies of scale alone are minimal relative to the overall battery cost.

Today's batteries also offer substantial trade-offs between capital cost, performance, and cycleability. In Chapter 3 I examine how these technology and performance tradeoffs impact the levelized cost of electricity delivered in a hybrid microgrid system. Although the electricity from hybrid systems was almost always more expensive than a diesel generator, high energy density, moderately expensive lithium-ion batteries were cost competitive with inexpensive but less efficient lead acid batteries. The improved performance of high power density lithium-ion batteries that offer excellent cycle life was insufficient to justify the much higher capital cost when compared to other storage options.

As battery energy storage use increases, we will need to develop new ways to minimize the environmental impact of producing these technologies, and ways to recover some of the valuable materials used to make batteries. In Chapter 4, I address the potential cost and emissions savings from a new battery recycling process, which directly recovers high-value cathode material, instead of a traditional pyrometallurgical recycling process. Using a lifecycle analysis that accounts for the emissions and energy consumption of manufacturing, recycling, and offsets from the recovered materials, I find that new, direct methods offer robust greenhouse gas emissions, while more traditional methods are not guaranteed to reduce emissions overall. Because of the costs associated with manufacturing cathode materials, there it is also possible that these new direct recovery methods can be profitable relative to other cathode manufacturing processes.

Chapter 5 begins to answer whether these materials that are recovered from the direct cathode recovery process have consumer support to be successful in the market. Using a choice-based conjoint survey of current electric vehicle owners, I examine whether consumers have strong preferences about battery materials (conventional, recycled, and refurbished) relative to other attributes that are related to battery performance (like range and warranty coverage of battery performance). We find that there is heterogeneity in consumer preferences, with PHEV owners overall having a slightly negative perception of recycled batteries, while BEV owners as one group are indifferent. However, within these groups we see a broader range of opinions, with some BEV owners having a positive opinion of refurbished batteries. For PHEV owners, roughly 40% of the respondents were considered risk-averse, requiring cost reductions of \$7,000 (\$600 - \$13,000) to

accept a recycled or refurbished battery pack. Additional examination of the demographics that may be associated with these different preferences is necessary, as is analysis of how recycled or refurbished battery performance could impact other attributes, like range and final range, that are consistently important to consumers.

Finally, Chapter 6 provides a summary of the findings of the previous chapters, along with policy recommendations to help to further reduce the costs of battery energy storage and its applications as the market continues to grow.

Chapter 2

Manufacturing costs of lithium-ion batteries: impacts of form factor, material inputs, and economies of scale

This chapter is based on work published in:

R. E. Ciez and J.F. Whitacre, "Comparison between cylindrical and prismatic lithium-ion cell costs using a process based cost model," *Journal of Power Sources*, Volume 340, 2017, Pages 273-281.

2.1 Introduction

Because of the significance of manufacturing costs, models of the production costs of lithium-ion batteries have been developed. The most notable model is the BatPaC model developed by Argonne National Lab. [7, 8] Using multiple battery pack configurations and lithium-ion chemistries, the model determines the cost per kWh, allowing for increases in production volume from the baseline rate of 100,000 packs year⁻¹. Additional work has been done to analyze some of the specific steps of pouch cell manufacturing outlined in the BatPaC model. Wood et al find that reducing the duration of solid-electrolyte interphase (SEI) formation and replacing expensive solvents can reduce the costs of manufacturing of small batches of batteries [9]. Both Wood et al [9]

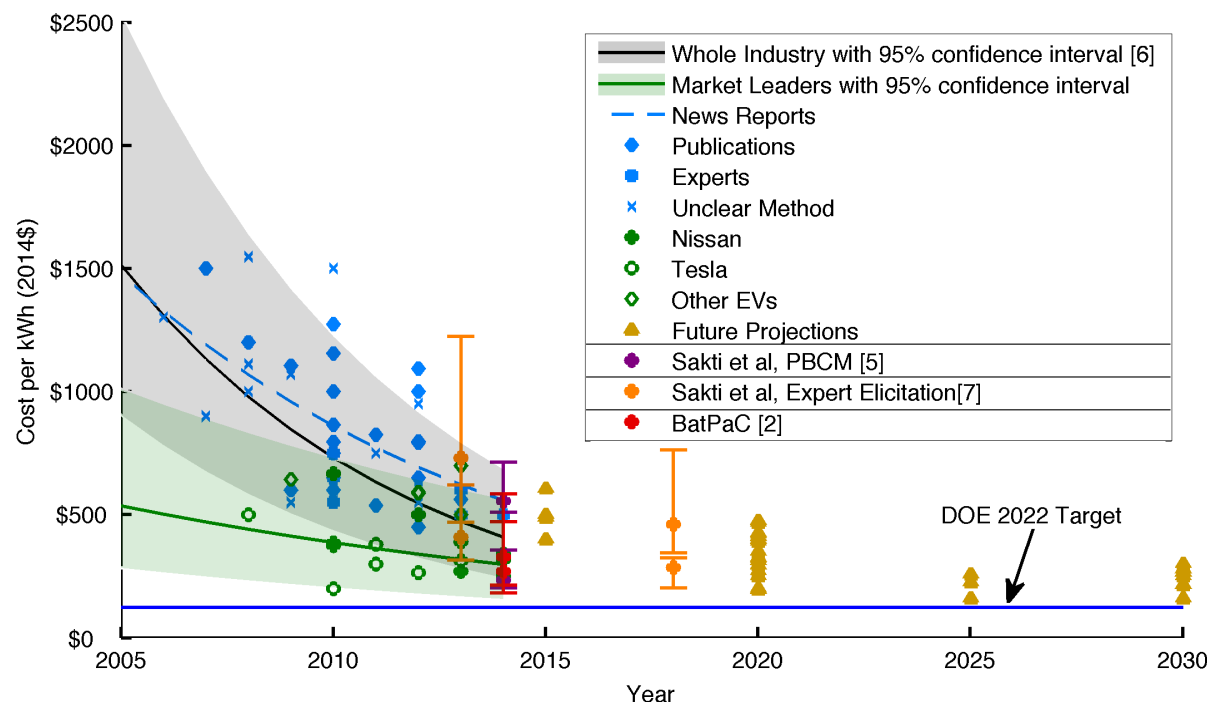


Figure 2.1: Historical prices and future cost predictions for lithium ion batteries. Estimates include both cell- and pack-level cost assessments, which is reflected in the significant variability in the cost estimates.

and Sakti et al [10] find that there are also cost savings when electrode thicknesses are increased, increasing the energy storage capacity of each cell.

All of these models produce cost estimates that are largely in line with current industry prices. Nykvist and Nilsson compiled stated predictions, news reports, and journal articles to analyze trends in lithium-ion cell- and pack-level prices [11]. Their data is reproduced in Figure 2.1, along with BatPaC estimates (using the May 2015 version), the estimates from Sakti et al [10], and expert predictions collected by Sakti et al [12].

However, since these models and analyses were introduced, the lithium-ion battery market has shifted. 419,000 battery vehicles (BEVs) and plug-in hybrid electric vehicles (PHEVs) were sold between 2010 and the end of 2015. The number of vehicles sold and the storage capacity of these vehicles varies significantly. The Tesla Model S, one of the most popular electric vehicles, has a battery pack that varies between 75 and 90 kWh, much larger than the 10.5 kWh average pack size for PHEVs and double the 42 kWh average for BEVs. These packs also use cylindrical lithium-ion cells, a departure from the prismatic cells examined in previous models. Electric vehicle sales and pack sizes also impact the most commonly used lithium-ion chemistries. Lithium Nickel Cobalt Aluminum Oxide (NCA) is the most common chemistry, accounting for half of the storage capacity

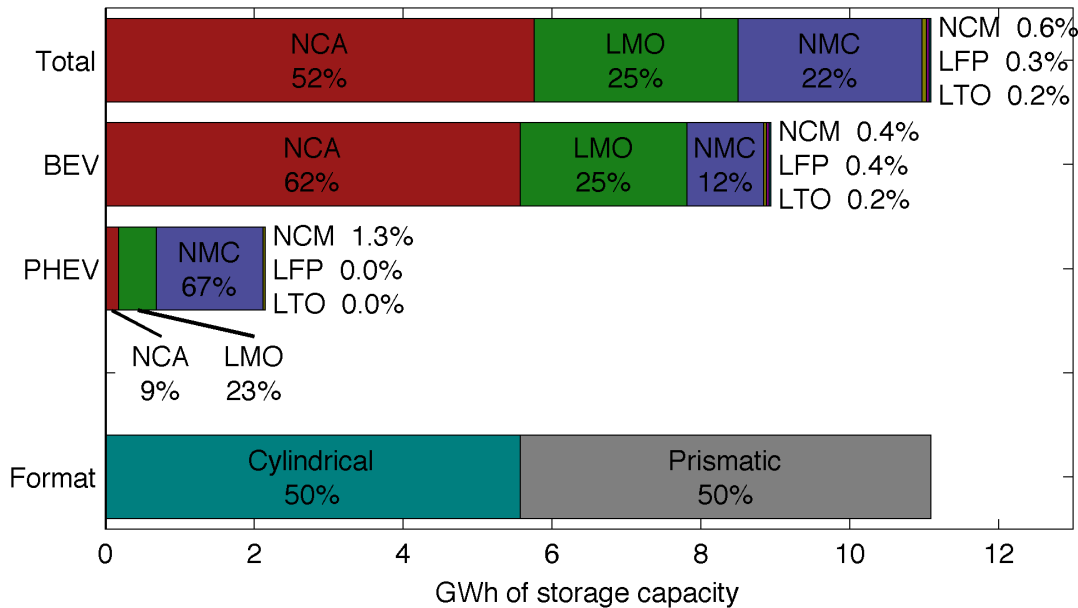


Figure 2.2: Estimate of storage capacity (by GWh), broken out by chemistry, format, and vehicle type. BEVs account for 79% of total capacity.

on the road today, and Lithium Manganese Oxide (LMO) and Lithium Nickel Manganese Cobalt Oxide (NMC) account for approximately a quarter each. Other chemistries have been used in niche applications (predominantly in California compliance cars and early electric vehicle models), but have largely been phased out. Figure 2.2 shows the split of battery chemistries and formats, and Appendix A provides full details on vehicle sales and associated battery storage.

Also as a result of these sales trends, on a per kWh basis, the majority of lithium-ion batteries on the road in the US today are cylindrical. To date, manufacturing process research and cost models have focused exclusively on prismatic cells, and there is no specific model to address the costs of manufacturing cylindrical cells. To address the disparity between the current EV battery market and research, we present a process-based cost model specifically adapted for manufacturing cylindrical lithium-ion cells.

The model uses common inputs from the BatPaC model for the steps that are identical for both prismatic and cylindrical cell manufacturing and accounts for the three chemistries most commonly used in electric vehicles. The model also allows for variations in the cylindrical cell dimensions. We use 18650 cells as a baseline (18 mm diameter, 65 mm height), but allow for 10% increases in cell height and diameter, allowing for a per-cell increase in storage capacity. We also account for variations in the cell electrode thickness. For any combination of parameters, we calculate the

Table 2.1: Cell BOM Parameters examined

Parameter	Values
Cell Chemistry	LMO (100 mAh/g), NMC (200 mAh/g), NCA (180 mAh/g)
Cell Dimensions	18650, 18720, 20650, 20720
Electrode Thickness	50, 70, 100 μm

manufacturing cost at various production volumes to compare the costs between chemistries and determine whether there are additional economies of scale that have not been realized. The manufacturing costs include in-house preparation of cathode active materials, which are commonly purchased at a markup by battery manufacturers.

2.2 Methods

The model consists of two parts: the first builds a cell based on desired cell dimension and chemistry, the second computes the per kWh cost of manufacturing these cells at varying production volumes.

2.2.1 Battery Cell Model

The model allows us to specify several parameters about the final form factor of the battery: the chemistry (LMO, NMC, or NCA), the diameter and height of the cells, and the electrode thickness. The upper bounds on the cell height and diameter are based on industry-specified limitations on heat transfer away from the cells. Similarly, the upper bound on the thickness of the electrode is limited by the cylindrical cell geometry. Unlike prismatic cells, where the electrodes are stacked, the electrodes in cylindrical cells must be wound. Since the current collecting foils are coated on both sides, the thickness of each individual coating cannot exceed 100 μm . Thicker electrode coatings would likely crack when wound because of the very small radius at the center of the cell. Electrode coatings are also somewhat limited by current manufacturing capabilities, as outlined in the interviews conducted by Sakti et al [12].

Depending on the parameter selections, the model calculates the bill of materials required to construct the battery, and determines the overall storage capacity of each cell. Table 2.1 lists the user-specified cell parameter selections. The energy storage capacity is determined by the active cathode material in each cell and the cell chemistry's specific energy storage capacity and voltage. Specific internal dimensions were based on a combination of the user specified param-

eters (namely the electrode thickness and height of the cell) and on published dimensions of the electrode thicknesses of prototype cylindrical cells [13]. The energy stored (E) in each cell is the product of the material voltage (V) and specific storage capacity (s) and the mass of cathode material (m), as shown in equation 2.1.

$$E = Vsm \quad (2.1)$$

The active material mass depends on the cathode volume (v_{CATH}), the density of the final cathode material (ρ_{CATH}), and the percentage of active material in the cathode (p_{ACT}) (equation 2.2).

$$m = \rho_{CATH}v_{CATH}p_{ACT} \quad (2.2)$$

The cathode volume is a product of the electrode height (x_H), cathode length (x_L), and the total (double-sided) thickness (x_T) as shown in equation 2.3.

$$v_{CATH} = x_H x_L x_T \quad (2.3)$$

The length of the cathode is determined by equation 2.4, which accounts for all of the interior volume of the cell, v_{cell} (assumed to be 85% of the cell volume calculated from exterior dimensions). Here, we assume that the anode and cathode foils (x_F) and active material coatings (x_T) are of the same thickness and height (x_H). However, the cathode and separators (with thickness x_S) are assumed to be 10% longer than the anode, in line with the dimensions specified in prototype cells [13]. The separator thickness is doubled to account for the two separators needed for the doublesided coating. The volume available within the cell is then divided by the volume of the electrodes (with varying lengths) and the volume of the separators, as shown in equation 2.4.

$$x_L = 1.1 \left(\frac{v_{CELL}}{x_H(x_T + x_F + 1.1(x_T + 2x_S + x_F))} \right) \quad (2.4)$$

2.2.2 Cost model

We model the cell cost using a process-based cost model (PBCM) for each of the steps involved in manufacturing cylindrical lithium-ion cells. This method has been applied to numerous industries, but it originated with the electronics industry, where design for manufacturing is a key concern

Table 2.2: Facility wide model parameters and sensitivity ranges

Input	Base	Units	Optimistic	Pessimistic
Working days per year	300	Days/year	360	240
8-hour shifts per day	3	Shifts/day	3	3
Unpaid breaks per shift	1	Hours/shift	0.5	1.5
Paid breaks per shift	0.75	Hours/shift	0.5	1
Building costs	\$3000	$\$/m^2$	\$1600	\$4000
Labor rate	\$18	\$/hour	\$15	\$25
Building useful life	20	Years	20	20
Capital useful life	6	Years	6	6
Discount rate	10%	%	10%	10%
Auxiliary equipment cost	10%	% of main machine cost	10%	10%
Maintenance	10%	% of main machine cost	5%	15%
Fixed overhead	33%	% of main machine, building, aux. equipment, and maintenance cost	30%	35%
Energy cost	3%	% of material and labor cost	3%	3%

Table 2.3: Material yield rates and associated manufacturing steps. Uncertainty in the cell yield rate is italicized and included below the baseline estimate

Material	Yield Rate	Step
Cathode material	92.2%	3.1 Cathode material mixing
Anode material	92.2%	3.2 Anode material mixing
Cathode foil	90.2%	3.1 Cathode coating
Anode foil	90.2%	3.2 Anode coating
Solvent recovery	99.5%	3.1 Cathode coating
Separators	98%	9 Cell winding
Electrolyte	94%	11 Electrolyte fill & seal
Cells	95% <i>90 - 99%</i>	15 Charge retention

[3, 14, 15]. Sakti et al also applied this method for calculating the cost of prismatic lithium-ion cells [10]. Here, we adapt this cost model to specifically focus on cylindrical cells. Figure 2.3 outlines each of the manufacturing steps included. Those in gray are the same for both cylindrical and prismatic cells. Those in green are specifically for cylindrical cells. The precursor preparation step (in blue) is common to all cell formats, but is not in the scope of the BatPaC model.

The total production cost in a PBCM is determined by summing material, equipment, auxiliary equipment, building, maintenance, labor, energy, and fixed overhead costs. The per-unit cost is the sum of these costs divided by the final output. Equipment and building costs are determined using discrete increases in required machinery necessary to produce increased production volumes, accounting for yield losses in the production process. Table 2.2 shows the facility-wide

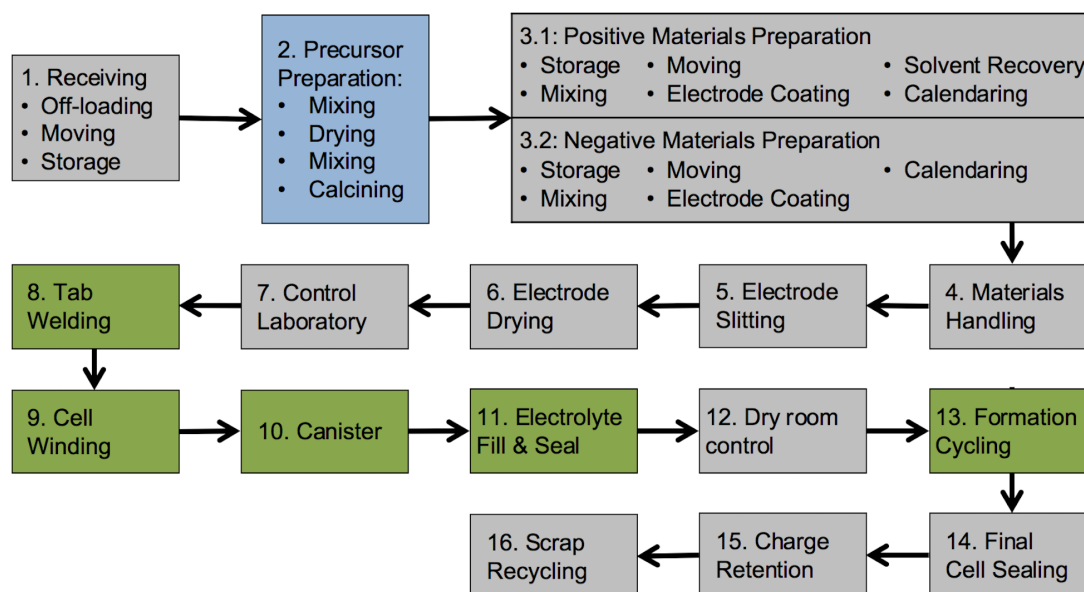


Figure 2.3: Historical prices and future cost predictions for lithium ion batteries. Estimates include both cell- and pack-level cost assessments, which is reflected in the significant variability in the cost estimates.

assumptions, and sensitivity ranges used to calculate the cost of each of the steps. Table 3 shows the equipment, area, and labor requirements for each step. For the steps common to both prismatic and cylindrical cells, these estimates are based on the BatPaC model, but are adjusted to 2015\$. Although the steps listed in Figure 2.3 are common to manufacturing all of the types of cylindrical cells derived from the cell model, there is equipment customization required for many of the steps depending on the cell electrode dimensions. As a result, the cost of switching a manufacturing process from one type of cell to another is very expensive, and would include not only additional equipment costs (as improperly tooled equipment would need to be replaced, possibly before its recovery period), but would also result lost production time to accommodate the installation. These costs are excluded from our analysis, and we look at the processes for a single cell format throughout.

Cylindrical Cell Steps

For the cylindrical-cell specific steps, we contacted a number of equipment manufacturers to obtain specific information about the machinery necessary for these steps. These estimates included equipment prices, footprint, process rates, and information on labor, and whether there are specific tooling requirements. These estimates are included in Table 2.4.

Precursor Mixing

The precursor mixing step calculations included assumptions about the specific precursor materials used, the costs of the precursor materials used, and the machinery and equipment necessary for this type of processing. Because of the steps and processes involved, it is very common for battery producers to outsource these steps to another company. However, doing so does increase the materials cost because of the additional markup that producers pay for the convenience of finalized active materials. Including an assessment of the in-house costs provides a better estimate of the true cost floor of battery manufacturing.

For the precursor material costs themselves, we used historical price data from the USGS 2015 Mineral Commodity Summary for each of the key constituent parts. The lithium price data listed is specifically based on lithium carbonate data (because of its dominance in the global market). For the other elements (Ni, Co, Al, Mn), we assumed that the price per unit mass of the constituent compound was determined entirely by the active element in the constituent compound. For example, the 5-year average nickel price is \$19/kg, NiSO₄ is 38% nickel by mass, so we assumed the cost per kg of NiSO₄ to be \$7/kg. Similar calculations were done for the other precursor materials, but we did correct for the impurity of the manganese prices quoted in the USGS data.

Table 2.4: Equipment, area, labor, and process rate assumptions for each manufacturing step. BatPaC point estimates are used for each of the steps common for all cell formats. Uncertainty bounds for the cylindrical cells and precursor preparation steps are italicized.

Step	Equipment Cost (millions of \$)	Footprint (m^2)	Fractional use of labor	Process Rate	Unplanned Downtime	Dedicated (Yes/No)
1 Receiving	3.6	900	3	6667 kg/shi.ft	20%	Yes
2 Precursor preparation						
Mixing	0.55	200	0.67	1000 l/shi.ft	25%	Yes
Drying	1.5	22	1	35 l/hr	25%	Yes
	1.2-1.8	20-25		29-44 l/hr		
Mixing	0.55	200	0.67	1000 l/shi.ft	25%	Yes
Calcining	1.5	22	1	20 l/hr	25%	Yes
	1.2-1.8	20-25		15-30 l/hr		
3.1 Positive Materials Preparation						
Cathode material storage	1.1	200	0.67	1000 l/shi.ft	25%	Yes
Cathode material mixing	0.55	200	0.67	1000 l/shi.ft	25%	Yes
Cathode material moving	0.55	750	0.67	1000 l/shi.ft	25%	Yes
Cathode coating	8.7	750	4	15 m^2/min	30%	Yes
Solvent recovery	3.3	225	2	212 kg/hr	20%	Yes
Cathode calendaring	1.1	225	0.67	15 m^2/min	30%	Yes
3.2 Negative Materials Preparation						
Anode material storage	1.1	200	0.67	1000 l/shi.ft	25%	Yes
Anode material mixing	0.55	200	0.67	1000 l/shi.ft	25%	Yes
Anode material moving	0.55	750	0.67	1000 l/shi.ft	25%	Yes

Anode coating	8.7	750	4	15 m^2/min	30%	Yes
Anode calendaring	1.1	225	0.67	15 m^2/min	30%	Yes
4 Materials handling	1.6	900	4	19 m^2/min	20%	Yes
5 Electrode slitting	2.2	300	4	19 m^2/min	20%	Yes
6 Electrode drying	0.2	38	0.25	600 $kg/shift$	20%	Yes
7 Control laboratory	1.6	300	4	121 kWh/hr	20%	Yes
8 Tab welding ^{ab}	0.13 0.12-0.15	6 5-7	1	30 $cells/min$ 25-35 $cells/min$	20%	Yes
9 Cell winding ^{ab}	0.42 0.25-0.59	5 4-5	1	15 $cells/min$ 12-20 $cells/min$	20%	Yes
10 Canister insertion ^{ab}	0.63 0.25 - 1	5 4 - 5	1	35 $cells/min$ 30 - 40 $cells/min$	20%	Yes
11 Electrolyte fill & seal ^{ab}	0.58 0.15 - 1	2 1 - 2	1	60 $cells/min$ 30 - 120 $cells/min$	20%	Yes
12 Dry room control	22	100	2	0.03 m^2/m^2	0%	No
13 Formation cycling ^a	0.2 0.13 - 0.25	4	0.23	31.25 $cells/hour$ 31.25 - 65.2 $cells/hr$	20%	Yes
14 Final cell sealing	2.2	450	2	30 $cells/min$	20%	Yes
15 Charge retention	0.01	1.2	0.004	1000 $cells/336hours$	20%	Yes
16 Scrap recycling	2.7	600	5	441 $kg/shift$	20%	Yes

^a Assumptions specific to cylindrical cells^b Steps enclosed in dry room control system, which is sized based on the building area required for these steps

Table 2.5: Precursor drying and calcining process assumptions

	Drying*	Calcining
Furnace length	15 feet	
Temperature (°C)	100	800
Cycle time (<i>hours</i>)	10 (8-12)	18 (12-24)
Power consumption (<i>kW</i>)	70 (63-77)	200 (180-220)

* NCA and NMC precursor manufacturing only

The steps and machinery required for precursor mixing depended on the specific chemistry. For both NMC and NCA, the cathode materials are prepared using a mixed hydroxide method, where the nickel, manganese, and cobalt compounds are pre-mixed and dried before adding lithium. [16, 17] The lithium compounds are then mixed with the hydroxide or oxide materials and calcined. For both mixing steps in the precursor preparation process, we used the assumptions listed for mixing equipment in the BatPaC model. For both the drying and calcining steps, we sourced quotes from manufacturers on both price and energy consumption for the required different operating temperatures. The equipment price, area requirements, labor requirements, and process rate are listed in Table 2.4. Additional assumptions about the drying and calcining processes are detailed in Table 2.5.

The power consumption values listed in Table 2.5 were used to calculate the additional cost of energy associated with precursor mixing. This step is fairly energy intensive, and the BatPaC assumption of energy costs (3% of the total material and labor cost) both excludes these steps and is not representative of the energy requirements of drying and calcining the precursor materials. Energy consumption for the mixing steps is negligible compared to the energy required for drying and calcining, and is excluded. The additional energy consumption is calculated based on the number of hours per year the machinery is operated for, and with an assumed electricity price of \$0.07/kWh, the median price of electricity for industrial customers in 2015. [18]

Cell Hardware Costs

Cell canister costs were based on inflation-adjusted unit costs of the cell container (\$0.22 per cell), but did not include additional expenses that result from additional mass. The positive and negative terminal assemblies for cylindrical cells differ slightly. One terminal, in this case, the negative terminal, uses the cell canister as the current conductor. There is also a polymer insulator inside

Table 2.6: Cathode active material costs per kg with uncertainty bounds, 2015\$

Battery Chemistry	Precursor PBCM	BatPaC assumed values
LMO	\$3.75 (\$2.60 - \$5.36)	\$10.9 (\$8.72 - \$21.8)
NMC	\$21.43 (\$16.89 - \$27.43)	\$28.34 (\$28.34 - \$31.61)
NCA	\$26.17 (\$21.53 - \$31.98)	\$35.97 (\$35.97 - \$40.33)

the cell. [19] This insulator costs on the order of \$0.05-\$0.10 per cell. The other terminal, in this case the positive terminal, include a polymer insulator and current interrupting device, in addition to a separate metallic cap. The cost of this terminal assembly is on the order of \$0.10-\$0.20 per cell. The safety devices are a substantial contributor to the assembly cost, and the cap contributes <\$0.05 per cell. [20] This puts the positive terminal assembly at a slightly lower cost estimate than the unit cost for prismatic cell terminals assumed in BatPaC.

2.3 Results & Discussion

2.3.1 Cathode Material Costs

When we account for all of the materials purchased, equipment, labor, and energy inputs required for each of the cathode active materials, we find that our estimates are lower than the assumed values in other models. Table 2.6 lists our costs per kg, with comparisons to other assumed values. Although these reductions could include some economies of scale savings over other production lines, much of the savings is likely attributable to elimination of profit margin markups for outside suppliers.

2.3.2 Unit Costs

Comparing the manufacturing costs of the baseline 18650 cell with 70 μm electrodes and 2 GWh of storage capacity produced annually, we find that the cost per cell is lowest for LMO cells (as shown in Figure 2.4). However, when we examine the cost on a per kWh basis, the LMO cells are significantly more expensive than both other chemistries we examine. While the active materials needed per cell are less expensive, the number of cells required to produce 2 GWh of storage capacity is roughly double the number of NCA or NMC cells necessary to store the same amount of energy.

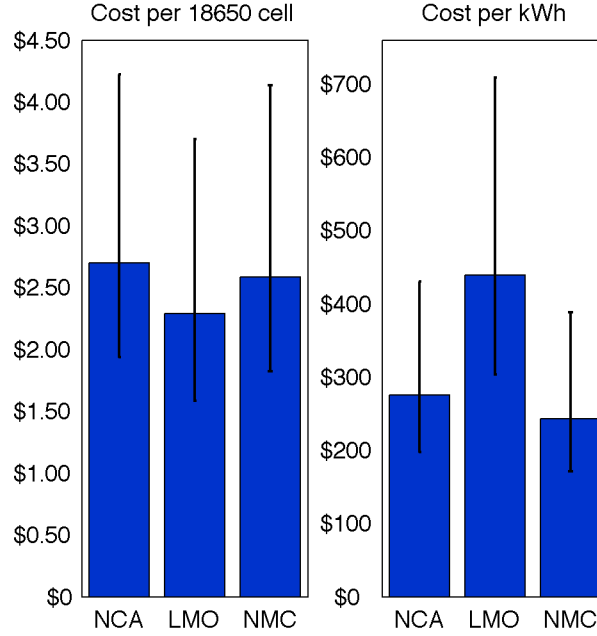


Figure 2.4: Cost per cell and per kWh for NCA, LMO, and NMC batteries, assuming 18650 cells, $70\mu m$ electrodes, and 2GWh of annual production

This cost pattern holds regardless of the production volume, as Figure 2.5 shows. The figure also shows that economies of scale of the production are largely reached at volumes of 1GWh/year with limited reductions in cost at higher volumes. Additional detail about the uncertainty in the cost estimates is provided in Appendix A.

2.3.3 Sensitivity Analysis

Because of the inefficiency of LMO batteries in this cylindrical format, we focus our further analysis on NCA and NMC chemistries. Figure 2.6 is a tornado plot that shows how the cost per kWh of storage capacity changes as we vary the model parameters specified. For both chemistries, we find that only decreasing the electrode thickness (from $70\mu m$ to $50\mu m$) is the only change that results in a higher price per kWh, as more of the battery volume is occupied by separators and current collectors instead of active material. While the per kWh cost increases with these thinner electrodes, this can be desirable in applications where a high power density battery is required, as is the case in PHEVs. Increasing the thickness (from $70\mu m$ to $100\mu m$), changing the format of the battery to be taller or wider (or both), and doubling or quadrupling annual production volumes all decrease the cost per kWh. However, none of these changes is alone sufficient to reach the DOE

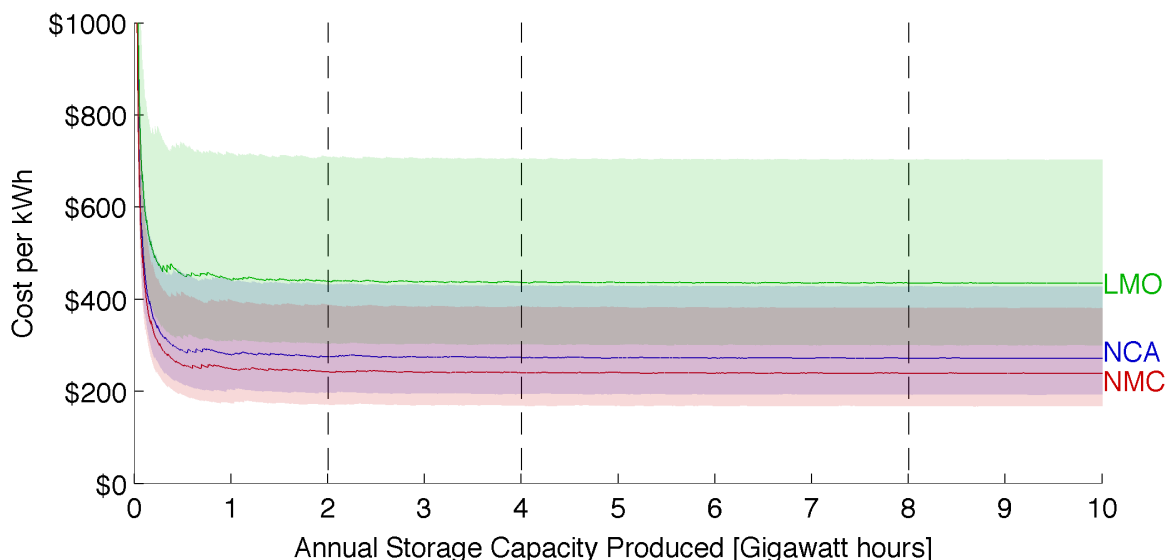


Figure 2.5: Cost per kWh of NCA, NMC, and LMO batteries generally reach economies of scale at 1 GWh of annual production, and remain stable as the annual production volumes increases. Production volumes used in later sensitivity analyses (2 GWh, 4 GWh, and 8 GWh) are highlighted.

energy storage target of \$125/kWh. Even in the most optimistic scenario, when the cells are the largest (20720), electrodes the thickest ($100\mu m$), and the production volume is 8 GWh per year, the cost per kWh is well above the DOE target of \$125/kWh: the NCA cells are \$206/kWh and NMC cells are \$180/kWh.

2.3.4 Cost Breakdown

For both our baseline model (18650 cells, $70\mu m$ electrodes, and 2GWh of production per year) and the most optimistic (20720 cells, $100\mu m$ electrodes, and 8GWh of production per year) combination of parameters, we find that the total cost is dominated by materials costs, which account for roughly 40% of the cost per kWh. Figure 2.7 shows the cost breakdown for both NCA and NMC cells in the baseline and most optimistic combinations of model parameters.

The dominance of material cost is also evident when we examine the costs per kWh associated with each step in the manufacturing process. Figure A.2 (included in the Appendix A) shows the most expensive steps (each with a cost of more than \$5/kWh) for manufacturing the baseline 18650 cells with either an NMC or NCA cathode. In both cases, we see that materials play a substantial role in the overall cost of many of these steps. Processes that have a long cycle time - formation cycling and charge retention - are also costly.

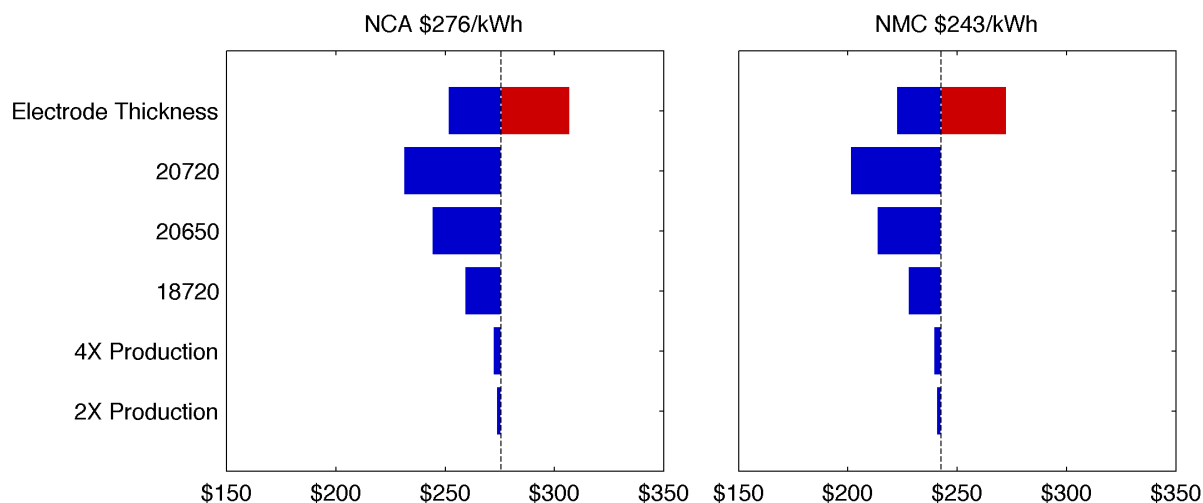


Figure 2.6: Change in cost per kWh for NCA and NMC batteries as production volumes, cell dimensions, and electrode thicknesses vary ($50\ \mu\text{m}$ to $100\ \mu\text{m}$)

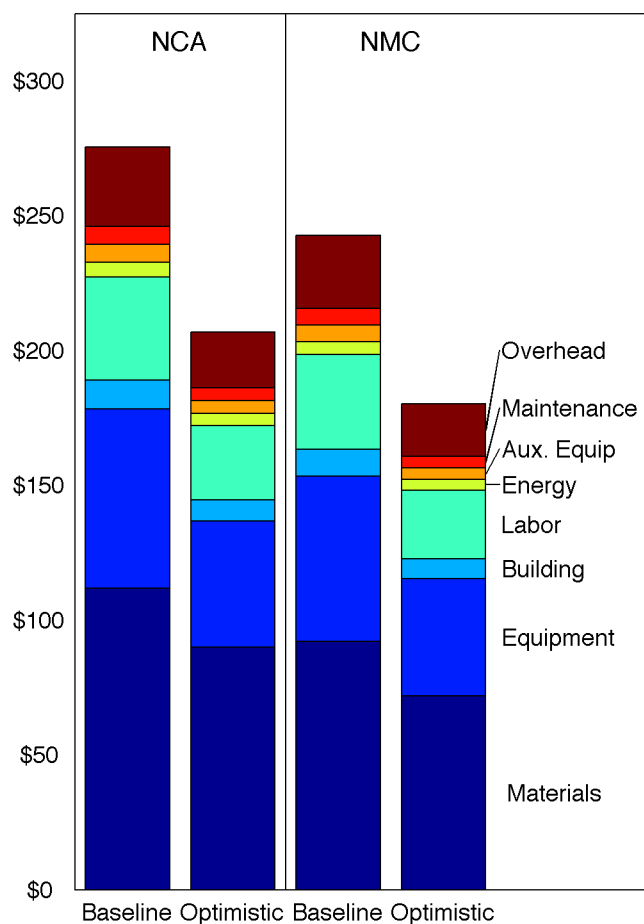


Figure 2.7: Per kWh baseline and optimistic cost breakdowns for NCA and NMC cells. Materials account for roughly 40% of the total cost.

Table 2.7: Impact of lithium prices on NCA and NMC cells in baseline and optimistic scenarios

Scenario	18650, 70 μm , 2GWh				20720, 100 μm , 8GWh			
Chemistry	NCA		NMC		NCA		NMC	
Li ₂ CO ₃ Price [\$/kg]	\$7.50	\$25	\$7.50	\$25	\$7.50	\$25	\$7.50	\$25
Cost of Li ₂ CO ₃ per kWh	\$6.10	\$20.30	\$5.60	\$18.66	\$6.10	\$20.30	\$5.60	\$18.66
Percentage of materials cost	5%	16%	5%	18%	7%	19%	8%	22%
Percentage of overall cost	2%	6%	2%	7%	3%	8%	3%	10%
Change in cost/kWh	-	+5%	-	+6%	-	+7%	-	+7%

The data also shows that many of the most expensive steps are associated with cell structural materials. Figure 2.8 breaks down the materials costs for both chemistries and baseline and optimistic scenarios. Nearly half of the materials cost is associated with cell hardware, including the container and terminal assemblies. These materials have been used in mass-produced cylindrical batteries (both primary and secondary) for decades, and are unlikely to have further cost reductions from large-scale production. Cathode precursor materials account for 27% of material costs for NCA baseline, 20% for NMC baseline, and play a larger role for larger cells with higher production volumes, where cell hardware, which scales by a combination of the number of pieces and size, contributes less to the cost per kWh.

It is important to note that these material costs are not driven by the price of lithium. Previous analysis shows that the price of lithium carbonate, the main source of lithium for batteries, has little impact on the overall cost of prismatic batteries, even if commodities prices undergo significant fluctuations. [21] This holds for cylindrical cells as well: even if the price of lithium carbonate increases to \$25/kg (from the baseline value of \$7.50), lithium never accounts for more than 10% of the total cell cost per kWh, and the resulting change in the cost per kWh is always below 10%, as shown in Table 2.7.

Although equipment costs are a relatively large percentage of the overall cost per kWh, they do decrease as the cell dimensions increase. This holds true even if we account for cascading downtime as a result of connected steps in the manufacturing process. Overall, the cost increase of more constrained system operation is relatively small ($\sim 10\%$). Additional details about the assumptions for cascading system downtime are available in Appendix A.5.

Figure 2.9 compares both the baseline and optimistic cost breakdowns for all 3 chemistries to prismatic cells with roughly 25 Ah of capacity. The exact prismatic cell dimensions and bill of materials is determined using BatPaC (version 4, May 2015), with three modifications. 1) We allowed the maximum electrode thickness constraint to increase to 200 μm , 2) we reduced the power

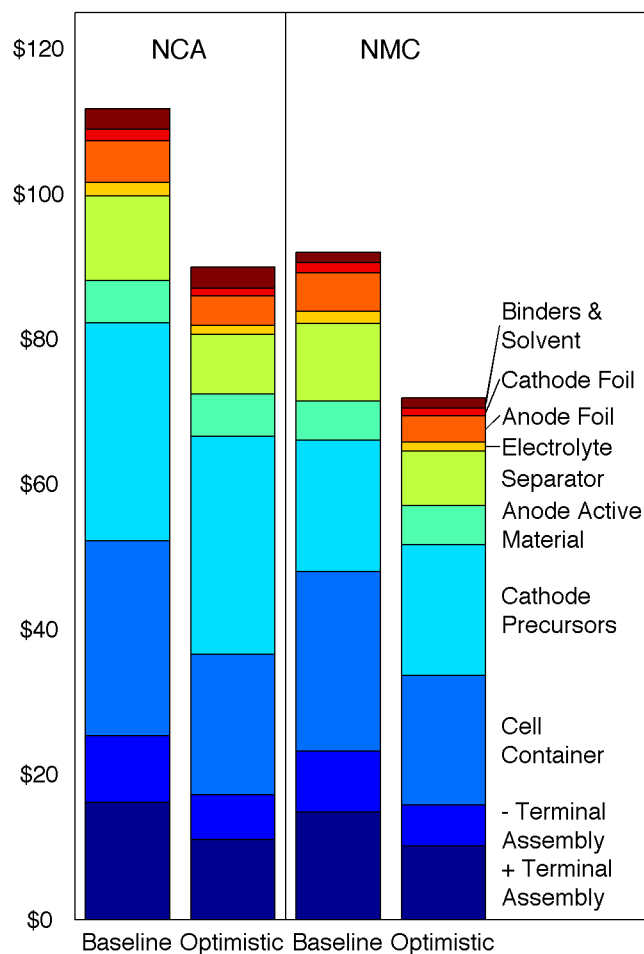


Figure 2.8: Per kWh material cost breakdown for NCA and NMC cells

requirement on the cells and 3) the specific capacities of the cathode materials was updated to match the assumptions included in Table 2.1. Costs are calculated using a process-based cost model adapted from Sakti et al with conversions to 2015\$ and using in-house precursor preparation. Specific information about the prismatic cell dimensions is provided in the supplementary information.

For all three battery chemistries, the cost per kWh for larger prismatic cells is lower than the cost for both types of cylindrical cells. This is consistent with previous analysis of the cost of prismatic LMO cells, which also showed that larger formats can offer reduced costs, even when electrodes are not allowed to increase to $200\mu m$. [21] Although the overall cost per kWh decreases, the cost of electrode materials per kWh increases slightly as larger amounts are scrapped per cell when there are manufacturing defects in prismatic cells. This effect is most pronounced when the overall annual storage capacity produced and the capacity of each cell is similar in magnitude.

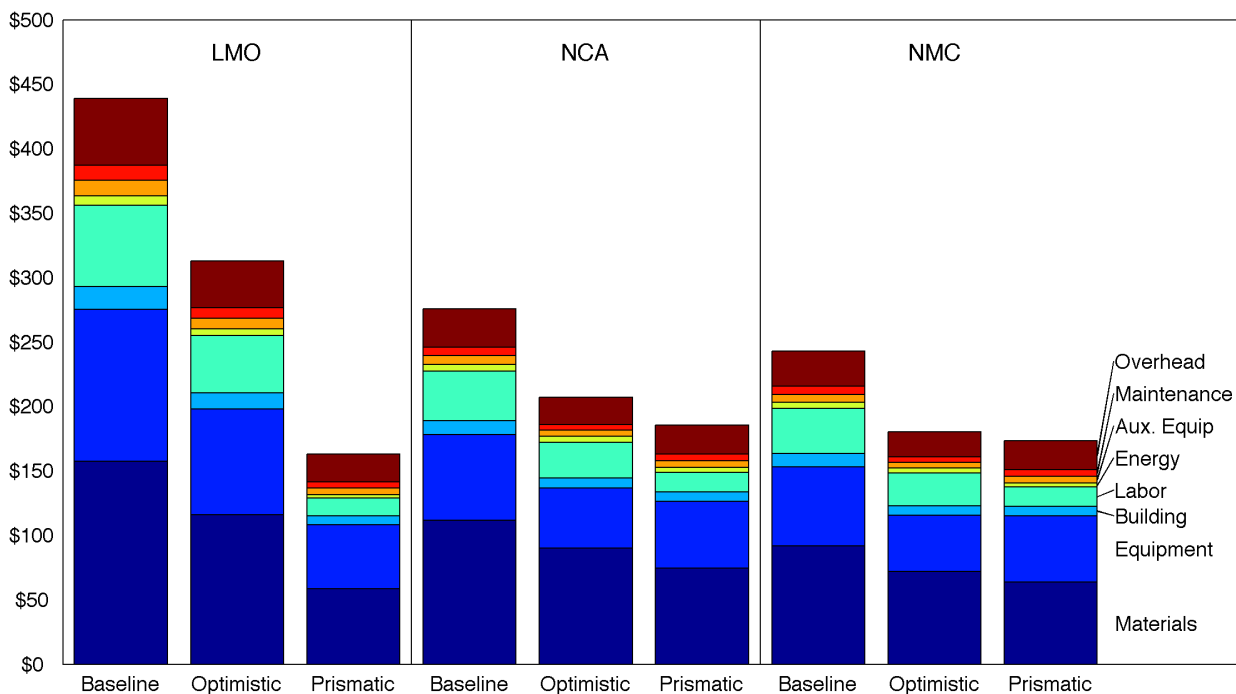


Figure 2.9: per kWh cost breakdown comparison for baseline 18650 cylindrical cells, optimistic 20720 cylindrical cells, and BatPaC prismatic cells

Overall, reduced hardware costs associated with larger cells more than offset the additional expense. Details about the material cost differences between the 18650 cells and prismatic cells are shown for NCA cells in Figure 2.10. It is also important to note that both of the NCA and NMC batteries are not able to deliver electricity at high power because of the relatively small electrode surface area relative to the thickness of the electrodes. The lower costs for prismatic cells persists even when purchased cathode materials are used instead of lower-cost in-house production, as shown in Figure 2.11.

2.4 Conclusions

The process-based cost model we construct for cylindrical lithium-ion cells shows that the cell chemistry has a significant impact on the per kWh cost of the batteries. For LMO batteries, with a low specific energy, the cylindrical cell format is too small and does not allow for the electrode thickness to increase sufficiently. As a result, additional cells are required to meet a specified energy storage production target. Prismatic LMO cells, which offer more opportunities for large cell formats with thicker electrodes and reduced hardware costs per kWh offer more opportunity

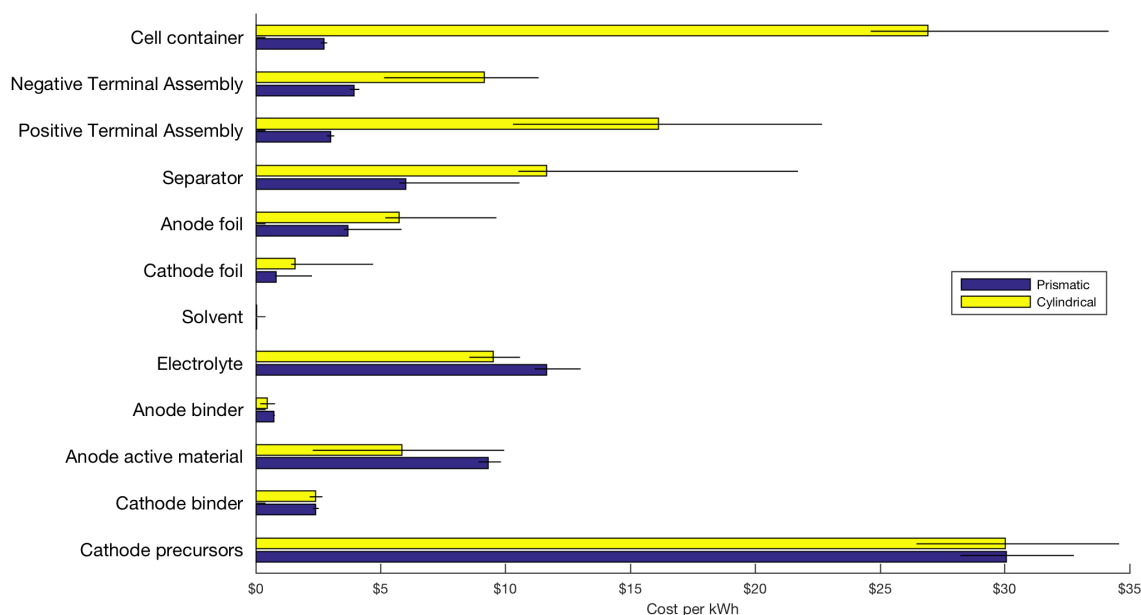


Figure 2.10: Material costs per kWh of 18650 cylindrical and prismatic NCA cells

for future cost reductions. Both NMC and NCA cylindrical batteries are less expensive per kWh to manufacture than LMO cylindrical cells, and further cost reductions are possible by increasing the cylindrical cell dimensions and the electrode thickness. While initial cost savings are possible from increasing production volumes, the possibility for cost reductions from scale alone are minimal past 1GWh of annual production, a volume which large battery manufacturers have already surpassed. At these higher production volumes materials play a significant role in the cost of energy storage per kWh, accounting for roughly half of the overall expenses.

Cathode material costs can be reduced by producing them from precursors in-house instead of purchasing them from suppliers. LMO is subject to the highest markup, at almost 200%, but the markup for NCA and NMC have substantial impacts on the cost per kWh as well. Like prismatic cells, lithium prices play a small role in the cost of NMC and NCA cylindrical cells. A more than 200% increase in the price of lithium carbonate leads to a less than 10% increase in the cost per kWh for each of the cell configurations considered.

Cell hardware is a significant contributor to the overall material cost per kWh. Prismatic cells, which have more design flexibility to account for specific chemistry characteristics, can be larger, requiring less hardware per kWh and reducing costs. This reduction is most pronounced for LMO prismatic cells, which can be manufactured for less than half the cost of cylindrical LMO cells. There is also potential for reducing the manufacturing cost for NCA and NMC cells using a pris-

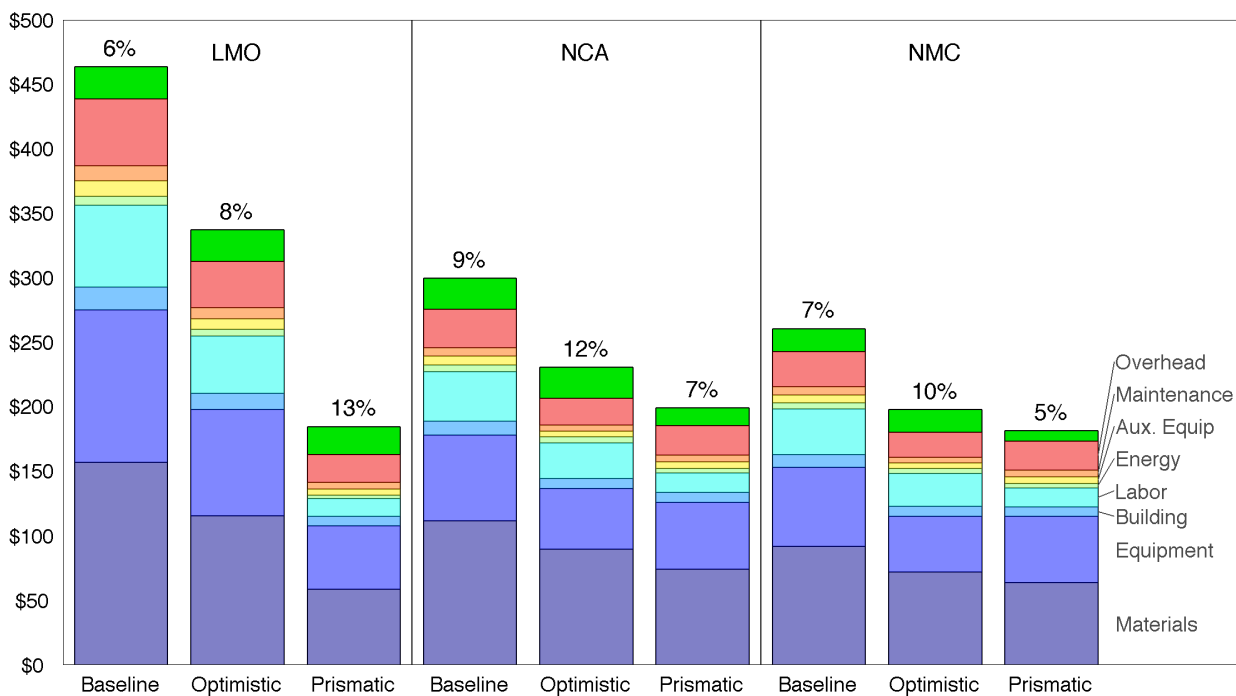


Figure 2.11: Additional cost per kWh for batteries made with purchased cathode materials (in green), relative to the cost per kWh for in-house manufacturing of active material for baseline 18650 cylindrical cells, optimistic 20720 cylindrical cells, and BatPaC prismatic cells

matic format, but the cells produced with that format are more rate-limited than LMO counterparts.

Chapter 3

Comparative Techno-Economic analysis of hybrid microgrid systems utilizing different battery types

This chapter is based on work published in:

R. E. Ciez and J.F. Whitacre, "Comparative techno-economic analysis of hybrid micro-grid systems utilizing different battery types," *Energy Conversion and Management*, Volume 112, 2016, Pages 435-444.

3.1 Introduction

Determining the appropriate balance between capital costs and technology longevity for distributed hybrid micro-grids with solar PV, battery storage, and diesel generation is particularly important as more markets incorporate small-scale energy storage and behind-the-meter energy storage policies. Germany and Japan have implemented subsidy programs to encourage behind-the-meter energy storage and independent power generation [22]. In the US, both Hawaii and California have issued energy storage requirements for grid operators, and California has approved subsidies for self-generation technologies, including energy storage [23–27]. There is also a rapidly growing demand in developing countries with poor electricity infrastructure and ample solar resources, and incentives from both development agencies (including the USAID's Beyond the Grid

Initiative) and home governments (like several state-run Renewable Energy Development Agencies in India) are in place to support this growth [28,29]. To examine how these policies align with the reality of battery operation in these applications, we focus on standalone micro-grids that utilize renewable (photovoltaic solar panels) and fossil fuel electricity generation resources (a diesel generator), combined with battery storage.

Long-term battery performance in these systems is influenced by many factors, including how deeply the battery is exercised per cycle, the rate and frequency of battery charging and discharging, and operating temperature. As new battery technologies, notably lithium-ion batteries of various chemistries and form factors, improve and become more widely available, interest has grown in determining how these batteries perform over the system life-time compared to widely available and inexpensive lead acid batteries that have historically been the technology of choice.

In the past, researchers have developed multiple models for lead-acid battery behavior in off-grid energy systems. The CIEMAT model, introduced by Copetti and Chenlo [30] and used by Achaibou et al. [31], and the model introduced by Manwell and McGowan [32] model lead acid batteries as an equivalent circuit, while Lander [33] modeled chemical dynamics. Empirical models are also available from case studies conducted by Protogeropoulos et al. [34], Spiers and Rasinkoski [35], West and Krein [36], Schiffer et al. [37], and Binder et al. [38]. Other models focus on the implementation of solar PV systems with battery storage. The model implemented by Bortolini et al. [39] provides detailed information on the power flows between system components, and uses this information to inform decisions on optimal system component size to minimize the levelized cost of electricity (LCOE), while accounting for the possibility of selling electricity to an electricity grid. Similarly, Kaldellis et al. [40] present a model of power flows for sizing the system components in a hybrid micro-grid for remote Greek islands that lack access to a larger electricity grid. However, both of these system models make broad assumptions about battery performance and technology, and do not deeply explore how different operating parameters impact the lifespan of the storage implemented. Neither the lead acid battery models or the PV system models offer a comparative assessment that incorporates the loss in function over the lifetime between lithium-ion batteries, which have inherent characteristics specific to the battery chemistry that cause each to age differently in different use cases.

Our model uses a realistic power versus time electrical load typical of a rural, multi-dwelling community without access to an electricity grid, along with appropriate temperature and solar data [41–43]. We model three contrasting battery types to provide energy storage. Specifically, a thin-

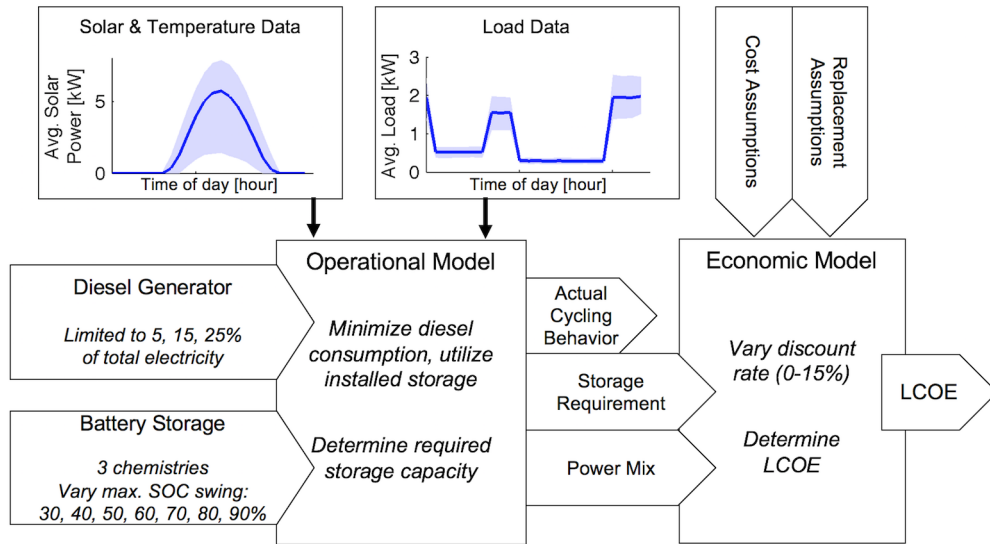


Figure 3.1: Model overview diagram

electrode, high power density lithium ion battery (similar to the A123 Systems M1 product), a thick-electrode high energy density lithium-ion battery (similar to the Panasonic NCR-18650 series) and a generic, low cost deep cycle lead-acid battery were considered. We choose to examine two distinct types of lithium-ion battery devices and the lead acid battery because these devices are predicted to be dominant in the distributed storage marketplace for at least the next five years [7]. While there are other emerging battery technologies that could be considered, we start with these since they are most relevant to the vast majority of the systems being implemented around the world today. The model then produces levelized costs of electricity for given combinations of battery type and size, fraction of energy allowed from the diesel generator, and discount rate. This model can be adapted in our future work to examine other emerging technologies. Further analysis examines what market conditions or policy incentives are required to induce a switch to hybrid generation systems over diesel-only systems. Although it is impossible to encapsulate all possible behavior of solar PV/battery storage hybrid systems, by using a consistent solar and load profile throughout our analysis, we are able to isolate the impacts on the batteries considered. In doing so, we highlight the general trends in the levelized cost of electricity that result from using different types of battery storage.

Table 3.1: Fixed System Parameters

Parameter	Values
Installed Solar PV capacity (kW)	7.5
Solar PV efficiency	15%
Diesel Generator capacity (kw)	2.5
Battery round-trip efficiency	90%
Storage retirement condition	80% of initial capacity

3.2 Methods

The model is composed of two parts: an operational model that dispatches power to find the minimum storage capacity required to meet specified operating parameters while minimizing diesel consumption, and an economic model of the costs associated with the system components and power mix that result from the operational model. A flowchart describing the process is provided in Figure 3.1. we use this process to compare the costs associated with 315 operating scenarios, with varying battery chemistries, state of charge swings, battery operational lifetime, and percentage of energy from renewable resources, and the costs associated for each system at varied discount rates. From this analysis, we could determine the scenarios for each battery chemistry that yield the lowest LCOE and compare amongst the three chemistries.

3.2.1 System Operational Model

The model combines a set of fixed components: a 7.5 kW solar PV array, a 2.5 kW diesel generator, and an off-grid micro-grid load profile with an average daily energy consumption of 20.5 kW h. Additional assumptions about these components are given in Table 3.1, and the average daily load and solar PV output profiles are plotted in Figure 3.1, with 95% confidence intervals. We selected the size of the PV array to provide enough power from solar resources to slightly exceed the average daily load, to meet both daily demand and provide surplus power to charge the batteries to provide power when solar was unavailable. Similarly, we size the diesel generator to meet full electricity demand in the event of insufficient insolation.

With these elements fixed, we then specify a number of operating conditions to apply to the battery storage. These conditions are the maximum allowable state of charge (SOC) swing, the maximum amount of electricity from the diesel generator (which dictates the amount of electricity from renewable sources), and the number of times the battery pack was replaced over the 20-year lifetime (dictating how long a pack was used). Table 3.2 shows a complete list of all of the operating

Table 3.2: Fixed System Parameters

Parameter	Values
Battery operational lifetime (years)	1, 2, 5, 10, 20
Maximum allowable SOC swing	30%, 40%, 50%, 60%, 70%, 80%, 90%
Maximum electricity from diesel generator	5%, 15%, 25%
Storage retirement	80% of initial capacity

parameters we consider and combine into 105 scenarios, which we repeat for each of the three battery chemistries. The selected values are a subset of all the possible number of replacements over the timeframe considered, and serve as bounding examples.

Under these operating conditions, we implement a battery chemistry and pack size, and optimize power flows to minimize diesel consumption over the entire specified lifetime. We iterate through different pack sizes until all of specified operating conditions are met, and the storage capacity remains above 80% of the initial capacity for the entire specified lifetime. This final storage capacity, and the power flows associated with it are used in the LCOE calculations.

Power flow optimization

The model assumes perfect information for both hourly solar availability and hourly load profile, thus providing a best-case scenario for energy storage utilization. Hourly temperature and solar data is combined with a load profile using documented electricity consumption for a rural community and HOMER Energy's load profile generation tool. These load and solar PV data are combined with battery storage and a diesel generator to deliver electricity to equal the demand for every hour in the time period considered. We iterate through different storage capacities to determine the minimum capacity required for the system to function for the specified number of years, t , and meet renewable energy targets, with the remaining electricity produced by the diesel generator when other sources were insufficient. Under these conditions, we minimize the costs associated with diesel generation, x_i^{GEN} , in all i time periods (Equation 3.1), so any additional storage capacity would be utilized in all time periods.

$$\min_x \sum_{i=1}^t x_i^{\text{GEN}} \quad (3.1)$$

The other constraint on the diesel generation is that the total electricity from the diesel generator ($\sum_{i=1}^t x_i^{\text{GEN}}$) could not exceed a certain percentage of the total electricity produced. The limits

are specified in Table 3.2.

We assume that the restrictions between the system components could be negligible, so the majority of the system constraints are on the battery storage component. The the model calculates energy stored in the batteries using data on the current level of energy stored in the previous hour, x_i^{BAT} , and the energy inputs, u_i^{CHARGE} , scaled with the round-trip efficiency, η , and the energy outputs, $u_i^{\text{DISCHARGE}}$ (Equation 3.2). We assume that because of the frequent battery cycling, self-discharge effects would be minimal; it commonly takes weeks or months for significant self-discharge to occur in these batteries. The model uses a load- following strategy, where only the solar PV panels can charge the batteries, to compute the power stored in the batteries at any given time. The specified maximum SOC swing, S , and the initial storage capacity determine the lower limit on the amount of energy stored. The values of S are specified in Table 3.2.

Stored energy is limited to the maximum storage capacity, C . Because batteries lose storage capacity as they are cycled, we recalculate this maximum storage capacity on a weekly basis over the course of the system operational lifetime, and use these calculations to update the constraints when computing the power flows for the following week (Equation 3.3). The formulae we use in these calculations are chemistry-specific and are outlined in Section 2.1.2. The model assumes that the batteries have to be operational (with capacity greater than or equal to 80% of their initial capacity) for the entire specified operating lifetime (1, 2, 5, 10, or 20 years) (Equation 3.4). If the system modeled violates these restrictions (Equations 3.3 and 3.4), or the initial restrictions specified (Table 3.2)., the storage capacity increases and the system recalculates the power flows until we find the minimum storage capacity to meet all of these requirements.

$$x_{i+1}^{\text{BAT}} = x_i^{\text{BAT}} + \eta u_i^{\text{CHARGE}} - u_i^{\text{DISCHARGE}} \quad (3.2)$$

$$(1 - S)C^{\text{INITIAL}} \leq x_i^{\text{BAT}} \leq C \quad (3.3)$$

$$0.8C^{\text{INITIAL}} \leq C \quad \forall i \in t \quad (3.4)$$

Battery degradation models

Different battery chemistries have vast disparities in response to different operating conditions, including temperature and depth of cycling. Generally, the deeper an electrochemical battery is cy-

Table 3.3: Battery chemistries and degradation models

Battery Chemistry	Sensitivity to SOC swing	Mathematical relationship between cycle life and SOC swing
Lead Acid	High	Power
High power-density Lithium-ion	Low	Linear
High energy-density Lithium-ion	Medium	Power

cled through its state of charge (SOC) window, the fewer total cycles possible over its lifetime. This effect is most profound in lead acid batteries, while some high-performing lithium-ion chemistries can endure thousands of cycles [44, 45]. These sensitivities are detailed in Table 3.3. The models we use attempt to capture these sensitivities, when sufficient data is available to differentiate the effects of temperature and SOC swing.

Lead acid battery

The degradation model for lead-acid batteries is based on the power-law relationship, characterized by increased degradation (fewer lifetime cycles) at higher SOC swings, with more cycles possible at lower SOC swings, as shown in Figure 3.2 [44]. As a result of this relationship, the total throughput over the battery's lifetime is higher if it is cycled shallowly for thousands of cycles, instead of deeply cycling the battery for a few hundred cycles. Equation 3.5 shows how we use this relationship to determine the capacity loss for lead acid batteries (C_{LA}^{LOSS}); using the average SOC swings between charge cycles over the weekly timeframe, S_{AVG}^{DAILY} and the number of cycles, Y .

$$C_{LA}^{LOSS} = \frac{(C^{INITIAL} - 0.8C^{INITIAL})}{(S_{AVG}^{DAILY}/12.838)^{-1.838}} Y \quad (3.5)$$

High power density lithium-ion battery

Data about the impact of both temperature and SOC swing on battery degradation are available for high power density lithium-ion batteries, which have a thin electrode system and a lower voltage LiFePO_4 cathode active material. For example, A123Systems provides battery data for the lifetime impacts for varied temperature and discharge conditions. Using the manufacturer specified data

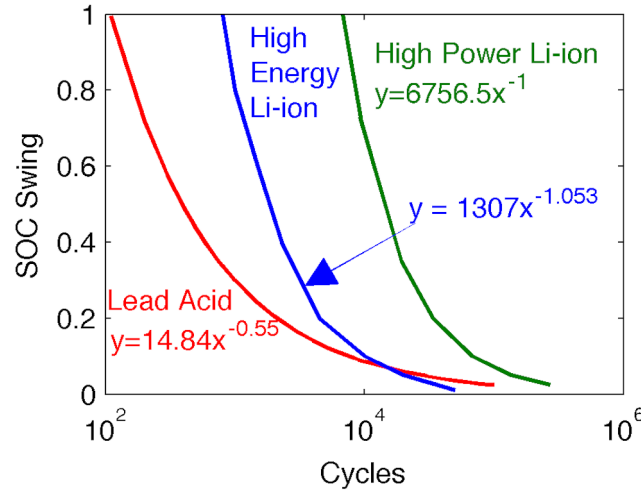


Figure 3.2: Relationships between the number of cycles and SOC swing for lead acid, high energy density Lithium ion, and high power density Lithium-ion batteries.

[46], along with the model operating temperature and the average percentage capacity lost per cycle at each of those temperatures, we calculate capacity losses (C_{HPL}^{LOSS}) using the formula in Equation 3.6:

$$C_{HPL}^{LOSS} = \left((5 \times 10^{-6}) T^{AVG} \right) Y C^{INITIAL} \quad (3.6)$$

where Y is the number of cycles and T^{AVG} is the average temperature over the time period for which capacity, C , is being recalculated. Charging and discharging limits are also based on manufacturer recommended levels, with charging voltage of 3.6 V and current of 3 A, and discharging voltage of 4.2 V at 5 A [46]. Previous testing by Peterson et al. [45] shows that manufacturer data are largely accurate, and that there is a linear, and relatively fixed, relationship between the SOC swing and the capacity processed by the cell. When plotted in terms of cycles available depending on the depth of battery cycling (Figure 3.2), the entire curvature is driven by the relationship between the depth of cycling and its relationship to a full charge cycle, and throughput is largely constant.

High energy density lithium-ion battery

Data about the performance of high-energy density lithium-ion batteries are very limited. Other models have previously identified the power law relationship that these lithium-ion batteries obey [44], although these models do not account for improvement in performance of these batteries

Table 3.4: System component cost assumptions

Component	Units	Cost (range)
Lead acid battery	\$/kWh	\$200 \$150 - \$250
High power density Lithium-ion battery	\$/kWh	\$680 \$530 - \$1000
High energy density Lithium-ion battery	\$/kWh	\$250 \$200 - \$300
Lithium-ion Pack costs	\$/kWh	\$40 \$35 - \$50
Diesel	\$/l	\$1.50
Generator Efficiency	l/kWh	0.3
Generator Capital Cost	\$	\$2,500
Solar PV Capital Cost	\$	\$24,000

over the past few years. Our cycle testing of high energy density batteries with a thick electrode layered metal oxide active cathode material (and a >4.1 V full state of charge) at different SOC swings shows that these batteries exhibit a power-law relationship between the number of cycles possible (until end of life) and the state of charge swing encountered on each cycle, similar to that of lead-acid batteries, and we use this data to scale the power law relationship to map to a current, if somewhat optimistic model of high energy density lithium-ion battery performance [44]. The results are plotted in Figure 3.2, which also shows that there is no appreciable difference in performance between lead acid and high-energy lithium ion batteries once the SOC swing drops below roughly 10%. Like the lead acid battery model (Equation 3.5), we use this relationship between SOC swing and the number of cycles to determine the weekly capacity loss (C_{HEL}^{LOSS}) using the relationship in Equation 3.7.

$$C_{HEL}^{LOSS} = \frac{(C^{INITIAL} - 0.8C^{INITIAL})}{(S_{AVG}^{DAILY}/1307.4)^{-0.95}} Y \quad (3.7)$$

The charging and discharging limits are based on manufacturer data (from Panasonic) specifying the maximum charging voltage as 4.2 V, and current of 1.925 A, and discharging voltage and current as 3.6 V and 2.75 A, respectively [47].

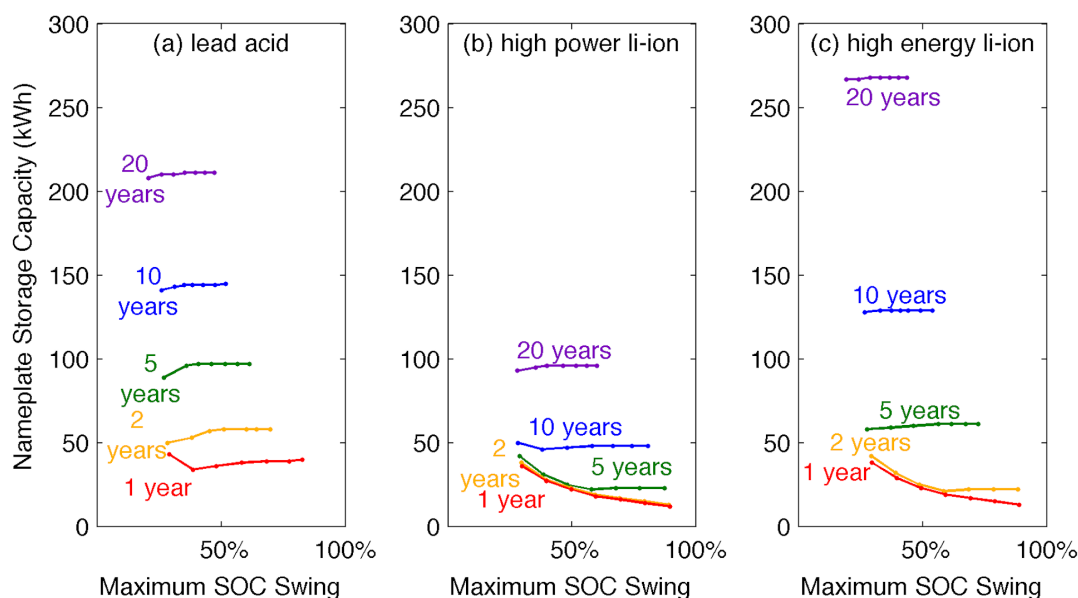


Figure 3.3: Nameplate storage capacity for different battery operational lifetimes as maximum state of charge swing varies with a 75% renewable requirement for a) lead-acid, b) high power density lithium-ion, and c) high energy density lithium-ion batteries.

3.2.2 Economic Model

Using the storage capacity determined by the power flow optimization for each set of operating conditions considered, we compute the LCOE of each complete system using a baseline discount rate of 5%, which is consistent with the discount rates used on capital-intensive projects. We also perform sensitivity analyses with discount rates ranging from 0% to 15%. Cost and efficiency assumptions for the system components are drawn from previous literature [48–50]. Many of these components are mature technologies, with easily sourced commercial prices. The main exception to this is the lithium-ion battery pack costs, which are a relative newcomer to the market. Battery pack cost assumptions (in \$/kW h) are sourced from both literature and direct communication with suppliers [10, 11, 46, 48, 51–54]. Their baseline values and ranges, and other system component costs are detailed in Table 3.4. Our assumptions have generally been confirmed, as additional information becomes available as new products (including the Tesla PowerWall, which has a pack cost of roughly \$55/kW h) become available [55].

3.3 Results

3.3.1 Battery operational lifetime

Using the power flow optimization outlined in 3.2.1 to dispatch power between the solar PV, diesel generator, and battery storage to meet the electricity demand, we determine the storage capacity required as the operating conditions specified in Table 3.2 are combined into 105 scenarios for each battery chemistry. Throughout our optimization, we implement the battery degradation models (Equations 3.5 - 3.7) for each chemistry to more accurately depict reductions in storage capacity. We find that the storage capacity required to meet or exceed the minimum specified operating requirements is highly dependent on the maximum allowable SOC swing and the number of years the batteries were used before replacement. This is shown in the storage capacities required for a subset of the scenarios where the maximum percentage of electricity from diesel is limited to 25%, with 75% or more from renewable sources, which is presented in Figure 3.3 for all 3 chemistries. With the fixed diesel generator contribution, both the maximum SOC swing and battery lifetime vary through the values specified in Table 3.2, and these 35 combinations are presented.

In the scenarios with short operational lifetimes, the storage capacity required drops as the maximum SOC swing increases (as shown for the lithium-ion and batteries operating for 1- and 2-years in Figure 3.3b and c), because more power is drawn from each battery. As the batteries are used over a longer time period, the batteries degrade to the point that they are unable to deliver the required number of cycles, especially at high SOC swings. To ensure the pack is functional for the designated lifetime, the storage capacity increases (as shown in the 2-year scenario for lead acid batteries Figure 3.3a).

While the storage capacity is increasing to ensure the batteries are functional for the designated time frame, the daily load profile is relatively consistent. This means that the average SOC swing on any given day falls, because the same amount of electricity is drawn from a larger battery pack. However, for the cases when storage capacity is just starting to increase to compensate for degradation, cumulative cycling may still result in a maximum SOC swing very close to the specified maximum. This is shown in Figure 3.4, which plots the average daily SOC swing with a 95% confidence interval, and compares it to the maximum SOC swing experienced by the high energy density lithium-ion batteries, with at least 75% of electricity from renewable sources. The storage capacity for these scenarios is plotted in Figure 3.3c. Points on the black line represent when

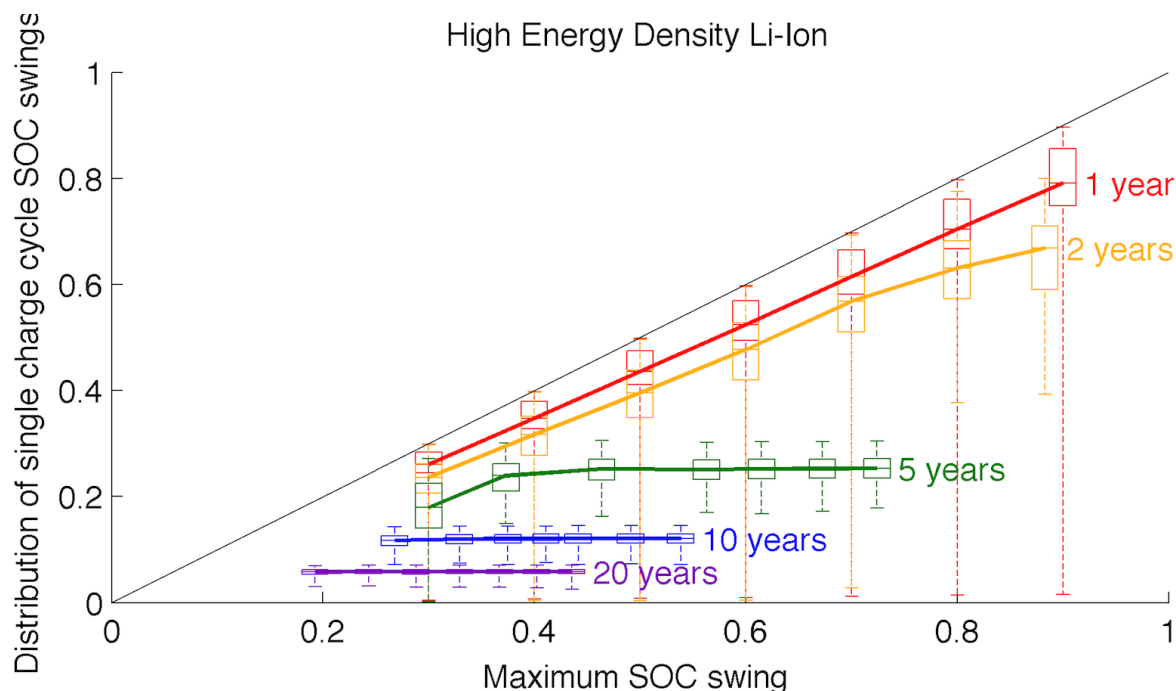


Figure 3.4: Median daily SOC swing (with 95% confidence interval) compared to the maximum cumulative SOC swing for high energy density lithium-ion batteries.

daily SOC cycles are equal to the maximum specified limit on the SOC swing. The line for the 2-year replacements shows how the storage capacity increases result in decreases in the daily SOC swing, but still have a high cumulative cycle. For the batteries operated for longer (5-, 10-, or 20-year) timeframes, while the daily SOC swing is generally fairly consistent, the more relaxed SOC swing constraints allow the maximum SOC swing (which is plotted on the x-axis in Figures 3.3 and 3.4), to vary in the rare events where the packs can cycle to lower depths over the span of several days, when solar resources are unavailable (full recharge of the battery at these capacities is not possible for the given solar resources). Such cycling is not possible when the maximum SOC swing is constrained to a lower value, and these systems rely on more diesel generation to compensate.

3.3.2 Levelized cost of electricity

Nameplate storage capacity has a direct impact on the levelized cost of electricity. We see this when we compare the storage capacities (plotted in Fig. 3) with the LCOE plotted in Figure 3.5 for the scenarios with a minimum of 75% renewable energy for all 3 battery chemistries. The uncertainty bounds in Fig. 5 reflect the uncertainty in battery prices and the values plotted use the

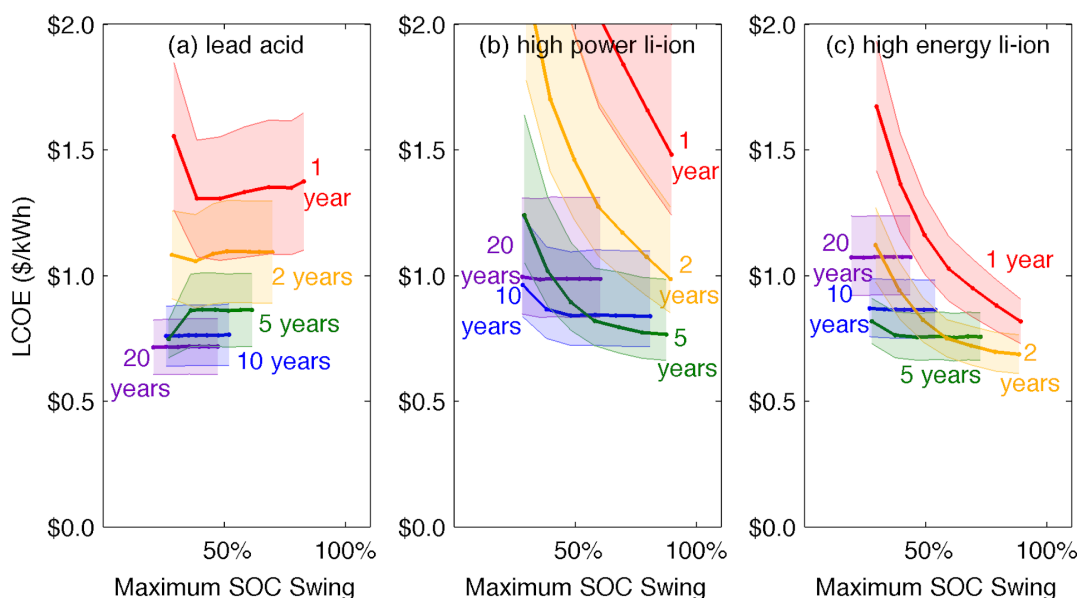


Figure 3.5: LCOE for different battery operational lifetimes with a 75% renewable requirement and 5% discount rate as maximum state of charge swing varies for (a) lead-acid, (b) high power density lithium-ion, and (c) high energy density lithium-ion.

base-line 5% discount rate. For the lead acid batteries, we find that very long operational lifetimes with high storage capacity cycled very shallowly over the system lifetime were less expensive than more frequent replacements. It should be noted that because of their volume, large battery packs could be subject to higher infrastructure costs, which are not included in the scope of this analysis.

Using the LCOE for each of the different chemistries and replacement schemes considered (and plotted in Figure 3.5), the number of battery sets over the 20-year time frame associated with the lowest LCOE is selected, as maximum SOC swing varied, and the LCOE and number of replacements are plotted in Figure 3.6c. For low maximum SOC swing, fewer replacements are favored. As SOC swing increased, more frequent battery replacements are required for lead acid batteries to attain the deep cycling, and frequent replacements with higher maximum SOC swings delivered lower cost electricity for both lithium-ion batteries. For both lithium-ion batteries, the least expensive scenarios occur while the batteries are able to cycle deeply for the entire specified lifetime, but operate for short enough timeframes that the sensitivity to SOC swing had not yet degraded the storage capacity to the point that additional storage was necessary. This results in less installed total battery capacity over the 20-year lifetime, and allows for further discounting of capital costs.

Comparing the lowest-cost LCOE profiles for each chemistry (plotted in Figure 3.7a), the

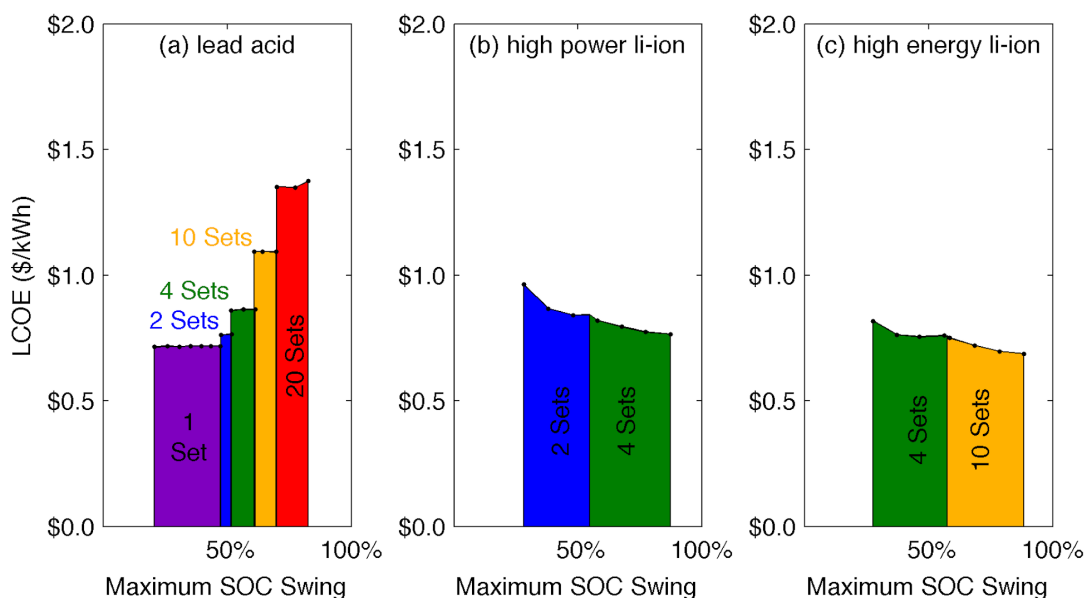


Figure 3.6: Optimal number of battery sets over 20 year lifetime with 5% discount rate as maximum SOC swing varies for a) lead-acid, b) high power lithium ion, and c) high energy lithium ion batteries.

lowest-cost storage option at a 5% discount rate is the high energy density lithium ion batteries cycled through a maximum of 88% SOC and replaced every 2 years, for a LCOE of \$0.69/kWh (see Figure 3.6). This is still higher than a diesel-only generation system, which has an LCOE of \$0.48/kWh at assumed capital and fuel prices. This was slightly lower than the cost of a lead acid hybrid system (\$0.71/kWh), with the high power density batteries offering the highest cost of electricity (\$0.77/kWh).

3.3.3 Sensitivity to discount rate

Changes to the discount rate play a significant role in determining which of the hybrid systems produced the lowest cost of electricity. We apply the discount rate to both the system costs and the output electricity when calculating the LCOE. For the lead acid batteries, which delivered lower cost electricity when a large battery pack is cycled shallowly for a long time period, lower discount rates meant that the return (total electricity produced in future time periods) is more highly valued, reducing the lowest LCOE for these systems. For both lithium-ion battery systems, reducing the discount rate means that future replacement expenses are higher, so while future electricity returns are more highly valued (lowering the LCOE), they are tempered by increased capital expenses. For the high-energy density lithium ion batteries, this is sufficient to make lead

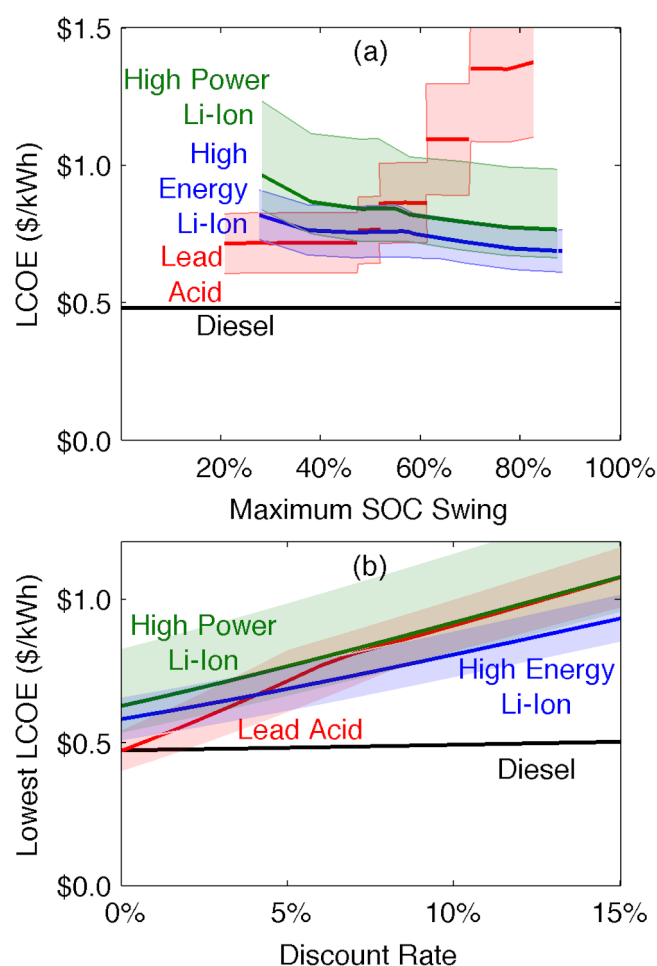


Figure 3.7: (a) Lowest LCOE envelope for each battery chemistry as maximum SOC swing varies with 75% renewable requirement at 5% discount rate and with a comparison to diesel-only generation and (b) how the Lowest LCOE for each chemistry varies with discount rate

acid hybrid systems more cost effective at low discount rates (less than 4%) as shown in Figure 3.7b. At higher discount rates, more frequent battery replacements are favored, even increasing the optimal number of replacements for the lead acid batteries. The high power density lithium-ion batteries are never the least expensive option under any of the discount rates considered. For the diesel-only system, capital costs are low, while the larger operating costs occur during the same time period as the electricity is generated. As a result, the LCOE is relatively insensitive to changes in the discount rate.

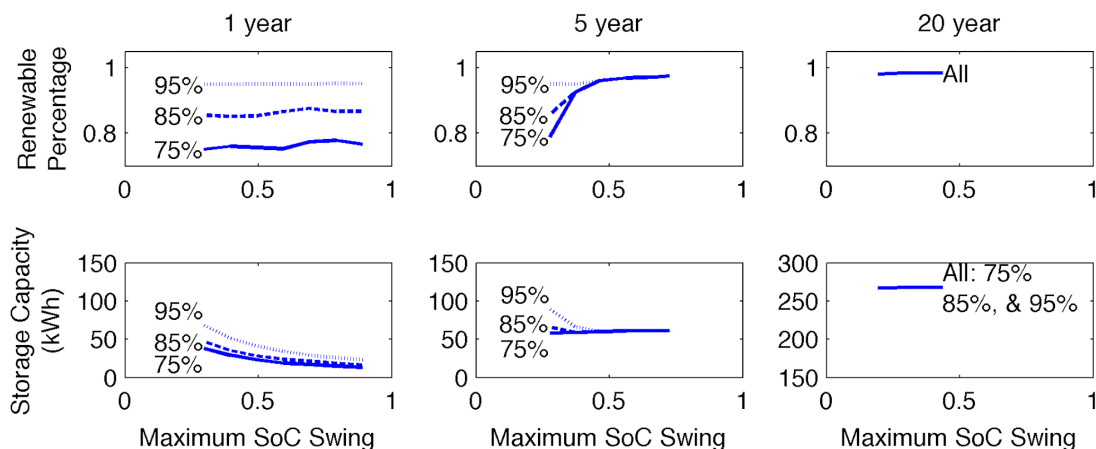


Figure 3.8: Required storage capacity and corresponding percentage of energy from renewable sources as the renewable target and operational lifetime of the high energy density lithium-ion batteries vary (1, 5, and 20 years)

3.3.4 Renewable energy requirement

Given that a common objective of hybrid systems is to reduce fossil fuel electricity generation, we examine three different limits on the maximum electricity from diesel generation: 5%, 15%, and 25% (specified in Table 3.1), with the remaining balance of the electricity coming from renewable sources. The results presented in Figures 3.3-3.6 are for a subset of these scenarios where the diesel contribution was limited to 25%, with the 75% or more of the total electricity coming from renewable sources. The impact of the renewable energy requirement varies depending on how deeply the batteries are cycled and how long they are operated for. For short operational lifetimes, where the batteries cycle through their maximum SOC swing on an almost daily basis, additional storage is required at an increasing rate to deliver larger percentages of renewable electricity. For longer operational lifetimes, the storage capacity is so large that daily battery cycling was lower than the maximum SOC swing allowed. The large capacity enables the system to exceed the specified renewable target, so no additional storage capacity is required to meet higher renewable targets. As the storage capacity continues to increase for longer battery operating lifetimes, the storage requirement begins to converge to one value that met all three of the specified renewable energy targets, as shown in Figure 3.8. For many of the lowest-cost replacement scenarios, the storage capacity was sufficiently large to exceed the specified renewable target, so the lowest LCOE for each battery chemistry is relatively insensitive to changes in the renewable requirement, with a maximum increase of \$0.04/kW h.

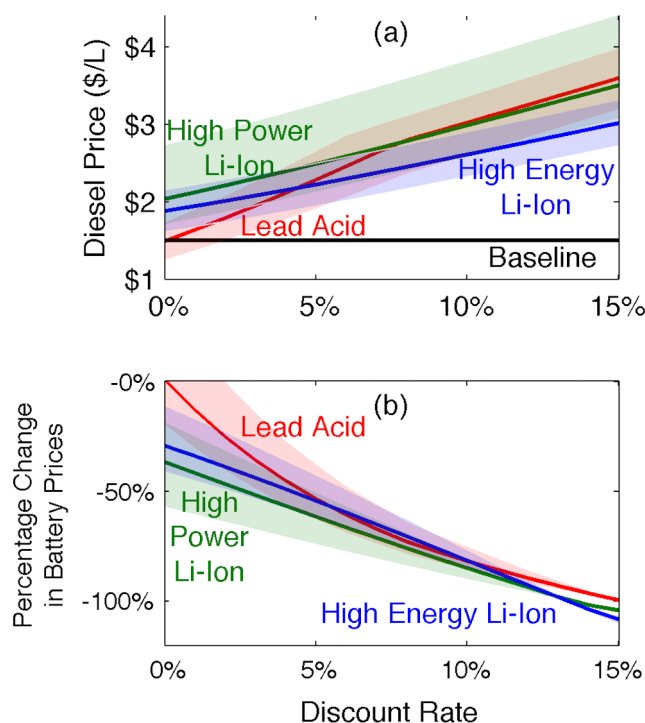


Figure 3.9: (a) Diesel prices required to switch to hybrid system depending on discount rate and assumed storage prices for each battery chemistry and (b) Battery price changes required to switch to a hybrid system as discount rate varies

3.4 Discussion

Because diesel-only generation is still less expensive than all of the off-grid hybrid micro-grid options considered, we examine the market changes necessary to induce a switch from diesel-only generation to a hybrid system, assuming no change in battery performance. Improvement in battery cycle life, or slight variations in chemistry or cost across manufacturers could alter the magnitude of the changes necessary to induce a switch to a hybrid system. However, the sensitivity analyses included for each intervention capture these variations, and show the same trends. The first market changes we examine are the changes in fuel and battery storage technology prices that would trigger a switch to hybrid generation. The other two forces are more policy-focused: feed-in tariffs on hybrid generation, and carbon emissions taxes. Finally, we comment on the efficacy and structure of some existing incentives policies for distributed generation and storage.

3.4.1 Price changes

Switchover analyses are conducted to determine (1) how much fuel prices need to increase to achieve parity with the three storage options considered and (2) what battery price changes are necessary to reach cost parity with the diesel-only generation system. The diesel prices required to trigger a switch to each of the three battery chemistries, and their associated uncertainties are plotted in Figure 3.9a, but to switch from diesel-only generation to the lowest-cost storage system at a 5% discount rate, diesel prices need to increase by almost 50% to \$2.20/l. These price increases could result from changes in market supply, higher taxes on fuel (as is common in Western Europe, where fuel prices have historically exceeded this amount) or from increased transportation costs to remote areas, which can cost an additional \$0.2/l for every 100 km of travel distance [56, 57]. Like the LCOE of the different systems, the required change in diesel prices is lowest at low discount rates, and increases as the discount rate increases. Similar percentage changes on battery prices are required to reach LCOE parity with diesel-only generation, as shown in Figure 3.9b. At the baseline 5% discount rate, lead acid and high energy density battery prices need to drop by 54% to \$93 and \$114/kW h, respectively, while high power density lithium-ion battery prices need to be reduced to \$261/kW h (a 62% reduction).

3.4.2 Feed-in tariffs

Feed-in tariffs are a common method for encouraging renewable electricity generation, and have been implemented by many developed and developing countries [41]. Tariff rates necessary to switch from diesel generation to a hybrid system at different discount rates are plotted in Figure 3.10a. At an assumed discount rate of 5% with the baseline price estimate of \$250/kW h of high energy density lithium ion batteries, the subsidy would have to be \$0.20/kW h to reach parity with diesel-only generation. This rate is on the higher end of the existing feed-in tariff rates in the US for systems of this scale. The full range of values available in the US is plotted in Figure 3.10a, with the lowest rate offered by the Tennessee Valley Authority (TVA) and the highest, offered by Madison Gas and Electric (WI). These rates are comparable to many feed-in tariffs offered in EU countries, and some developing countries, but are much higher than the subsidized feed-in tariffs proposed as part of a globally managed Green Climate Fund, which are less than \$0.06/kW h [58–60]. Even larger subsidies would be required to be competitive with lower-cost grid electricity [61, 62]. Determining a tariff to reach grid electricity parity is highly dependent on local electricity prices

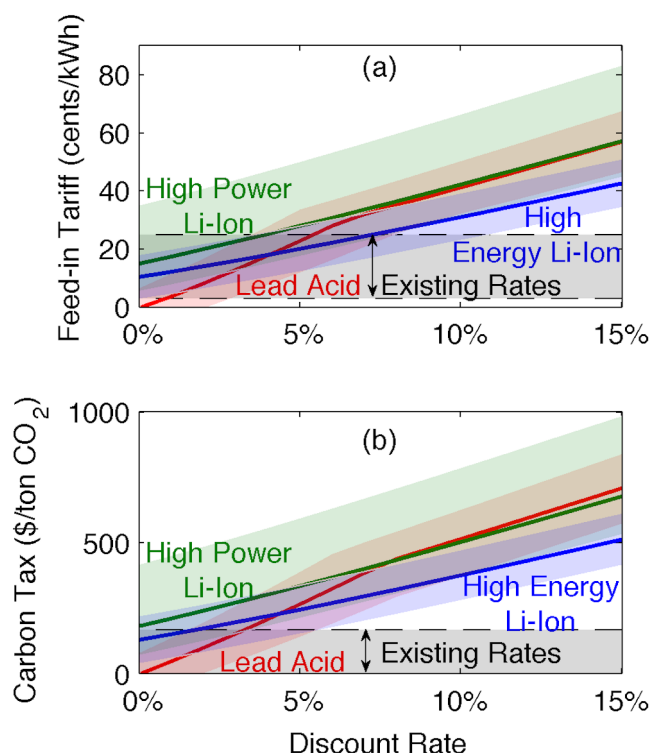


Figure 3.10: Incentives policies to induce switch to a hybrid system with variation in discount rate. Feed in tariffs (a) required to reach LCOE parity between lowest-cost systems and diesel-only generation, with comparison to the highest and lowest US electricity provider Feed-In Tariff rates and (b) Carbon taxes required to switch to a hybrid system, with comparison to existing global tax rates.

and is outside of the scope of this study.

3.4.3 Carbon tax

Assuming that carbon taxes would only be applied to fossil fuel resources, they would need to be fairly substantial to increase the LCOE of diesel-only generation to reach parity with the lowest-cost hybrid system. At the assumed price of \$250/kW h for high energy density lithium-ion batteries and 5% discount rate, the required carbon tax is \$245/ton of CO₂. At lower discount rates, no tax would be necessary, with taxes increasing as the discount rate increases (see Figure 3.10b). These carbon tax values are higher than existing carbon taxes, which are generally on the order of \$10-\$30/ton CO₂e, and exceed the Swedish carbon tax - the highest in the world - of \$168/ton [63].

3.4.4 Other policy recommendations

As shown in Figure 3.5, many of the lowest-cost hybrid generation options utilize more frequent battery replacements. However, many incentives programs, including California's Self-generation incentive program, require all subsidized technologies to have a ten-year warranty [27]. These frequent replacements (1) generally require fewer batteries overall to meet the same demand and (2) allow consumers to spread the capital costs of these systems over several years. Considering the 20-year timeframe we use in this model, the California program would choose to subsidize 2 high- energy density lithium ion battery packs, each used for 10 years, with a total lifetime storage capacity of 258 kW h over a system with 10 battery packs, each used for 2 years, with a total lifetime storage capacity of 220 kW h. Discounting the replacement costs at 5%, the system with 10 packs is \$17,000 less expensive than the system with 2 battery packs. Assuming the costs of 8 additional replacements is less than this amount, more frequent replacement is more cost effective.

3.5 Conclusions

A time-step battery degradation model was implemented for three types of batteries. The model combined multiple operating variables to determine the energy storage required to meet specified performance targets. It is important to note that this model did not use a smart battery management or predictive controller. Such a controller could be used to restrict battery charging and discharging when not needed, which would allow the system to utilize less storage during some time periods, reducing the overall battery degradation over time.

Using the combinations of storage capacity and diesel utilization from the model, we determined the lowest levelized costs of electricity for each type of battery. These costs were then compared with each other and diesel-only generation.

- At assumed prices and discount rates of 1% or higher, diesel- only generation is the most cost-effective option.
- For low (<4%) discount rates, lead acid batteries are the lowest cost hybrid option. At higher discount rates, high energy density lithium ion batteries are have the lowest LCOE.

- The optimal number of battery sets over the 20-year system lifetime varies substantially, with only one, very large pack favored for lead-acid batteries, and smaller packs replaced more frequently for both lithium-ion batteries.
- High power density lithium-ion batteries have the highest LCOE for all discount rates considered.
- Discount rate is significant in calculating the LCOE, determining which storage technologies in hybrid systems are competitive, and how large price changes (on diesel or batteries) or policy incentives (feed-in tariffs or carbon taxes) need to be to induce a switch to a hybrid system.

Chapter 4

Prospects for reducing battery manufacturing emissions from direct material recovery

4.1 Introduction

Electric vehicles are quickly becoming one of the largest markets for lithium-ion batteries, with approximately 16 GWh of storage capacity and 80,000 tons of cathode material on the roads today in the US alone. As they have become more prevalent, a number of jurisdictions have imposed regulations requiring their safe disposal. The European Union requires that 45% of all rechargeable batteries be collected and that half of those batteries must be recycled, [64] while many US states have similar requirements. [65, 66] These regulations will become increasingly important as the non-lead-acid automotive battery market continues to grow. Although the lithium-ion battery market for EVs is currently larger than the market for grid-scale projects, electric vehicles still account for a very small portion of US vehicles ($\sim 0.25\%$). If even 1% of US vehicles were plug-in hybrid vehicles, with an average capacity of 11kWh, that would nearly double the current battery capacity on the road to approximately 29 GWh, requiring roughly 145,000 metric tons of cathode material per year. If manufacturers like Tesla and GM were to meet their 2020 production targets, annual production capacity would be on the order of at least 40 GWh/year, or 200,000 tons of cathode material annually. [67, 68]

Today there are relatively few facilities that can process used lithium-ion batteries, and the

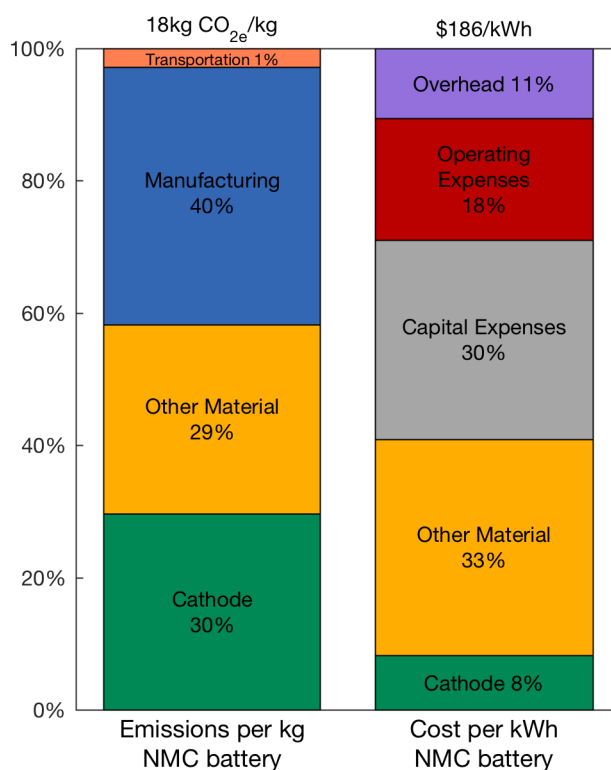


Figure 4.1: Cathode materials are a substantial contributor to overall costs and CO_{2e} emissions for manufacturing NMC cylindrical cells.

methods they employ are limited, typically relying on a pyrometallurgical process where materials are either downcycled into inputs for cement making or undergo significant processing for to be useful in other applications. Most efforts to improve recycling processes have focused on recovering specific valuable metals, especially cobalt. [69–75] More recently, direct physical processes, [76] which recover battery materials as a mixture, rather than as individual metals have been developed. These processes take advantage of the limited battery chemistries and pack formats of electric vehicles to target the known cathode materials. This focus on cathode materials is a logical choice since they are the second largest contributor to cell material costs (after cell packaging materials) and account for nearly one third of the emissions associated with battery manufacturing, as shown in Figure 4.1. Dunn et al conducted an early analysis of the life cycle carbon emissions associated with employing a direct recycling process on lithium manganese oxide (LMO) cathode materials. [77]

Here, we compare the environmental impacts and economic costs of battery manufacturing and recycling using both pyrometallurgical and direct cathode recycling methods for the two most common chemistries in US electric vehicles: lithium nickel manganese cobalt oxide (NMC) and

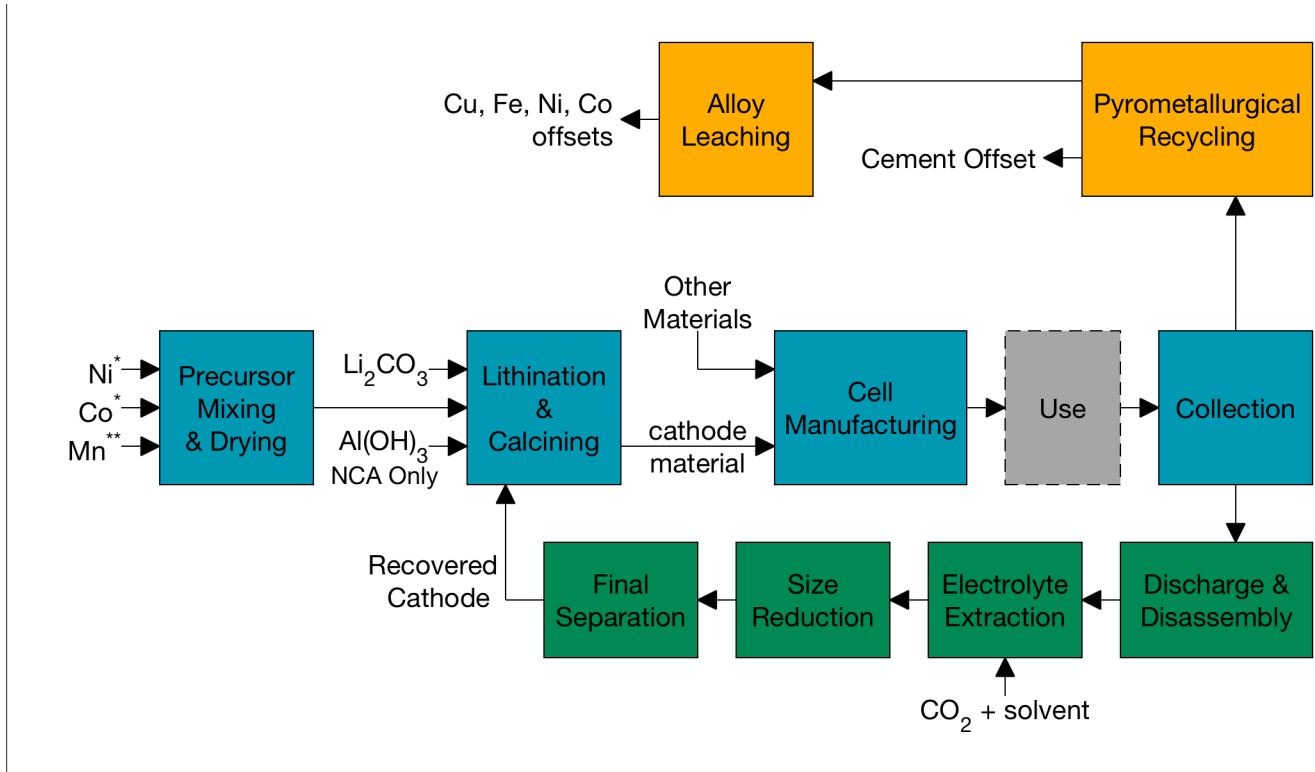


Figure 4.2: Manufacturing (in blue), pyrometallurgical (in yellow), and direct cathode recycling (green) pathways for NCA and NMC cells. Ni, Co, and Mn inputs can be sourced from either sulfates or nitrates. Mn is only an input for NMC cells, Al(OH)_3 is only for NCA cells. We do not consider the emissions for cell use.

lithium nickel cobalt aluminum oxide (NCA). We also focus on cylindrical cells, which make up roughly half of the storage in EVs. [2] To make this comparison, we use an attributional life cycle analysis to determine the greenhouse gas emissions and input energy resources that result from mining raw materials, shipping, manufacturing, and recycling processes. We consider three different electricity grid assumptions to illustrate the impact of grid emissions on manufacturing and recycling: the US average, a low emitting grid (NWPP NERC subregion), and a higher-emitting grid (RFCM NERC subregion). Using a process-based cost model, we determine the cost of manufacturing cathode materials from raw inputs and use this to find a breakeven recovery cost for direct cathode recycling to be competitive with other sources. Finally, we comment on other waste streams produced by these processes, and how pyrometallurgical and direct cathode recycling align with recycling regulations.

4.2 Methods

We use a Monte Carlo simulation to conduct an attributional life cycle assessment of the materials, manufacturing, and recycling of lithium-ion batteries. We focus our analysis just on the greenhouse gas emissions and energy consumption of these steps, and do not include the emissions or energy associated with their use in electric vehicles. Figure 4.2 outlines the manufacturing, pyrometallurgical, and direct cathode recycling processes modeled.

The cell bill of materials for each simulation was constructed based on literature estimates of cell contents for two cell dimensions: 18650 (18 mm diameter, 65 mm tall) and 20720 (20mm diameter, 72 mm tall). [13] Additional information about the cell material inputs and dimensions is provided in Tables C.1 and C.2. We considered two types of inputs to produce the cathode precursors: nitrate and sulfates. Tables C.1 - C.6 detail the required inputs for both pathways. [78] These precursors are then combined with lithium carbonate and calcined to produce the final cathode material (details included in Tables C.7 and C.8).

The pyrometallurgical process, outlined in an Umicore patent, [1] involves firing the battery materials with slag, limestone, sand, and coke to produce a metal alloy, which can be separated into its constituent materials, and a slag that can be repurposed to make cement. The direct cathode recycling process involves discharging and disassembling the batteries, extracting the electrolyte using liquid or supercritical CO_2 , [79–82] then reducing the size of the recovered components and separating out the cathode materials. [76, 79, 83]

For each process considered, we present the resulting emissions in carbon dioxide equivalent using 20 year warming potentials and energy consumption in MJ. [84, 85] We also use two different functional units: kg of battery manufactured (including cell electrode materials, separators, and packaging) and kWh of battery manufactured (including all cell components).

4.2.1 LCA Assumptions

The energy inputs and carbon emissions for the cell material inputs are modeled in GREET 2016, [86] often including a range of assumptions depending on the recycled content of the source materials. Tables C.10 and C.11 list the specific assumptions and distributions used to model these contributions to the overall greenhouse gas emissions and energy resources for cell manufacturing.

For the energy consumed at the battery manufacturing and recycling facilities, we assess the damages from natural gas consumption using GREET 2016 assumptions for a kiln using north American shale gas. For grid electricity emissions, we use EPA eGRID 2014 data. [84] Specifically, we consider the emissions associated with using a US average grid, the NWPP subregion grid, and RFCM subregion region grid. These subregions were selected based on known EV manufacturing locations, and the emissions assumptions are summarized in Table C.9. We use average emissions assumptions because the processes modeled operate continuously.

Transportation Assumptions

We also use the location assumptions to create rough estimates of the distances to ship both raw materials and to collect the used cells for recycling. Estimates for the distances traveled were calculated using information about both where materials are produced and tools that calculate distances between major ports. For steel and graphite, we assumed that the materials would be shipped from Shanghai to Long Beach (for NWPP) or Newark (RFCM), [87] and then would be shipped via rail for 600 miles each (approximately the distance between Newark and Detroit and Long Beach and Reno). Most of the bauxite used in the US is imported from Jamaica (GREET 2016), [86] so we calculated the distance from Kingston to Newark, and then the shipping distance by rail). Aluminum, copper, nickel, cobalt, and manganese are all produced in North America, and the USGS has maps with locations of these production facilities. [4, 88] Distances between these facilities and approximate locations were calculated and attributed to rail shipping. For the other input chemicals, production is not tied to a specific location, and we assumed 500 miles rail. For all the inputs, we assumed 50 miles of road transport to reach the final destination. The distances assumed for different modes of transportation (water, rail, road) [87, 88] and damages per ton mile are listed in Table C.12 and C.13. We also conduct a sensitivity analysis on these estimates to determine the impact of shipping on overall emissions and energy consumption.

Recycling Process Emissions, Energy Consumption, and Offsets

The pyrometallurgical process is based on the process detailed in US Patent 7,169,206 B2, [1] where batteries are mixed with other input materials (listed in C.14 and heated to produce a metal alloy and slag material. Process and heat inputs (listed in Table C.15) are fixed regardless of the

specific cell chemistry or format. Estimates of the energy consumed for the leaching processes to separate the metal slag are drawn from Dunn et al. [83]

The direct cathode recycling process consists of four main steps: discharge and disassembly, electrolyte extraction, size reduction, and final separation. The electricity consumption assumption for the discharge and disassembly step of 0.034 mmBtu/ton of battery comes from the Dunn et al [83] assumption for the total electricity required during the formation cycle of battery cells. The primary driver of electricity consumption for the electrolyte extraction step is the energy used to compress the CO₂ used as a solvent. Recent research [79–82] has focused on the optimal combination of CO₂, duration of the extraction process, and additional solvents, but we use the assumptions from Grutzke et al. [79] They use liquid CO₂ to fill a 100ml chamber, along with an ACN/PC mixture. We use a triangle distribution to estimate the number of times the chamber is filled (peak of 2, bounds of 1 and 4), and then scale this by the cell volume treated. To estimate the energy consumed to produce the liquid CO₂ we also use a triangle distribution, with a peak of 0.0981 kWh/kg, [79] and bounds of 0.0719 kWh/kg (from Zahid et al) [82] and 0.1609 kWh/kg (from Dunn et al). [83] For both the size reduction and final separation steps, we use the estimates provided by Dunn et al, [83] but with triangular distributions to represent the uncertainty to the functional unit. We use a triangular distribution to divide the 0.22 mmBtu for the size reduction step, and divide it by the total cell mass, the cell mass that is present at that step, and the mass of cathode material. We use the same functional units to divide the 0.02mmBtu assumed for the final separation step.

To determine the environmental benefits of recycling, we calculate the greenhouse gas emissions offset by the final products. For pyrometallurgical recycling, this includes copper, iron, nickel, cobalt, and cement slag. The total amount of each material present in the smelted material is calculated based on cell inputs and the amount of each metal recovered is calculated based on the yield rates from the process patent, listed in C.15. For the direct cathode recycling process the emissions and energy offsets include the sum of the embodied energy and emissions of the cathode precursor materials, the transportation of these materials, and the energy consumed during the cathode precursor drying step. The offsets are then scaled based on the yield rate of the cathode recovery process.

4.2.2 Cost Model

We use a process-based cost model to estimate the cost to produce cathode materials from raw inputs. This modeling technique originated in the electronics industry, where it was used to inform design decisions by estimating manufacturing costs. [14] The method has since been adopted for product design more broadly, [3, 15] and has been used to examine battery manufacturing costs. [2, 10]

Process-based cost models disaggregate the many factors that come together during a manufacturing process into discrete units that increase with production volumes. Labor, capital equipment, and input materials are allocated for each step in the manufacturing process, with the possibility of sharing resources between steps where appropriate. Production volumes at each step are adjusted based on yield rates of the downstream processes. This type of bottom-up modeling makes it possible to make more granular comparisons between process technologies, to determine the production volumes required to reach economies of scale, and to identify the inputs and processes that contribute the most to product cost. These characteristics mean that process based cost modeling can provide more substantive reasons for why technology costs are falling, and because process models can be adapted for technologies that do not currently exist, it offers a distinct advantage over models that examine overall learning rates or price curves, which rely on historical sales or price data to make predictions. [89]

We leverage knowledge from this previous work examining battery manufacturing costs to focus on the manufacturing costs of the cathodes from raw materials, and contrast this with the costs associated with the cathode materials from a direct cathode recycling process. The reprocessing of the cathode materials from the direct cathode recycling process is essentially the same as the lithiation step of cathode manufacturing, so we can isolate the breakeven cost of recovering the cathode material. Assumptions about equipment, labor, material, and energy costs are detailed in Tables C.16 - C.18.

4.3 Results

4.3.1 Cell Manufacturing Emissions

As Figure 4.3 shows, greenhouse gas emissions associated with cell input materials are a substantial contributor to the overall emissions from the manufacturing process. These emissions

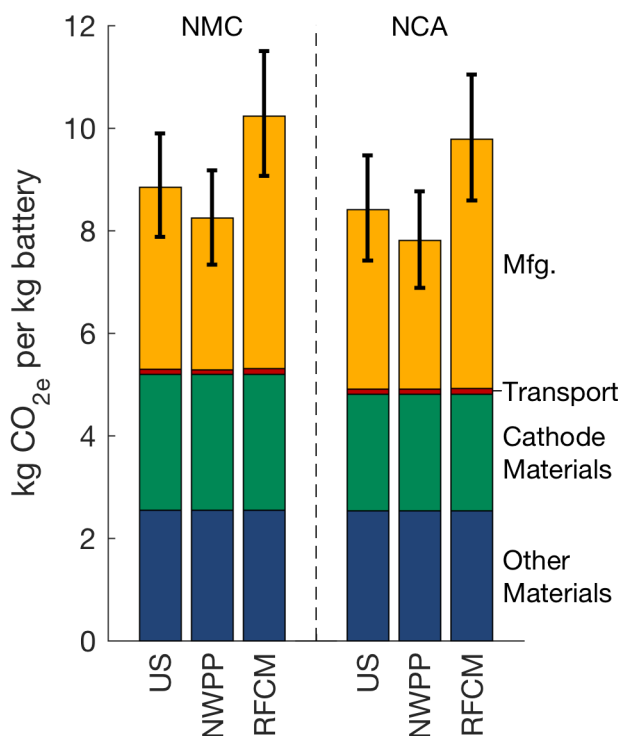


Figure 4.3: kg CO_{2e} per kg of cell emitted during the manufacturing of NMC and NCA cylindrical batteries using US average, NWPP, and RFCM average grid emissions data. Manufacturing includes processing of cathode material preparation

play a larger role for facilities that utilize lower-emitting electricity grids. For NMC cells, if the facility is located in the RFCM subregion, which is higher emitting than the US average, materials account for 50% of total emissions per kg of battery, while they account for 60% of the total if the facility is in the NWPP subregion, which is lower emitting. Figure 4.3 also shows that our baseline transportation assumptions have a minimal impact on the emissions per kg of battery produced. Although there is a difference in the median CO_{2e} emissions depending on the grid assumptions, there is sufficient uncertainty in emissions from the input materials that there isn't a statistically significant difference in the total CO_{2e} emissions between any of the grid locations. Similar plots listing the uncertainty in greenhouse gas emissions and the input energy required per kg of battery, as well as the greenhouse gas and energy inputs per kWh of battery are provided in supplementary Figures C.1 - C.4. As the data provided in Table 4.1 show, our estimates of the greenhouse gas emissions and energy consumption per kg of battery are largely in line with other analyses of the battery manufacturing process. Table C.19 provides the same information on a per kWh basis.

Table 4.1: Comparison of greenhouse gas emissions and energy inputs to cell manufacturing between this and other studies

Reference	Cathode Chemistry	Specific Energy [kWh/kg]	Greenhouse gas emissions [kg CO _{2e}] & input energy [MJ] per kg battery		
			Materials	Manufacturing	Total
Notter et al (2010) [90]	LMO	0.114	5 kg <i>86 MJ</i>	0.98 kg <i>18 MJ</i>	6 kg <i>100 MJ</i>
Zackrisson et al (2010) [91]	LFP	0.10	7.7 kg -	9.5 kg -	17 kg -
Majeau-Bettez et al (2011) [17]	NCM	0.112	16 kg <i>130 MJ</i>	6 kg <i>80 MJ</i>	22 kg <i>210 MJ</i>
	LFP	0.088	16 kg <i>130 MJ</i>	6.1 kg <i>80 MJ</i>	22 kg <i>210 MJ</i>
Dunn et al (2012) [77]	LMO	0.13	4.8 kg <i>72 MJ</i>	0.27 kg <i>2.7 MJ</i>	5.1 kg <i>75 MJ</i>
EPA (2013) [92]	Average	0.15	11 kg <i>160 MJ</i>	0.09 kg <i>1.4 MJ</i>	11 kg <i>160 MJ</i>
EPA (2013) <i>cells only</i> [92]	Average	0.09	7.2 kg <i>110 MJ</i>	3 kg <i>55 MJ</i>	10 kg <i>160 MJ</i>
Ellingsen et al (2014) [93]	NCM	0.11	6.8 kg -	11 kg -	18 kg -
Ellingsen et al (2014) <i>cells only</i> [93]	NCM	0.17	9.2 kg -	19 kg -	28 kg -
Kim et al (2016) [94]	LMO/NCM	0.08	6.1 kg -	5.2 kg -	11 kg -
Kim et al (2016) <i>cells only</i> [94]	LMO/NCM	0.14	4 kg -	9.1 kg -	13 kg -
<i>This study</i> (US average power mix, 95% confidence intervals)	NMC	0.21	5.2 kg (4.5 - 6.0 kg) <i>69 MJ</i>	3.6 kg (3.0 - 4.2 kg) <i>49 MJ</i>	8.9 kg (7.9-9.9 kg) <i>120 MJ</i>
			<i>61 - 76 MJ</i>	<i>41 - 57 MJ</i>	<i>108 - 130 MJ</i>
			4.8 kg (4.0 - 5.6 kg) <i>64 MJ</i>	3.5 kg (2.9 - 4.1 kg) <i>48 MJ</i>	8.4 kg (7.4 - 9.5 kg) <i>114 MJ</i>
	NCA	0.19	<i>(55 - 73 MJ)</i>	<i>(40 - 56 MJ)</i>	<i>(101 - 126 MJ)</i>

4.3.2 Cell Recycling Emissions

Figure 4.4a shows the CO_{2e} emissions associated with each kg of battery manufactured and recycled using both pyrometallurgical and direct cathode recycling methods and an average US power grid. Figure 4.4b shows the median and 95% confidence intervals for the greenhouse gas emissions avoided by using both recycling processes. For both chemistries, a direct cathode recycling process leads to net emissions savings. However, using a pyrometallurgical process for either cell

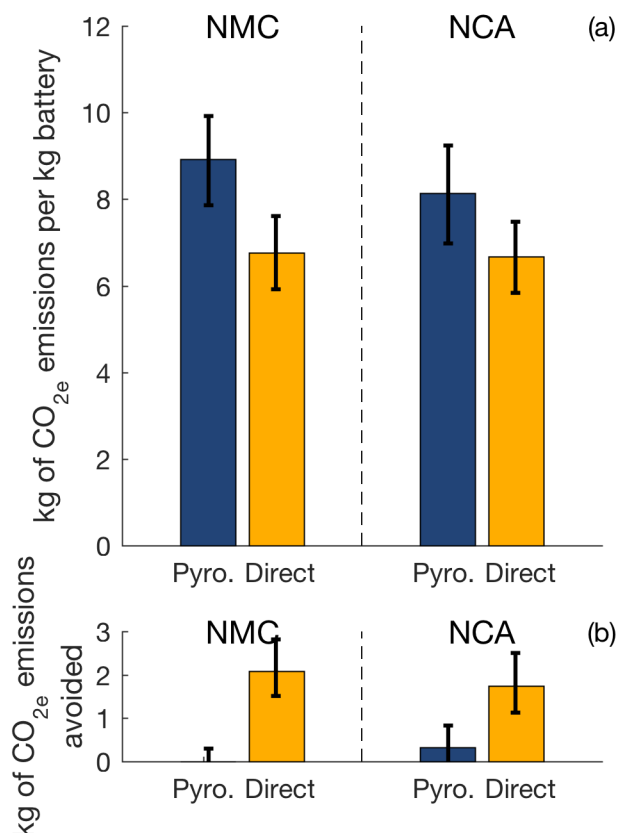


Figure 4.4: CO_{2e} emissions per kg of battery for (a) manufacturing and recycling processes (pyrometallurgical and direct cathode recycling) less the emissions offsets from recovered materials, and the (b) net CO₂ emissions avoided by using a recycling process for NMC and NCA cells and recovering material. All processes use the US average electricity grid.

chemistry does not guarantee such savings. For both chemistries, much of the pyrometallurgical recycling emissions offsets are derived from using the output slag as a substitute for cement inputs. The other differences in pyrometallurgical emissions are the result of differences in the cathode chemistries. While the median emissions for pyrometallurgical recycling of NCA cells shows some net savings, for NMC cells only a few scenarios result in emissions savings. This trend is largely driven by the presence of manganese as a cathode material present in NMC cells, but not NCA cells. Manganese is not recovered during the pyrometallurgical recycling process, and global recycling rates of manganese are very low, so the manganese for these cathodes is assumed to be mined for each application. [95] The nickel and cobalt can be recovered by either pyrometallurgical or direct cathode recycling. Although the metals recovered in a pyrometallurgical process must be refined, the energy and associated emissions are less substantial than the emissions and energy required to mine the material. However, for the metals recovered (nickel, copper,

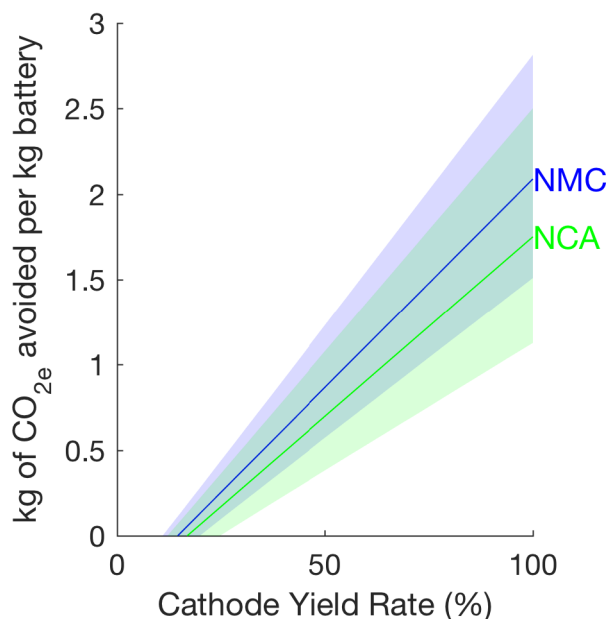


Figure 4.5: net kg of CO_{2e} emissions avoided per kg battery when combining manufacturing with direct cathode recycling over using no recycling method after manufacturing. As the cathode yield rate from the direct recycling process decreases, so do emissions benefits. Pyrometallurgical recycling does not offer significant greenhouse gas emissions reductions.

iron, and cobalt) there are already a variety of other recycling pathways, pathways that have lower emissions than pyrometallurgical recycling of lithium-ion batteries. Because these existing recycling pathways play such a large role in the current markets for these metals, pyrometallurgical recycling does not offer significant greenhouse gas emissions reductions in any grid (shown in Figure C.5). Similar trends hold when we consider different functional units. Figure C.7 shows that when we consider emissions per kWh of battery, pyrometallurgical recycling of NMC cells does not offer net reductions in emissions. Figures C.6 and C.8 consider the input energy per kg and kWh, respectively.

Figure 4.4 assumes that 100% of the cathode material is recovered during the direct cathode recycling process, but we are interested in determining how effective this process needs to be at recovering cathode material to have net emissions benefits. Since the pyrometallurgical process does not have significant environmental benefits for either chemistry, we compared the benefits of using a direct cathode recycling method over doing nothing after the batteries are manufactured. Holding fixed our assumptions about cell construction and the quantity of materials input, we compare the avoided CO_{2e} emissions as the yield rate for the direct cathode recycling process varies from 0 to 100%. As Figure 4.5 shows, using direct cathode recycling for NMC cells offers

slightly larger emissions savings than using the direct cathode recycling process for NCA cells. Additionally, choosing a direct cathode recycling process makes sense for NCA cells only if the direct cathode recycling yield rate is above 17% (13-25%), while the yield rate for direct cathode recycling of NMC cells need only be 15%(11-20%) for direct cathode recycling to be more beneficial than doing nothing. Figures C.9 - C.12 show the breakeven emissions and energy input savings for different direct cathode recycling yield rates on a per kg and per kWh basis, for all three electric grid options (US average, NWPP, and RFCM).

Because of uncertainty in the emissions associated with pyrometallurgical and direct cathode recycling, the confidence intervals when comparing the emissions differences between the two are much larger than when comparing direct recycling to no recycling after manufacturing. For NMC cells, direct recycling yield rates must be 15% (2-29%) to be more favorable than pyrometallurgical recycling. Because pyrometallurgical recycling has more potential for emissions offsets for NCA cells, the recovery rate for cathode materials to outperform pyrometallurgical recycling is 33% (9-61%). Figures C.13 - C.16 show the emissions as the recovery rate for direct cathode recycling compare to pyrometallurgical recycling for all three electric grid options.

4.3.3 Impact of Transportation

Transportation of the input materials and for collecting the batteries before recycling is responsible for only a small fraction of the total energy input into the process, and in turn only a small amount of the greenhouse gas emissions. Under the baseline assumptions for an average US location, transportation only accounts for 0.33 kg CO_{2e}/kg battery, roughly 4% of the total when using a pyrometallurgical process, and 5% when using a direct cathode recycling method.

Of the 0.33 kg of CO_{2e}, 70% is attributed to battery collection. Because of strict regulations on how batteries must be shipped, they are transported on trucks (the highest emitting form of transportation). [96] Because of the limited number of facilities, we also assumed that the distance traveled was 2,500 miles. Doubling the emissions factors, or both the emissions factors and distances traveled has a relatively small impact on the total emissions per kg. Doubling the emissions factors increases CO_{2e} emissions per kg battery by 4% while doubling both the emissions factors and distances traveled increases the total CO_{2e} emissions per kg battery by 12%.

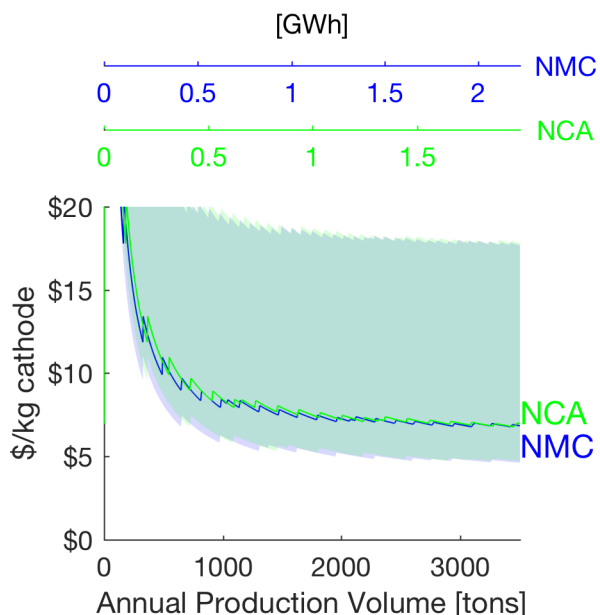


Figure 4.6: Relithination cost per kg of cathode material for NMC and NCA cells as production volumes vary. The process reaches economies of scale at roughly 1,500 tons of annual production.

4.3.4 Breakeven Recovery Cost

Our process-based cost model of cathode material manufacturing shows that at scale, the cost of manufacturing one kg of NCA cathode is \$24 (\$19-\$40), and for an NMC cathode is \$20 (\$15 - \$37). The at scale cost of relithinating the cathode materials recovered from a direct cathode recycling process is approximately \$6/kg (\$5-\$18) for both NMC and NCA cathodes, assuming 50% of the lithium is replaced. and economies of scale are reached (depicted in Figure 4.6) at relatively low volumes: approximately 1,500 metric tons/year, enough for roughly 1 GWh of cells, well within current manufacturing capacities. That allows direct cathode recycling to be profitable at \$18/kg (\$15-\$27) for NCA and \$15/kg (\$12-\$24) for NMC cells.

Relithination costs depend on how much lithium carbonate is required. Figure C.17 shows both the cost of relithination and the breakeven cost for direct recycling to be profitable as the percentage of lithium required during relithination varies from 0 to 100%. In practice, the maximum amount of lithium that would need to be added during reprocessing is 60% as the crystal structure of the cathode material collapses if more than 60% of the lithium is lost. [97] Figure C.18 - C.21 show that the variation in lithium added during reprocessing has a minimal impact on the net emissions and energy consumed by implementing a direct recycling process and the associated offsets.

4.4 Discussion

Although there is potential for both economic and environmental benefits to using a direct cathode recycling process over a pyrometallurgical process, there is some contrast between these environmental and economic objectives. The significant manganese content in NMC based cells increases the potential environmental benefit from using a direct cathode recycling process, but makes manufacturing the cathode from raw input materials less expensive. This narrows the potential window for economic viability without any incentives. For NCA cells, which have a higher percentage of high-value metals (cobalt and nickel), the cost associated with manufacturing the cathodes from raw materials is higher, increasing the potential payoff from a direct cathode recycling process, especially because of recent increases in cobalt commodity prices. [98,99] However, the environmental benefit of a direct recycling process over a pyrometallurgical process is smaller in this case, because both processes recover all of the constituent metals in NCA cathodes, which is not true of today's NMC pyrometallurgical recycling.

While recycling programs for lead acid automotive batteries have largely been successful (especially in the US, where 99% of lead acid batteries are recycled), [100] the prognosis for lithium-ion batteries is less clear; in the US, federal law requires lead acid batteries to be recycled, and many states have enacted exchange mandates: sellers must accept old batteries at the time of new purchases. The lead acid recycling process is also relatively simple and profitable. [101] In contrast, lithium-ion batteries have no overarching federal regulation, and the recycling requirements vary by state. Implementing consistent regulations for automotive lithium-ion batteries across state lines, and adopting policies like refundable deposits with battery purchases could increase collection rates. Non-refundable deposits could help to fund battery collection and transportation to recycling facilities, easing the financial burden on recyclers and allowing more financial resources to be devoted to recovering higher value materials.

The European Union also has regulations requiring lead acid automotive batteries to be recycled, although collection rates have lagged the US. [102] They also have requirements for lithium-ion battery recycling. The EU battery directive requires 50% by weight of the total battery content be recycled. [64] For pyrometallurgical recycling, much of the cathode material, in addition to some current collector and cell canister material is output as part of the metal alloy. The other non-combustible cell components are output as part of slag that can be repurposed as cement input materials. As such, combined, the metal alloy and slag material satisfy the requirement that

50% by weight of battery materials be recycled to be compliant with EU regulations.

For direct cathode recycling, ensuring compliance with EU regulations depends on additional recycling, despite the more substantial environmental benefits. Assuming a 100% yield, the cathode material recovered during direct recycling accounts for approximately 30% of cell mass, less than the 50% required. Others have noted similar mismatches between the environmental impact of recycling and the mass requirements of manufacturing for other waste streams. [89] Recovering and recycling other components, like current collectors (~10% of cell mass) and cell canisters (~30% of cell mass) in addition to the direct recycling of the cathode could bring direct recycling process into compliance. Selling them as scrap metal could also be another source of income from the direct recycling process. Whether this combination of processes, potentially undertaken at multiple facilities by multiple actors, would be considered compliant depends on how the EU directive defines the boundaries of recycling facilities and the yield rate of the direct recycling process.

4.4.1 Recycling and future market demand for metals

Demand for many metals used in lithium-ion batteries is expected to continue to increase in the coming decades, [95, 103] with potential implications for both the economic viability and environmental benefits for both pyrometallurgical and direct cathode recycling. Although some individual metal prices are particularly volatile (in 2017 cobalt has been trading at roughly double the price in 2016), [4, 99] prices of individual metals have relatively small impacts on the cost of producing cathode material. Less dramatic but more systematic increases of input prices have more substantial impacts. For example, cobalt prices have roughly doubled in the past few months, Anonymous:6NX6dEld but the overall cost per kg of cathode material would only increase by ~\$3/kg (roughly 12.5%). An increase of 50% for all cathode input materials increases the cost per kg of material produced by roughly 25%.

As demand for different metals increases, less favorable sources will be mined at lower efficiencies, requiring additional energy and producing more emissions, [103] but also potentially shifting the amount of material recycled through other pathways. These currently unused recycling methods for non-battery materials would also likely consume more energy than the recycling methods currently in use. These changes would shift both the upper bound and the peak for the triangular distributions we used to assess the emissions associated with input materials like cobalt and nickel, thereby increasing the emissions and energy offsets for both recycling processes. Al-

though increases in the underlying emissions and energy consumed for input materials could make pyrometallurgical recycling environmentally beneficial, the benefits would still be larger for direct cathode recycling, especially because the direct cathode recycling process can better capitalize on grid electricity emissions reduction trends.

Chapter 5

Evaluating Consumer Risk Perceptions of Recycled Batteries in the Electric Vehicle Market

5.1 Introduction

Reducing transportation emissions will require both widespread adoption of alternative fuel vehicles and low-carbon sources for these fuels. After decades of investment and policy support, electric vehicles are now becoming accessible for many vehicle owners. This, combined with more widespread adoption of carbon-free electricity generation technologies creates a promising path for reducing transportation emissions. However, we need widespread consumer buy-in to achieve emissions reductions. Much research has already been conducted to determine what attributes are most important to consumers considering electric vehicles, and they rank vehicle price and attributes related to the battery (vehicle range, recharge time) among the most important [104].

Despite recent declines in lithium-ion battery costs [10, 11], they are still a substantial contributor to the overall cost of electric vehicles. In addition to advancing cell chemistries to increase storage capacity, recent efforts to reduce battery costs have also focused on recycling [76, 105] and refurbishment methods to reduce material costs and insulate battery costs from global commodity bottlenecks [2, 106].

While these recycling and refurbishment methods may be successful in reducing the costs of electric vehicle batteries, this cost reduction may come with a penalty in battery performance.

This could result in higher premature failure rates (currently about 1 in 10 million new cells) [107], or accelerated capacity fade over time. Premature cell failures are low probability events, and the impacts can be mitigated through the pack design, while accelerated capacity fade directly impacts the electric range of the vehicle.

To assess how much of a trade-off in performance consumers are willing to accept, we use a discrete choice survey to assess electric vehicle owners' willingness to pay for different attributes associated with battery health and usefulness over its lifetime, including warranty coverage of the battery, whether the battery pack is made of recycled or refurbished materials, and initial vehicle range.

5.1.1 Literature review

Discrete choice techniques have been widely applied to assess consumer preferences, including vehicle preferences, although the types of data used and questions asked varies between studies. The earliest example of this type of analysis is by Lave and Train, who used survey responses from recent vehicle purchasers [108]. The multinomial logit model used in that original study has been adapted and applied to other cases since them, including cases that use revealed preference data. Berry et al use a combination of consumer level and aggregate data to improve predictive power [109]. Historical sales data has also been used to assess the effectiveness of policies like fuel economy standards, as in Whitefoot and Skerlos [110] and Allcott and Wonzy [111] or other incentives programs as in Greene et al [112]. Other extensions of the basic multinomial logit model include the random coefficients logit model used by Boyd and Mellman [113], and the mixed logit model used by Berry et al [114] and Train and Winston [115]. The mixed logit model allows for heterogeneity in consumer preferences and accounts for substitution patterns.

Others have used similar analytic techniques to assess stated-choice data. The surveys to collect these stated preferences often utilize choice-based conjoint questions, where respondents are given a selection of combinations of attributes and asked to select one they'd most likely purchase, although other methods, like the interactive survey in Axsen et al [116], where respondents select their ideal combination of attributes within some constraints can collect similar information.

Many of these choice-based conjoint studies use multinomial logit [117–120] models, and mixed logit models have also been used to estimate heterogeneous preferences [117, 121–123]. More recently, latent class models, which can account for heterogeneity in consumer preferences, without necessarily knowing what the underlying attribute driving the differences between groups,

have been applied to vehicle and other transportation preference questions. Greene and Hensher [124] compared the results of latent class models against mixed logit models for different long-distance road travel. Both Shen [125] and Zito [126] use latent class analyses to compare between different transit options. Latent class analyses have also been applied to different vehicle types. Hidrue et al [127] used latent class analysis to identify an electric vehicle oriented from gasoline vehicle oriented consumers, while Axsen et al [128] surveyed recent vehicle purchasers and used latent class analysis to identify distinct groups based on vehicle preference (electric and conventional) and lifestyle factors (like environment or technology-oriented lifestyles).

5.2 Theory: Revealed and Stated Preference Studies

Both revealed and stated choice methods used to assess consumer preferences, and both methods have strengths and weaknesses [129]. Revealed preference studies have the benefit of reflecting actual decisions that consumers make in the market. However, revealed preference studies can be subject to endogeneity problems that arise because it is impossible to account for all possible attributes that consumers consider, especially as the complexity of the product in question increases. Multicollinearity can also be a problem, as certain attributes often influence each other [130–132]. The market data may also present very low variations in the attributes of vehicles. This is particularly true for electric vehicles, where manufacturers are offering a limited number of models with relatively little variability in their attributes. The limited number of manufacturers and models is particularly limiting for attributes like warranty, which is highly correlated with the vehicle brand [133]. Most importantly, the technology we want to examine (recycled and refurbished battery materials) is not currently available for mass-produced electric vehicles.

Stated preference studies, on the other hand, can encompass wider variations in attribute levels, including forward-looking levels that are not currently available. While there is this freedom to expand the decision space, there is a possibility that respondents behave differently in surveys than when they are making actual purchases, particularly with respect to the importance of price [134]. In some contexts, it is possible to design stated preference studies with incentives that can align the consumer responses with more realistic trade-offs with other purchases, although that is best suited for lower-cost items [135]. Otherwise, it is possible that respondents will be less sensitive to price in a stated preference choice than they would be in a real decision scenario, although it would not affect the rank order of importance for the other attributes included in the

survey. Additionally, although the attribute levels can vary more than is possible in revealed preference studies, stated preference studies are subject to saliency problems because respondents are forced to examine attributes that may rank fairly low on their overall list of priorities when making an actual purchase.

For this study, we chose to use a stated preference method because of the flexibility to include technologies (recycled and refurbished batteries) that have not yet been introduced into the market, and present attribute combinations that are not currently offered in today's market (like variation in different warranty packages). To minimize the impact of the relative insensitivity to price that can occur during stated choice tasks, we bound the price attribute levels based on our knowledge of the current electric vehicle the respondent owns. We also include a "none of these" option so that respondents were not forced to make a choice between two unaffordable combinations. Additional details about the survey design and attributes are detailed below.

5.3 Methods

We use a choice-based conjoint analysis survey instrument to measure the consumer preferences for different electric vehicle attributes that are directly related to the battery performance and price of the vehicle. Below are details about the survey design, the attributes and levels used in the survey, and information about how participants were recruited.

5.3.1 Survey Design

The objectives of the survey design were to isolate the respondents focus on the battery package attributes rather than other parameters that factor into consumer vehicle purchase decisions (like brand, technology features, etc.), to make the attribute levels included in the survey match the attributes of electric vehicles available today, and to minimize the cognitive burden of each choice task.

Our recruitment strategy focused on attracting current electric vehicle owners, who have experience and resolved preferences because of their interactions with the operation of an electric vehicle/how batteries impact it. We screened respondents based on whether they owned an electric vehicle, and if they did, whether they owned a battery electric vehicle, a plug-in hybrid electric vehicle, or if they were unsure about the type of electric vehicle they owned.

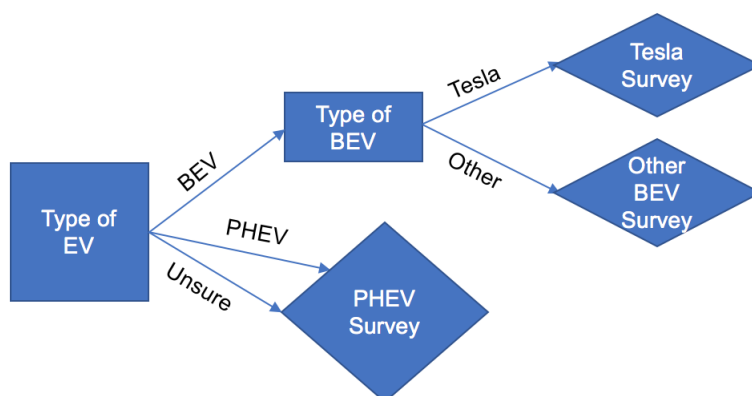


Figure 5.1: Flow chart for survey version decision based on current vehicle owned

Attributes and Levels

Our choice experiment included five attributes related to electric vehicle batteries: price (the final price after all government incentives), initial range (refers to the distance you can travel (in miles) on a full battery charge when the vehicle and battery pack are new), percentage (the energy storage capacity guaranteed under the warranty period. If capacity drops below this amount, the battery will be replaced), warranty (the duration (in years) the battery is covered by a manufacturer warranty), and battery material type (whether the battery pack is made from conventional materials, made from recycled materials, or if the batteries are refurbished). The levels for each of these attributes were drawn from current electric vehicle market data. Additional details about this market data are available in the Supplementary Information (Section D). Because many of the attribute levels, especially price and initial range, are very different depending on the type of vehicle (BEV or PHEV) and brand, we fielded three different versions of the survey. Figure 5.1 shows how survey respondents were sorted based on their answers to questions about their current vehicle, with one version of the survey one if they had a Tesla Model S or Model X, one if they had another battery electric vehicle, and one if they currently own a plug-in hybrid. If respondents were unsure of the type of vehicle they own, they were given the plug-in hybrid version of the survey. The levels for each attribute for each version of the survey are listed in Table D.2.

Table 5.1: Attribute Descriptions

Attribute	Description
p_j	Price the final price after all government incentives
x_j^{RANGE}	Range the distance you can travel (in miles) on a full battery charge when the vehicle and battery pack are new
$x_j^{PERCENT}$	Percentage the percentage of battery capacity guaranteed under warranty
$x_j^{WARRANTY}$	Warranty the length (in years) a manufacturer will guarantee battery performance
$x_j^{RECYCLED}$	Recycled a dummy variable that specifies whether the battery pack is made from recycled materials
x_j^{REFURB}	Refurbished a dummy variable that specifies whether the battery pack is refurbished
x_j^{OG}	Outside Good a dummy variable that signifies whether the outside good option was selected
$x_j^{RANGE} x_j^{PERCENT}$	Final Range the range (in miles) guaranteed during the warranty period. If the vehicle range drops below this guaranteed range during the warranty, the manufacturer will replace the battery.
$x_j^{RANGE} x_j^{PERCENT} x_j^{WARRANTY}$	Final Range Under Warranty the benefit of an additional mile of range guaranteed with an additional year of warranty coverage

Choice experiment

The choice section of the survey had one practice choice task and 15 randomized choice tasks. Both the practice task and choice task featured 3 options: 2 vehicle battery packages and a “neither of these” option. For the practice task, we specified one clearly dominant option, with clearly preferable levels for price, range, percentage, and warranty. Since we do not know whether consumers have a positive or negative perception of battery materials, both options presented in the sample task included conventional battery materials. The practice task also included directions that walked the respondents through each attribute and specified which option to select.

To reduce the cognitive burden of the survey on respondents, we made 2 key decisions in the design of the choice tasks. First, we displayed the percentage attribute as the product of the percentage of vehicle range and the initial vehicle range to display the final vehicle range guaranteed by warranty in miles (the product of the initial range (x_j^{RANGE}) and percentage ($x_j^{PERCENT}$)). Second, we displayed this final range in conjunction with the warranty attribute (in years of cover-

age) together, so that for each decision respondents were only comparing across four metrics. A sample question is shown in Figure 5.2.

Suppose these were the two battery options available for your BMW i3. Which would you choose? Choose by clicking one of the buttons below:

(1 of 15)

Price	BMW i3 \$40,000	BMW i3 \$45,000	Neither: I would choose another vehicle.
Vehicle Range with New Battery	250 miles	175 miles	
Vehicle Range Guarantee	200 miles for 8 years	158 miles for 7 years	
Battery Type	Recycled	Conventional	
	<input type="radio"/>	<input type="radio"/>	<input type="radio"/>

← →

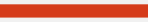
0%  100%

Figure 5.2: Sample discrete choice question

5.3.2 Data Collection

Participants were recruited using Facebook ads and posts. Ads were targeted to those Facebook users who were in the United States, 18 years old or older, and had expressed an interest in electric vehicles. In the ads and posts, users were directed to an off-site survey link.

Of the completed survey responses (214), a number of responses were removed from the final analysis. Responses were removed if 1) the respondent did not own an electric car, but some other type of electrified vehicle (motorcycle, etc.), 2) if the respondent did not select the correct, dominant option as instructed for the practice task (described in 5.3.1, 3) if the respondent completed the survey in less than 5 minutes (the minimum time determined through preliminary testing) or took an excessive amount of time to complete the survey (>2 hours) and 4) if the respondent answered all of the choice questions by selecting the same option for all questions. We were left with 83 EV survey responses, and 80 PHEV survey responses. Respondents were

also asked a series of demographics questions at the end of the survey, which helped us to determine the age, gender, income, and education level of the participants.

5.3.3 Model Specification

We estimate consumer utility using a multinomial logit model (MNL) in the willingness to pay space, which is a transformation of a preference space utility model. In the preference space, the utility (u_{ij}) that a respondent i gains from alternative j is modeled as:

$$u_{ij} = v_{ij} + \epsilon_{ij} = \beta'_i \mathbf{x}_j + \epsilon_{ij} \quad (5.1)$$

In the willingness to pay space, the utility of alternative j is:

$$u_{ij} = v_{ij} + \epsilon_{ij} = \alpha (p_j + \gamma'_i \mathbf{x}_j) \quad (5.2)$$

Where p_j is the price of alternative j and the coefficients, γ , are equal to the preference-space coefficients, β divided by the price coefficient, α . Assuming that the unobservable utility, ϵ_{ij} , is independent and identically distributed extreme value distribution, the closed-form solution for a choice probability is given by:

$$P_{ij} = \frac{\exp(v_{ij})}{\sum_{j=1}^J \exp(v_{ij})} \quad (5.3)$$

We also explore the possibility of heterogeneity in consumer preferences using latent class (LC) models. The theory of latent class models assumes that individuals are implicitly sorted into Q classes, and that membership in these classes depends on both observable and unobservable attributes. The latent class model uses the same closed-form logit model to assess the probability that individual i selects alternative j in choice task t [124]. Assuming that each choice task t is independent, the contribution of each individual i to the overall likelihood in class q is the cumulative probability:

$$P_{iq} = \prod_{t=1}^{T_i} P_{it|q} \quad (5.4)$$

We first use a simple latent class model with no covariates [136], so the probabilities of each individual being a member of class q in Q is H_{iq} , where

$$H_{iq} = \frac{\exp(\mathbf{z}_i \theta_q)}{\sum_{q=1}^Q \exp(\mathbf{z}_i \theta_q)} \quad (5.5)$$

Where \mathbf{z} simplifies to 1 because this model does not account for different covariates, and θ is a parameter maximized like the parameters of the utility function. Here, θ for class 1 is set to equal zero, and we solve for $Q - 1$ values of θ . The overall likelihood function is then given by:

$$\ln L = \sum_{i=1}^N \ln \left(\sum_{q=1}^Q H_{iq} \left(\prod_{t=1}^{T_i} P_{it|q} \right) \right) \quad (5.6)$$

Since the number of true classes is unknown, there is no specific test to determine if the correct number of classes have been included in the model. However, metrics including the Akaike Information Criterion (AIC) and Bayesian Information Criterion (BIC) have been commonly used to guide the selection of the number of classes, with lower values for both criterion suggesting the model may be preferred to others [124, 125].

For each of these methods, we examined a number of model specifications using the attributes listed in Table 5.1. Our baseline model (given in Equation 5.7) included price, a logarithmic transformation of range, a logarithmic transformation of the final range, additional years of warranty over the lowest warranty period offered, an interaction term between the additional years of warranty coverage and final range, a recycled dummy variable, a refurbished dummy variable, an interaction between recycled batteries and the initial range, an interaction between refurbished batteries and the initial range, and an outside good term. Warranty is scaled to be additional years of warranty coverage over a 7 year warranty period (the lowest warranty period level included in our model).

$$\begin{aligned} v_j = & \alpha(p_j + \gamma_1 \log(x_j^{RANGE}) + \gamma_2 \log(x_j^{FINALRANGE}) + \gamma_3 x_j^{WARRANTY} + \\ & \gamma_4 \log(x_j^{FINALRANGE}) x_j^{WARRANTY} + \gamma_5 x_j^{RECYCLED} + \gamma_6 x_j^{REFURB} + \\ & \gamma_7 x_j^{RECYCLED} \log(x_j^{RANGE}) + \gamma_8 x_j^{REFURB} \log(x_j^{RANGE}) + \gamma_9 x_j^{OG}) \end{aligned} \quad (5.7)$$

We chose to use a logarithmic transformation of range and final range because when we compared models with both linear and logarithmic range parameters to a partworth model, we found that the logarithmic model more closely aligned with the utility specified by the partworth model, which does not make any assumptions about the relationship between attribute levels and

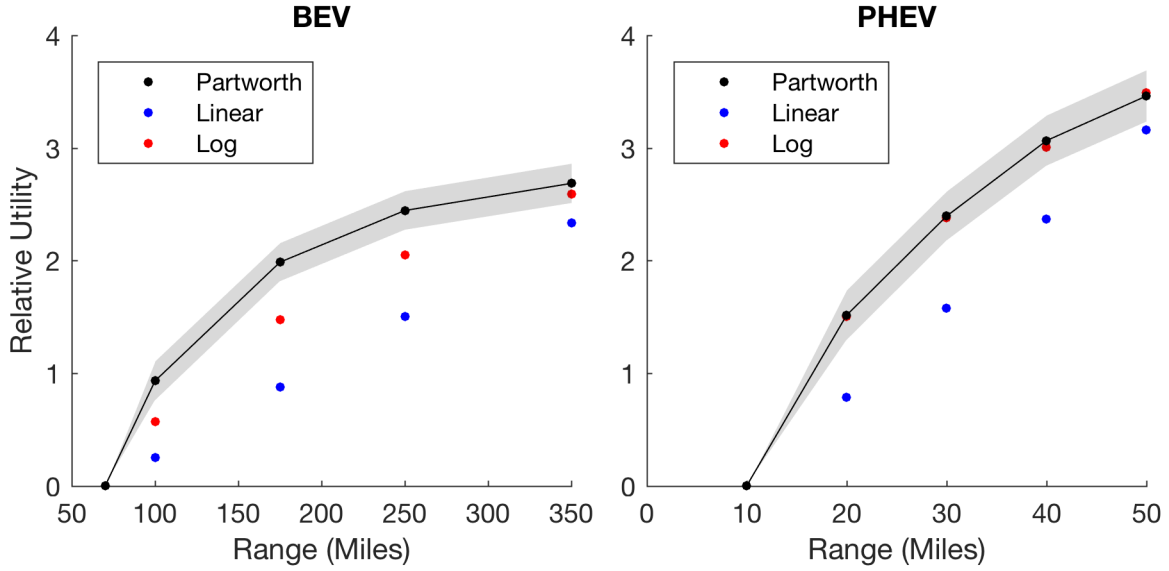


Figure 5.3: Partworth, Linear, and Logarithmic models of range for BEV and PHEV data. A logarithmic model is a better fit to the partworth data than a linear model for the vehicle range attribute.

utility. Figure 5.3 shows how the utilities of linear and logarithmic range models compare to the partworth model.

The interaction terms on final range and warranty examine whether the value of an additional year of warranty coverage is dependent on also having a longer final range guaranteed. The interactions on battery material and initial range examine whether consumer willingness to pay for different battery materials is dependent on how much they are willing to pay for a vehicle with a longer range (and similarly larger battery pack).

We also examine a simplified model, which does not include any interaction terms outside of the final range term, which is a product of the percentage of battery capacity guaranteed and the initial range. This simplified model is given in Equation 5.8.

$$v_j = \alpha(p_j + \gamma_1 \log(x_j^{RANGE}) + \gamma_2 \log(x_j^{FINALRANGE}) + \gamma_3 x_j^{WARRANTY} + \gamma_4 x_j^{RECYCLED} + \gamma_5 x_j^{REFURB} + \gamma_6 x_j^{OG}) \quad (5.8)$$

Table 5.2: Respondent Demographic Data

	BEV	PHEV
Sample Size	86	79
Age (average)	49.2	45.9
<i>Household income</i>		
"<\$25,000	0.0	2.5
\$25,000-\$49,999	12.8	8.5
\$50,000-\$74,999	16.3	15.3
\$75,000-\$99,999	12.8	11.9
\$100,000-\$124,999	19.8	12.7
\$125,000-\$149,999	2.3	12.7
\$150,000-\$174,999	5.8	6.8
\$175,000-\$199,999	7.0	4.2
\$200,000-\$224,999	11.6	3.4
\$225,000-\$249,999	2.3	3.4
\$250,000-\$274,999	2.3	4.2
\$275,000-\$299,999	0.0	2.5
>\$300,000	1.2	4.2
Household Size (average)	2.7	3.1
<i>Education</i>		
High school degree or equivalent	3.5	3.8
Some college	26.7	22.8
Associate degree	5.8	15.2
Bachelors degree	33.7	31.6
Masters degree	18.6	19.0
Professional degree	5.8	2.5
Doctoral degree	5.8	3.8
<i>Living Situation</i>		
Married or living with a partner	80.2	74.7
Singe	16.3	19
Divorced	3.5	3.8
Widowed	0.0	1.3
<i>Sex</i>		
Male	89.5	89.9
Female	9.3	8.9

5.4 Results

Here, we present the results of both model specifications in the willingness to pay space, with latent class analysis on the simplified model. Similar results in the preference space are available in Appendix D. The data for BEV and PHEV respondents is analyzed separately and the results are presented in Table 5.3 (BEVs) and Table 5.4. For each of the models we investigate, we find that price is always significant, and range is almost always significant in determining overall utility.

Table 5.3: BEV Willingness to pay results

Attribute	Baseline Model	Simplified Model
Price	0.025*** (.003)	0.025 *** (.003)
ln(Range)	44.602 *** (10.859)	40.011 *** (9.113)
ln(finalrange)	8.320 ** (3.346)	9.897 *** (3.039)
Warranty	-3.126 (4.933)	1.422 (1.602)
Warranty*ln(finalrange)	1.105 (1.144)	
Recycled	37.569 (46.7)	-1.273 (4.226)
Refurbished	30.823 (46.81)	-3.003 (4.263)
Recycled*ln(Range)	-7.468 (8.957)	
Refurbished*ln(Range)	-6.505 (8.967)	
Outside good	185.390 *** (49.281)	168.070 *** (38.737)
Log Likelihood	1051.400	1052.300
Observations	1290	1290
Note:	*p<0.1; **p<0.05; ***p<0.01	

For our baseline model for BEV owners and PHEV owners, we see that price, range, and final range are significant in their decision-making process. for BEV owners, the outside good is also a significant predictor. Because none of the interaction terms are significant for either group, we focus most of our additional analysis on the simplified model.

As with the baseline model, we find that for BEV owners as a whole, price, range, final range, and the outside good are the most significant factors when determining the overall willingness to pay for a vehicle. The logarithmic transformation on range and final range means that both BEV and PHEV owners are willing to pay the same amount for percentage increases in range and final range, but overall willingness to pay for additional miles of range and final range decreases as the overall range or final range increases. Figure 5.4 shows PHEV owners' diminishing willingness to pay for range and final range as the miles of range and range covered increases.

Examining multiple latent class models using our simplified model (see full tables in Appendix D), we find that for BEV owners, a 4-class latent class model meets the different criteria we examine and captures four distinct groups of consumers. Of these four groups, three are indifferent to

Table 5.4: PHEV Willingness to Pay Results

Attribute	Baseline Model	Simplified Model
Price	0.067 *** (.003)	0.067 *** (.003)
ln(Range)	15.489** (7.423)	17.994*** (6.874)
ln(finalrange)	7.604 ** (3.69)	7.142 ** (3.469)
Warranty	0.763 (2.316)	0.199 (.723)
Warranty*ln(finalrange)	-0.215 (.843)	
Recycled	-6.694 (15.566)	-3.291 * (1.992)
Refurbished	-23.284 (16.279)	-1.848 (1.997)
Recycled*ln(Range)	0.986 (4.52)	
Refurbished*ln(Range)	6.264 (4.72)	
Outside good	19.643 (18.039)	26.977 * (15.166)
Log Likelihood	801.330	802.350
Observations	1185	1185
Note:	*p<0.1; **p<0.05; ***p<0.01	

the type of battery materials and one group (Class 2), which we refer to as the environmentally-conscious group, has a positive valuation of refurbished battery materials. This group represents roughly 35% of the respondents. Table 5.5 shows the latent class coefficients in the willingness to pay model.

For PHEV respondents, we find that as one group, there is a weakly negative perception of recycled batteries, with consumers willing to pay on average \$3,000 less for a car that has a recycled battery. As we segment this group into more distinct classes, we find that when there are four latent classes, there is one group (Class 3 in Table 5.6) that has very negative perceptions of recycled and refurbished materials. We refer to this group of PHEV owners as the risk-averse group, and they require price reductions of approximately \$7,000 to accept a recycled or refurbished battery pack. Figure 5.5 shows that the risk-averse PHEV owners' willingness to pay for both recycled and refurbished batteries is significantly different from zero. All other groups of PHEV owners are indifferent to the type of battery materials in their vehicle.

Table 5.5: Latent classes for BEV owners in the willingness to pay space. Environmentally-conscious owners, with a positive opinion of refurbished materials, make up 35% of the sample population.

Attribute	Class 1	Class 2 Environmentally conscious	Class 3	Class 4
Price	0.181*** (.028)	0.168*** (.022)	0.188*** (.018)	0.001*** (.)
ln(Range)	2.935 (7.203)	14.558*** (4.963)	14.909*** (3.639)	63.834 (65.024)
ln(finalrange)	14.420*** (7.)	13.613*** (4.91)	4.107 (3.451)	-70.695 (62.54)
Warranty	-0.756 (.975)	0.612 (.661)	0.606 (.487)	0.932 (8.728)
Recycled	-3.614 (2.636)	2.378 (1.667)	-1.256 (1.248)	3.991 (23.07)
Refurbished	-4.155* (2.475)	3.923** (1.724)	-1.280 (1.288)	5.769 (23.219)
Outside good	62.273*** (14.844)	67.498*** (18.556)	61.487*** (6.108)	16.897 (92.111)
Class		1.065*** (.389)	1.092*** (.399)	0.272 (.432)
	12%	35%	36%	16%
Log Likelihood	755.11			
AIC	1572.211			
BIC	1732.245			
Observations	1290			
Note:	*p<0.1; **p<0.05; ***p<0.01			

5.5 Discussion

Knowing that some PHEV owners are concerned with recycled and refurbished battery materials, we need to contextualized whether manufacturers can maintain demand at current levels by cutting pack costs to match consumers' willingness to pay. Assuming that the batteries cost approximately \$200/kWh (\$125 - \$300/kWh), the \$7,000 (\$600-\$13,000) price differential represents a relatively large portion of the total pack cost. For PHEVs with small and relatively inexpensive battery packs, the average \$7,000 reduction that consumers want in order to accept a vehicle with recycled batteries is a much larger portion of overall pack costs, even exceeding the total pack costs of some small PHEV battery packs available today. Figure 5.6 shows how the price differential compares as a percentage of the total cost for different battery storage capacities. If the risk-averse PHEV owners' actual willingness to pay is closer to the lower end of the range, and is actually unaffected by changes in the vehicle range, recycling would need to reduce the cost

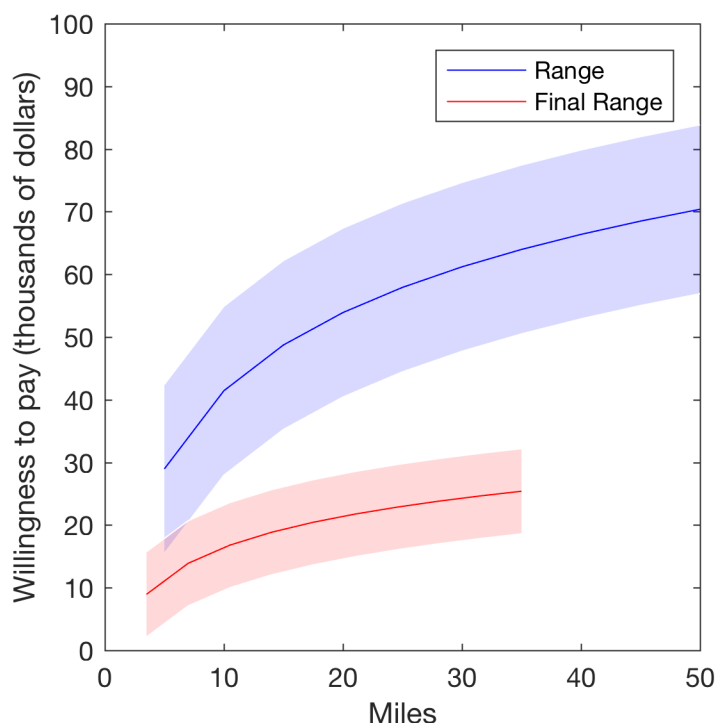


Figure 5.4: PHEV owners willingness to pay for miles of range and final range (when percentage is 70%). There is decreasing willingness to pay as the miles of range available increases

of the battery by roughly 50%, which is difficult to achieve. Refurbished options might be able to meet these lower cost targets because refurbishing batteries avoids many of the steps required for remanufacturing batteries, but there is still a high degree of uncertainty in the overall willingness to pay.

However, on a per kWh basis, BEVs make up a much more substantial portion of the overall automotive energy storage market than PHEVs (Figure 2.2), so recovering the materials used in BEV batteries, where consumers seem to be less sensitive to the type of battery material, or even have a positive valuation of refurbished materials, will have a larger net impact on reducing manufacturing emissions.

5.5.1 Limitations and Future Work

Additional work is necessary to determine the demographic or other behaviors that are driving membership in different classes. Income, education level, and age could all be important factors that influence consumer behavior, and these potential relationships were not fully explored here. These demographics are also important to identify to determine how the members of different

Table 5.6: Latent classes for PHEV owners in the Willingness to pay space. Risk-averse owners make up 40% of those sampled.

Attribute	Class 1	Class 2	Class 3 Risk-Averse	Class 4
Price	0.207*** (.063)	0.136*** (.013)	0.079*** (.007)	0.126*** (.023)
ln(Range)	-10.331 (20.713)	20.229*** (5.875)	24.547*** (8.695)	-29.356*** (10.867)
ln(finalrange)	32.449 (20.118)	1.975 (5.649)	25.589*** (8.627)	43.573*** (10.305)
Warranty	3.567 (2.777)	-0.854 (.77)	1.859 (1.179)	0.399 (1.335)
Recycled	-2.092 (5.714)	-2.032 (2.068)	-6.908** (3.203)	-2.266 (3.675)
Refurbished	-8.841 (5.406)	-0.767 (2.189)	-6.620** (3.169)	2.435 (3.702)
Outside good	52.972* (32.085)	34.817*** (7.307)	89.057*** (11.749)	-65.202*** (14.642)
Class	7%	1.706*** (.483) 40%	1.707*** (.481) 40%	0.613 (.546) 13%
Log Likelihood	568.22			
AIC	1198.44			
BIC	1355.84244			
Observations	1185			
Note:	*p<0.1; **p<0.05; ***p<0.01			

latent classes compare to the population overall.

Although we found that the interaction terms between battery type and vehicle range were insignificant for the overall BEV and PHEV respondents, additional analysis is necessary to determine if there is a significant interaction between range (and commensurate pack sizes) and consumer willingness to pay for different battery materials, whether that is the environmentally-conscious BEV owners or risk-averse PHEV owners.

Beyond the additional analysis of how demographic or other behaviors influence how consumers are sorted into different latent classes, it is also important to examine how the performance of recycled or refurbished batteries compares to conventional cells, and whether those differences impact attributes (like range or final range) that are consistently ranked as important to larger groups of EV owners.

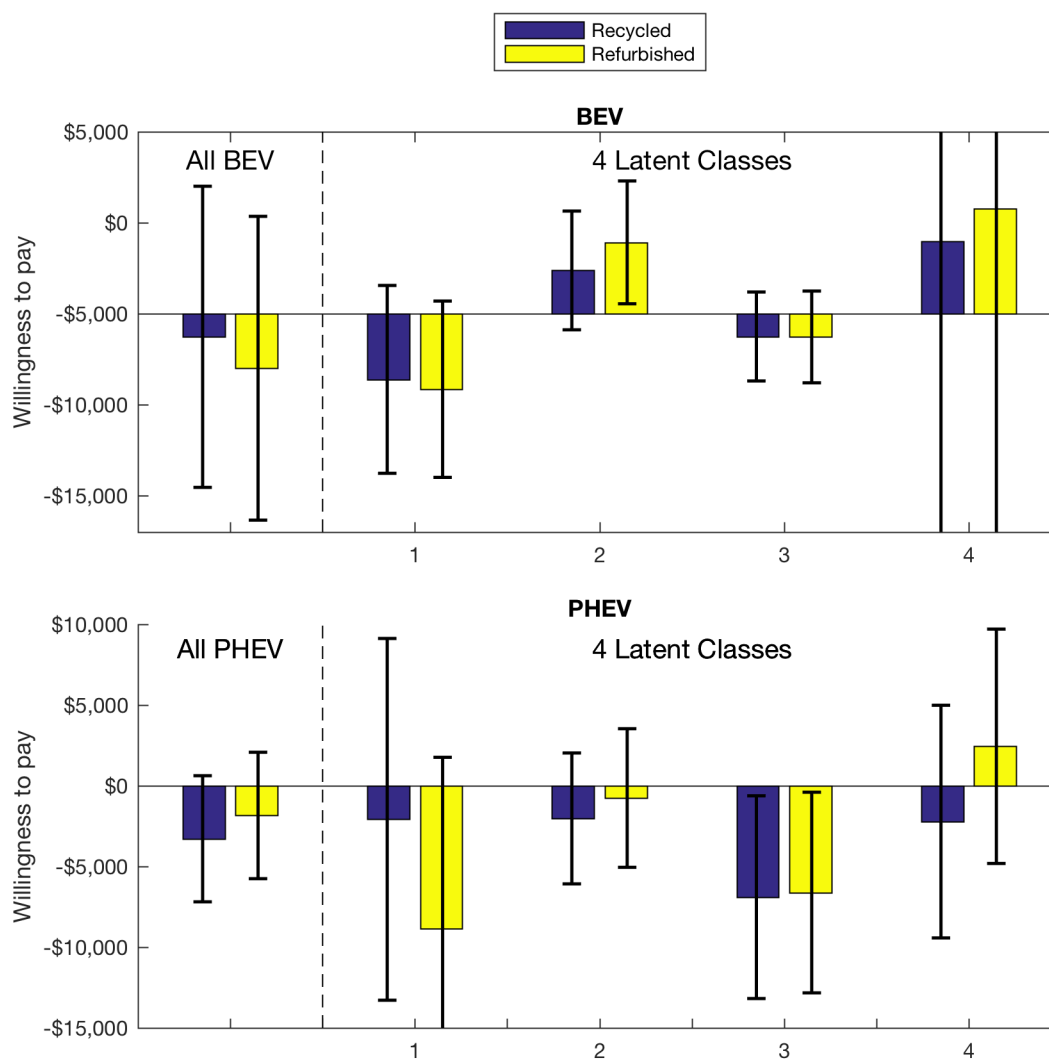


Figure 5.5: Overall and latent class perceptions of recycled and refurbished batteries for BEV and PHEV owners. Error bars represent the 95% confidence interval. The environmentally-conscious group of BEV owners (class 2), and risk-averse PHEV owners (class 3) are the only groups that have a willingness to pay that is significantly different from zero.

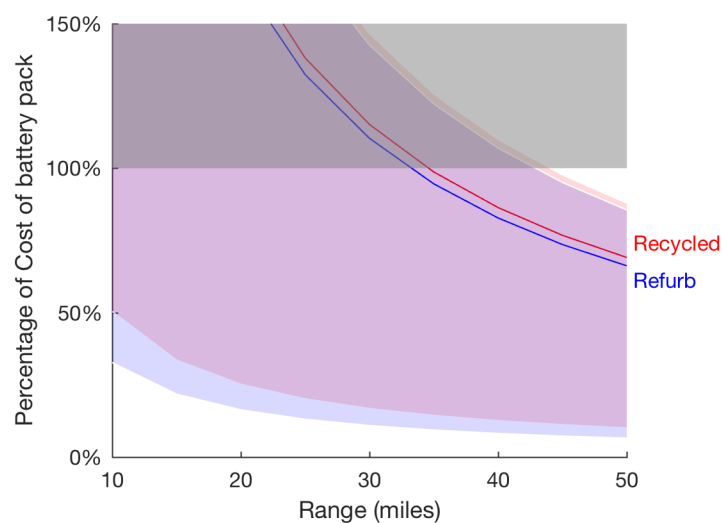


Figure 5.6: Percentage reduction in pack costs for risk-averse PHEV owners to be willing to accept recycled and refurbished battery materials. Accounting for the uncertainty in their aversion to both types of battery packs, the cost reductions for recycled battery packs to be competitive for very short range vehicles are high relative to overall pack cost at nearly 50%. Additional work is necessary to determine if there are any segments of the overall PHEV owners group where range influences overall willingness to pay for recycled and refurbished materials.

Chapter 6

Conclusions

Electrochemical energy storage has the potential to play an increasing role in decarbonized electricity and transportation sectors. However, to fully realized the technological potential, changes to the manufacturing, use, and retirement of batteries for widely-implemented storage applications may need to differ from initial innovations and policies.

6.1 Summary of Results

From the process based cost model of Chapter 2, we see that simple economies of scale increases will not be sufficient on their own to further reduce the cost of large-format lithium-ion cells. However, design decisions about the cell format and dimensions can reduce manufacturing costs by taking advantage of a lower ratio of non-storage components to electrode material. We also see that differences in cathode chemistry can exacerbate these differences, with lower specific-capacity materials that require cheaper input materials, more poised to take advantage of these changes in cell design. For example, for NMC and NCA cylindrical cells, the cost per kWh from shifting to larger cylindrical cells is somewhat dramatic ($\sim 25\%$ reduction), but switching from large cylindrical cells to prismatic cells offers relatively modest cost reductions. However, for LMO cells, with a lower specific energy storage capacity, the cost per kWh is halved when switching from cylindrical to prismatic cells, to a cost of roughly \$150/kWh.

The hybrid microgrid considered in Chapter 3 is one possible application of the lithium-ion batteries manufactured in Chapter 2. Although the cost of diesel electricity generation is still lower than the hybrid options considered, the performance of some lithium-ion batteries, combined with more moderate prices, is sufficient to make some lithium-ion batteries competitive with very inex-

pensive lead acid batteries. Depending on the assumed discount rate, high energy density lithium-ion batteries were the least expensive technology because of the ability to stagger replacements throughout the system lifetime. Very high performance lithium-ion batteries, which also have a high capital cost, were never the lowest cost option in this application, which requires more consistent, longer-duration charging and discharging to provide electricity when solar PV is not available.

The comparison of different battery recycling methods in Chapter 4 shows that traditional pyrometallurgical recycling is not an effective way to reduce the greenhouse gas emissions associated with disposing of lithium-ion batteries. However, direct cathode recycling, which recovers the high-value cathode materials does offer substantial emissions benefits by offsetting additional mining of materials and reducing the processing steps to manufacturing new batteries. Leveraging some of the process-based cost model information from Chapter 2, I also find that there is a window for the recovery of these materials to be cost competitive with cathode material that is manufactured from scratch.

However, the ability to sell this recovered cathode material is contingent on a market that is willing to accept recycled materials. In Chapter 5, I examine EV owner preference for these recycled battery materials. Although there is evidence that some consumers have a negative view of recycled battery materials, there is heterogeneity in their preferences, and for some consumers, the cost reductions offered by recycled and refurbished materials could outweigh any negative perceptions. Other vehicle attributes, like range and battery capacity over the warranty are generally more important, and additional analysis is necessary to determine if recycled or refurbished batteries would have an impact on those parameters.

6.2 Policy Recommendations

- Innovation for new batteries should focus on both higher energy-density materials, but also new ways of designing cells to minimize the costs of non-storage battery components.
- Energy storage incentives programs should allow for flexible duration of the technology use. In some applications, more frequent replacements of smaller energy storage components can offer lower costs than larger battery storage systems designed to operate for a longer time between replacements.
- Government regulations for automotive li-ion batteries should be at national level, ideally with

standardized labeling of the cell chemistry and manufacturer to enable more environmentally beneficial recycling methods.

Appendix A

Electric Vehicle Market Information and Process Based Cost Model Assumptions

A.1 Electric vehicle battery analysis

Combined BEV and PHEV vehicle sales in the US were roughly 419,000 from 2010 to the end of 2015, with a fairly even split between both types of electric vehicles (51.2% BEVs and 48.8% PHEVs). The total storage capacity of these vehicles is 11 GWh (8.9 - 12 GWh). However, the average storage capacity of BEVs and PHEVs varies significantly, with BEVs having a weighted average of 42 kWh (34-43 kWh), almost four times the capacity of PHEVs, which have an average of 10.5 kWh. Because of this difference, BEVs account for 81% (76%-82%) of the total storage capacity of EV batteries currently on the road.

The most abundant battery chemistry also differs for BEVs and PHEVs. For BEVs, NCA (lithium nickel cobalt aluminum oxide) batteries dominate. This is driven by both the popularity of the Tesla Model S, and the large storage capacity of the Model S, which varied between 60-90 kWh since the vehicle's introduction in 2012 [137, 138]. For plug-in hybrids, the dominant battery chemistry is also driven by one vehicle, the Chevrolet Volt, which features a larger than average 16-16.5 kWh storage capacity and high sales numbers. The Volt uses a combination LMO-NMC battery, and these two chemistries are the top two contributors in energy storage by kWh for PHEVs. While the chemistry was developed in partnership with Argonne National Lab, the exact

ratio of these two chemistries is uncertain [139, 140]. The baseline approximation results in NMC accounting for 67% (65%-77%) of all of the storage capacity in PHEVs, and 23% (10%-28%) of capacity in LMO batteries. Other manufacturers, including GS Yuasa and AESC have also filed patents for layered cathode materials, although it is unclear which exact chemistries, if any, have been implemented in vehicles, and is thus not included in these estimates [141–143].

NCA batteries are the most abundant in the US, with LMO making up the second largest portion. Lithium- nickel/manganese/cobalt oxide batteries with different ratios of the transition metals account for the 3rd and 4th largest portions. LFP and LTO batteries are the smallest contributors. However, it should be noted that LTO batteries are not currently being installed in new vehicles, and LFP batteries being installed in the Mercedes S550 PHEV, with both a small storage capacity and limited sales [144]. The use of LFP batteries in the Chevrolet Spark was discontinued in 2015, and the Honda Fit EV, which used LTO batteries, was intended to be a CARB compliance car, and was discontinued in 2014 [145–147]. Globally, the breakdown in cell chemistry may vary, particularly as China integrates LFP batteries into electric buses [148].

Table A.1: U.S. BEV sales and storage capacity, 2010-2015. Blank cells indicate no vehicle sales

Make & model	Chem.	2010/2011 Capacity Sales [kWh]	2012 Capacity Sales [kWh]	2013 Capacity Sales [kWh]	2014 Capacity Sales [kWh]	2015 Capacity Sales [kWh]	Sources
BMW i3	NMC				22 6,092	22 11,024	[149, 150]
Chevrolet	LFP			21.3 539	21.3 1,145		[151, 152]
Spark	LMO					5.7 2,629	[139, 145, 153]
	NMC					13.3	
Fiat 500e	NMC			24.0 2,310	24.0 5,132	24.0 6,194	[154, 155]
Ford Focus	LMO		6.9 680	6.9 1,738	6.9 1,964	6.9 1,582	[139, 156, 157]
Electric	NMC		16.1 680	16.1 1,738	16.1 1,964	16.1	
Honda Fit	LTO		20.0 93	20.0 569	20.0 407		[146, 147]
EV							
Kia Soul	NCM				27.0 359	27.0 1,015	[158, 159]
EV							
Mercedes	NCA				28.0 774	28.0 1,906	[160]
B-Class ED							
Mitsubishi	LMO	16.0 80	16.0 588	16.0 1,029	16.0 196	16.0 115	[161, 161]
i-MIEV							
Nissan	LMO	24.0 9,674	24.0 9,819	24.0 22,610	24.0 30,200	24.0 17,269	[143]
LEAF							
smart ED	NMC			17.6 923	17.6 2,594	17.6 1,387	[162]

Tesla Model S*	NCA		85.0	2,650	85.0	17,650	85.0	17,300	85.0	25,700	[137, 138]
Tesla Model X*	NCA								90.0	214	[163]
Toyota Rav-4 EV	NCA		41.8	192	41.8	1,096	41.8	1,184			[164]
Volkswagen e-Golf	NMC						24.2	357	24.2	4,232	[165, 166]

* Tesla reports sales at the time of purchase, not time of vehicle delivery

Table A.2: U.S PHEV sales and storage capacity, 2010-2015. Blank cells indicate no vehicle sales

Make & model	Chem.	2010/2011	2012	2013	2014	2015	Sources
		Capacity Sales [kWh]	Capacity Sales [kWh]	Capacity Sales [kWh]	Capacity Sales [kWh]	Capacity Sales [kWh]	
Audi A3	LMO					2.6	[167, 168]
	NMC					6.2	
BMW i8	NMC				7.1	2,265	[149, 169]
BMW X5	NMC					9.0	[170, 171]
Cadillac ELR	LMO			5.0	5.0	5.0	
	NMC			11.6	11.6	11.6	[139, 153, 172]
Chevrolet Volt	LMO	4.8	4.8	5.0	5.0	5.0	
	NMC	7,671	23,461	23,094	30,200	15,393	[139, 151, 173]
		11.2	11.2	11.6	11.6	11.6	
Ford C-Max Energi	NMC		7.6	7.6	7.6	7.6	[174, 175]
			2,374	7,154	8,433	7,591	
Ford Fusion Energi	NMC			7.6	7.6	7.6	[174, 176]
				6,089	11,550	9,750	
Honda Accord PHV	LMO			6.7	6.7	6.7	[151]
				526	449	64	
Hyundai	LMO					2.9	[177–179]
						160	

Sonata PHV	NMC						6.9	
Mercedes S550 PHV	LFP						8.7	118 [144]
Porsche Cayenne- SE	NCM					10.8	10.8	1,103 [180–182]
Porsche Panamera- SE	NCM			9.4	86	9.4	9.4	407
Porsche 918 Spyder	NCM						6.8	203 [181, 182]
Toyota Prius PHV	NCA	4.4	12,750	4.4	12,088	4.4	4.4	4,191 [166, 183, 184]
Volvo XC 90	LMO NMC						2.8 6.4	86 [153, 185, 186]

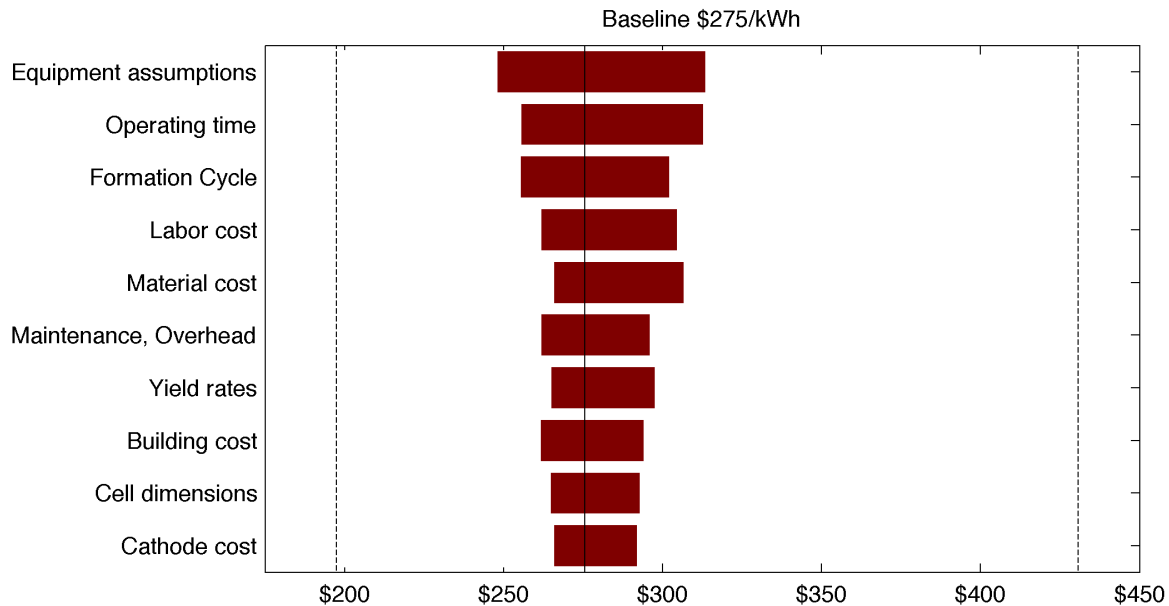


Figure A.1: Material costs per kWh of 18650 cylindrical and prismatic NCA cells

A.2 Uncertainty Analysis

There were many sources of uncertainty within the model. The sources are listed below, and their individual uncertainty contributions are shown in Figure A.1

A.2.1 Equipment Assumptions

This included capital equipment, process rates, labor, and footprint assumptions for the precursor preparation and cylindrical cell-specific steps included in the model (Steps 2, 8-11, 12 in Table 2.4).

A.2.2 Operating Time

The total operating time varied depending on the operating days per year and the length of breaks per shift (both paid and unpaid), as listed in Table 2.2.

A.2.3 Formation Cycle

This included the capital equipment, process rate, labor, and footprint assumptions for the formation cycle step of the model (Step 12 in Table 2.4). These assumptions are also included in the

sensitivity analysis on all of the equipment assumptions, but the formation cycle dominates these impacts because of the expense associated with the long duration of the process and the low batch size.

A.2.4 Labor Cost

The hourly price of labor varied from \$15-\$25/hour from a baseline of \$18/hour (Table 2.2)

A.2.5 Cell dimensions

The cell dimension uncertainties were related to how much material was actually contained per cell. The active volume (or volume of the cell not devoted to the housing structure), porosity of the separator (which affected how much electrolyte was necessary), and the anode density all varied. Values are listed in Table A.3

Table A.3: Cell dimension parameter values

Cell dimension parameter	Baseline	Units	Lower	Upper
Active volume	85	%	90	80
Separator porosity	42	%	40	44
Anode density	1.38	g/cm ³	0.6	2.1

A.2.6 Cell Yield rates

The cell yield rate varied from 90-99% from a baseline of 95%, as listed in Table 2.3.

A.2.7 Material Cost

Uncertainty in the materials cost included the cathode precursor material uncertainties (listed in Table A.4), along with the uncertainties on the material inputs presented in BatPaC.

Table A.4: Material cost values (excluding cathode precursors)

Material	Baseline	Units	Lower	Upper
Cathode foil	\$0.33	\$/m ²	\$0.33	\$0.87
Anode foil	\$1.31	\$/m ²	\$1.31	\$1.96
Separators	\$1.31	\$/m ²	\$1.31	\$2.18
Electrolyte	\$18.53	\$/l	\$18.53	\$19.62
Cell container	\$0.25	\$/cell	\$0.24	\$0.30

A.2.8 Maintenance and overhead

There is uncertainty on the percentage markup for maintenance and overhead. Maintenance costs varied from 5-15% of the annualized equipment expense, while overhead varied from 30-35% of the sum of annualized capital equipment cost, annualized building expenses, auxiliary equipment expenses, and maintenance.

A.2.9 Building cost

The cost per square meter varied from \$1600 to \$4000 from a baseline value of \$3000 (as listed in Table 2.2).

A.2.10 Cathode Cost

Cathode material cost uncertainties were based on market uncertainty and the content of the materials in other compounds. They are listed in Table A.5.

Table A.5: Cathode precursor cost assumptions

Material	Baseline	Units	Lower	Upper
Li ₂ Co ₃	\$7.46	\$/kg	\$6.63	\$8.67
Mn ₃ O ₄	\$0.01	\$/kg	\$0.01	\$0.01

A.3 Cost drivers by process step

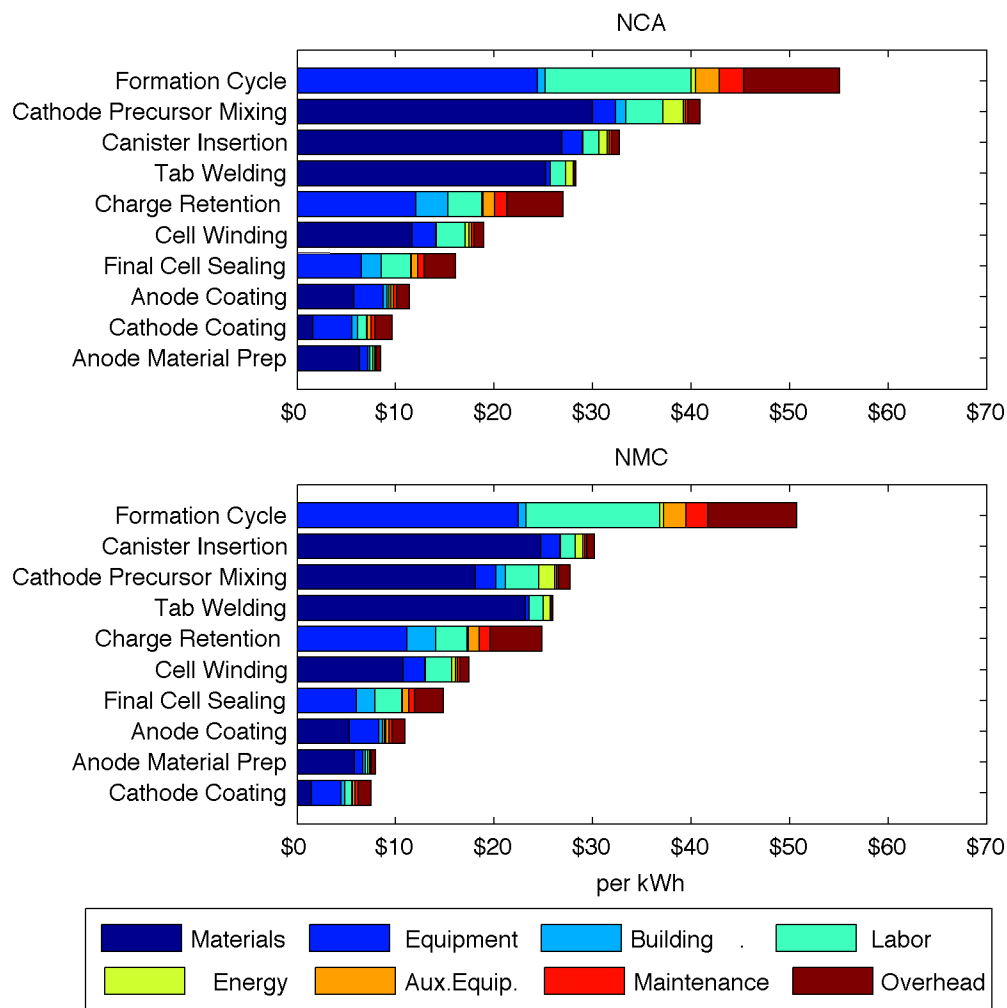


Figure A.2: Per kWh costs by manufacturing step for baseline NCA and NMC cell production

A.4 Assumptions for prismatic cells

Table 2.3 lists the equipment assumptions for cylindrical cell manufacturing, including steps 8-11 and 13, which are specific to cylindrical cells. For the prismatic cell cost comparison, we used different equipment assumptions (drawn from Sakti et al and updated for 2015\$) [10]. Those assumptions are listed in Table A.6. The physical parameters used to determine the materials per cell are listed in Table A.7.

Table A.6: Prismatic cell step assumptions

Step	Equipment Cost (millions of \$)	Footprint (m ²)	Fractional use of labor	Process rate	Unplanned Downtime	Dedicated (Yes/No)
8 Cell stacking [†]	1.09	150	1.25	225 bicell layers/min	20%	Yes
9 Tab welding [†]	1.09	150	1.25	5 cells/min	20%	Yes
10 Enclosing Cells [†]	0.82	150	0.75	5 cells/min	20%	Yes
11 Filling & first seal [†]	1.36	225	1.25	5 cells/min	20%	Yes
13 Formation cycling	0.93	63	0.23	500 cells/16 hours	20%	Yes

[†] Steps enclosed in dry room control system, which is sized based on the building area required for these steps

Table A.7: Prismatic cell physical parameters

Chemistry	LMO spinel	NMC $\text{Li}_{1.05}(\text{Ni}_{4/9} \text{ Mn}_{4/9} \text{ Co}_{1/9})_{0.95} \text{ O}_2$	NCA $\text{LiNi}_{0.8} \text{ Co}_{0.15} \text{ Al}_{0.05} \text{ O}_2$
Cell capacity	26.8 Ah	28.9 Ah	29.3 Ah
Cell Volume	258 cm ³	192 cm ³	201 cm ³
Bicell Layers	10	10	9
Cathode Thickness	200 μm	147 μm	160 μm
Anode Thickness	121 μm	200 μm	200 μm
Power limit per cell	0.55 kW	0.24 kW	0.27 kW

A.5 Cascading Unplanned Downtime in Sequenced Processes

Several of the steps in the manufacturing process are connected very closely to preceding or following steps, thus the assumption that the unplanned downtime for each step is independent from others is not entirely correct. The equipment assumptions included here do not account for perfectly scaled equipment where the process rates are exactly the same for each step in the process, and we assume some allowances for material handling between lines.

However, for some portions of the process, these steps are connected and have similar processing rates. The combinations of steps where this is the case are listed in Table A.8, along with the cumulative operating probability (calculated with the same unplanned downtime assumptions from Table 2.4. Overall, the impact of these larger cumulative downtimes is fairly minimal on the overall cost per kWh of cells produced. The cost per kWh, along with the changes from the original

Table A.8: Connected Manufacturing Steps and Cumulative Operating Time

Steps	Cumulative Operating Probability
Cathode Coating, Solvent Recovery, Cathode Calendaring	39%
Anode Coating, Anode Calendaring	49%
Electrode Slitting, Electrode Drying	64%
Cell Winding, Tab Welding, Canister Insertion, Electrolyte Fill & Seal	41%

Table A.9: Change in cost per kWh as a result of cascading unplanned downtime

	Production Volume	NMC		NCA	
		18650	20720	18650	20720
Cost per kWh	2 GWh	\$270 (\$197 - \$436)	\$204 (\$147-\$325)	\$303 (\$223-\$483)	\$232 (\$169 - \$367)
	4 GWh	\$266 (\$193-\$432)	\$200 (\$144-\$323)	\$302 (\$219-\$481)	\$228 (\$167-\$363)
	8 GWh	\$265 (\$192-\$420)	\$199 (\$143-\$320)	\$300 (\$218-\$479)	\$227 (\$165-\$362)
Cost Increase per kWh	2 GWh	\$23 (\$14-\$48)	\$16 (\$8-\$33)	\$22 (\$14-\$53)	\$18 (\$9-\$36)
	4 GWh	\$21 (\$12-\$47)	\$15 (\$9-\$34)	\$23 (\$13-\$52)	\$16 (\$10-\$37)
	8 GWh	\$21 (\$12-\$47)	\$15 (\$9-\$34)	\$23 (\$13-\$51)	\$17 (\$9-\$38)
Percentage Increase	2 GWh	9% (8% - 12%)	8% (6% - 11%)	8% (7% - 12%)	8% (6%-11%)
	4 GWh	9% (7% - 12%)	8% (7% - 12%)	8% (6% - 12%)	8% (6%-11%)
	8 GWh	9% (7% - 12%)	8% (7% - 12%)	8% (6% - 12%)	8% (6%-12%)

assumptions, are listed in Table A.9

Appendix B

Calculation Details for Battery Model Calculations

B.1 Carbon Tax Calculations

Using Excel Solver, diesel prices need to increase by 20.5% to \$1.82/l to become indifferent between diesel-only generation and a hybrid system with lead-acid batteries

There are 22.38 pounds of CO₂/gallon of diesel (5.91 lbs CO₂/L)

$$\frac{\$1.82 - \$1.50}{1 \text{ L}} \bigg| \frac{1 \text{ L}}{5.91 \text{ lbs CO}_2} = \$0.054/\text{lb CO}_2 = \$108.25/\text{ton CO}_2$$

B.2 Generation Subsidy Calculations

The required subsidy per kilowatt hour was calculated by reducing the system operation costs on a per kilowatt-hour basis for the net present value calculation for the system levelized cost of electricity. It was assumed that the \$0.092/kWh subsidy was applied to all power generated by the hybrid system. If the subsidy is applied only to the power produced from renewable resources, the subsidy required increases slightly to \$0.095/kWh.

B.3 Power Flow Optimization

Objective $\min_{\mathbf{x}, \mathbf{u}, \mathbf{p}, \mathbf{q}} f(\mathbf{x}) = \sum_{i=1}^T x_i^{GEN}$

Minimize diesel generation costs

Where state variables: $\mathbf{x} = \begin{bmatrix} x_i^{GEN} \\ x_i^{BAT} \end{bmatrix} \forall i \in T$

Power from generator

Power stored in batteries

control variables: $\mathbf{u} = \begin{bmatrix} u_i^{GEN} \\ u_i^{CHARGE} \\ u_i^{DISCHARGE} \end{bmatrix} \forall i \in T$

Change in power from generator

Power to charge batteries

Power to discharge batteries

slack variable: $\mathbf{p} = \begin{bmatrix} p_i^{GEN} \\ p_i^{SOLAR} \\ p_i^{BAT} \\ p_i^{LOAD} \end{bmatrix} \forall i \in T$

Power flows from generator

Power flows from solar PV

Power flows from batteries

Power flows to load

slack variable: $\mathbf{q} \in \mathbb{R}^{4 \times T}$

Subject to $\mathbf{x}_{i+1} = \mathbf{A}\mathbf{x}_i + \mathbf{B}\mathbf{u}_i \quad \mathbf{A} = \begin{bmatrix} 1 & 0 \\ 0 & 1 \end{bmatrix}, \mathbf{B} = \begin{bmatrix} 1 & 0 & 0 \\ 0 & \eta & -1 \end{bmatrix}$

$\mathbf{p} = \mathbf{B}^{ELEC} \mathbf{q}$

$p_i^{GEN} = x_i^{GEN} \forall i$

$p_i^{BAT} = u_i^{DISCHARGE} - u_i^{CHARGE} \forall i$

Power from batteries is difference between discharging and charging

$p_i^{SOLAR} \leq E_i^{SOLAR}$

Power from solar less than or equal to available solar resources

$p_i^{LOAD} = E_i^{LOAD}$

Power to load must equal demand

$\begin{bmatrix} 0 \\ (1-S)C^{INITIAL} \end{bmatrix} \leq \mathbf{x} \leq \begin{bmatrix} 100 \\ C \end{bmatrix}$

Generator limit

Battery state of charge limits

$\begin{bmatrix} -100 \\ 0 \\ 0 \end{bmatrix} \leq \mathbf{u} \leq \begin{bmatrix} 100 \\ l^{CHARGE} \\ l^{DISCHARGE} \end{bmatrix}$

Ramping constraints

Battery charging limit

Battery discharging limit

Table B.1: Power Flow Optimization Parameters

Parameter	Value	Description
T	169	Calculated timeframe, equal to 1 week in hourly increments + 1
η	0.9	Battery round-trip efficiency
\mathbf{B}^{ELEC}	$\begin{bmatrix} 100 & 0 & 0 & -100 \\ 0 & 200 & -100 & -100 \\ 0 & -100 & 200 & -100 \\ -100 & -100 & -100 & 300 \end{bmatrix}$	DC power flow susceptance matrix
E_i^{SOLAR}	varies	Solar power resources available
E_i^{LOAD}	varies	Electricity demand
S	varies (0.3 - 0.9)	State of charge swing
$C^{INITIAL}$	varies	Initial total storage capacity
C	varies	Current storage capacity, recalculated on weekly basis
I^{CHARGE}	varies	Limit on power flow to charge battery
$I^{DISCHARGE}$	varies	Limit on the power flow to discharge the battery

B.4 Battery Degradation Models & Manufacturer Data

Storage capacity was recalculated on a weekly basis to appropriately model the reduction in available storage over time. $C \in \mathbb{R}^N$ where N is the number of weeks in the simulation

$$C_{n+1} = C_n - C_n^{LOSS} \quad (\text{B.1})$$

Where C^{LOSS} is a function dependent on the properties of the battery chemistry (see Table B.2) and the number of cycles, Y :

$$Y_n = \frac{\sum_{i=1}^{T-1} u_i^{DISCHARGE}}{C^{INITIAL}} \quad (\text{B.2})$$

Limits on the power flow to charge and discharge the batteries also varied for the different chemistries considered. These limits are listed in Table B.3. C was not allowed to drop below 80% of the initial capacity ($0.8C^{INITIAL}$). If it did, the initial storage capacity was increased, and new capacity degradation was recalculated.

Table B.2: Capacity Loss Calculations for different battery chemistries

Battery Chemistry	Formula
Lead-acid	$C_n^{LOSS} = 0.0002 \times C^{INITIAL} \times Y_n$
A123	$C_n^{LOSS} = (5 \times 10^{-6} t^{AVG}) Y_n C^{INITIAL}$ where t^{AVG} is the average temperature in week n
Panasonic	$C^{LOSS} = 0.0005 \times C^{INITIAL} \times Y_n$

Table B.3: Charging and Discharging Power Flow Limits

Battery Chemistry	Charging Limit (l^{CHARGE})	Discharging Limit ($l^{DISCHARGE}$)
Lead acid	$C_n/4$	$C_n/4$
A123	10.8 W/cell [†]	16.5 W/cell [†]
Panasonic	8.09 W/cell [†]	9.9 W/cell [†]

[†] Based on manufacturer data, scaled to the number of cells per 1kWh capacity stack and the number of stacks

B.5 Matlab Solvers

Power flow optimization calculations to minimize diesel consumption were computed using the YALMIP toolbox with an SDPT3 solver in MATLAB. YALMIP is capable of solving linear, quadratic, and second-order cone programs using semidefinite programming. The problem formulated is an affine system with a convex linear objective function, with linear constraints. SDPT3 is a second-order cone programming solver capable of handling this problem formulation.

Appendix C

Recycling Model Assumptions and Detailed Results

Table C.1: Cell Input Assumptions for NMC Cells. Baseline assumptions are listed along with upper and lower bounds (italicized)

Input	Units	Cell Dimensions		Distribution
		18650 canister, 70m electrode	20720 canister, 100m electrode	
Steel	g	13.23 <i>(12.74-24.47)</i>	18.87 <i>(17.42-34.83)</i>	Triangular
Aluminum	g	1.65 <i>(1.55-1.74)</i>	1.69 <i>(1.59-1.79)</i>	Triangular
Copper wire	g	4.97 <i>(4.67-5.26)</i>	5.1 <i>(4.8-5.4)</i>	Triangular
Cathode Active Material	g	14.93 <i>(14.06-15.81)</i>	21.92 <i>(20.63-23.21)</i>	Triangular
Graphite	g	6.78 <i>(2.78-10.93)</i>	9.95 <i>(4.07-16.04)</i>	Triangular
PVDF	g	1.2 <i>(0.94-1.46)</i>	1.76 <i>(1.37-2.15)</i>	Triangular
LiPF ₆	g	0.81 <i>(0.75-0.86)</i>	1.12 <i>(1.04-1.19)</i>	Triangular
Electrolyte (EC/DC)	g	4.43 <i>(4.13-4.94)</i>	6.12 <i>(5.72-6.82)</i>	Triangular
Polypropylene	g	0.84 <i>(0.79-0.89)</i>	0.86 <i>(0.81-0.91)</i>	Triangular
Specific Capacity	mA/g	200		Point Estimate
Voltage	V	3.57		Point Estimate

Table C.2: Cell Input Assumptions for NCA Cells. Baseline assumptions are listed along with upper and lower bounds (italicized)

Input	Units	Cell Dimensions		Distribution
		18650 canister, 70m electrode	20720 canister, 100m electrode	
Steel	g	13.23 (12.74-24.47)	18.87 (17.42-34.83)	Triangular
Aluminum	g	1.65 (1.55-1.74)	1.69 (1.59-1.79)	Triangular
Copper wire	g	4.97 (4.67-5.26)	5.1 (4.8-5.4)	Triangular
Cathode Active Material	g	15.33 (14.43-16.23)	22.5 (21.18-23.83)	Triangular
Graphite	g	6.78 (2.78-10.93)	9.95 (4.07-16.04)	Triangular
PVDF	g	2.25 (1.93-2.58)	3.3 (2.83-3.79)	Triangular
LiPF ₆	g	0.81 (0.75-0.86)	1.12 (1.04-1.19)	Triangular
Electrolyte (EC/DC)	g	4.43 (4.13-4.94)	6.12 (5.72-6.82)	Triangular
Polypropylene	g	0.84 (0.79-0.89)	0.86 (0.81-0.91)	Triangular
Specific Capacity	mA/g	180		Point Estimate
Voltage	V	3.55		Point Estimate

Table C.3: Material inputs and output for cathode precursor mixing step using nitrate precursor materials

Input	Units	NMC (NiMnCo(OH) ₂)	NCA (NiCo(OH) ₂)
Ni(NO ₃) ₂	g	81.2	153.86
Co(NO ₃) ₂	g	20.33	28.89
Mn(NO ₃) ₂	g	79.53	0
Energy	kWh	0.34	0.34
Output	g	91.07	92.75

Table C.4: Material inputs and output for cathode precursor mixing step using sulfate precursor materials

Input	Units	NMC (NiMnCo(OH) ₂)	NCA (NiCo(OH) ₂)
NiSO ₄	g	68.78	130.32
CoSO ₄	g	17.22	24.47
MnSO ₄	g	68.78	0
NaOH	g	79.99	79.99
NH ₃ OH	g	7.01	7.01
Energy	kWh	0.34	0.34
Output	g	91.07	92.75

Table C.5: Material and energy inputs for manufacturing sulfate precursor materials

Input	Units	NiSO ₄	CoSO ₄	MnSO ₄
Transition Metal	kg	334.06	438.17*	330.22
Sulfuric Acid	kg	574.96	574.25	598.74
Energy (natural gas)	kWh	193.43	0	0
Output	kg	907.18	907.18	907.18
Source		Dunn et al (2014) [83], GREET 2016 [86]	Calculated	Dunn et al (2014) [83], GREET 2016 [86]

* cobalt oxide

Table C.6: Material inputs for manufacturing nitrate precursor materials

Input	Units	Ni(NO ₃) ₂	Co(NO ₃) ₂	Mn(NO ₃) ₂
Transition Metal	kg	292.11	371.95*	70.94
Nitric Acid	kg	625.05	625.05	126.04
Output	kg	907.18	907.18	178.96
Source		Wang et al [78]	Wang et al (2015) [78]	Calculated

* cobalt oxide

Table C.7: Material inputs and output for lithiation of NMC and NCA

Input	Units	NMC	NCA
Precursor	g	86.51	88.11
Li ₂ CO ₃	g	38.79	35.95
Al(OH) ₃	g	0	3.9
Energy	kWh	0.61	0.62
Output	g	93.48	96.08

Table C.8: Energy inputs for cathode drying and calcining

Chemistry	NMC	NCA
Precursor Drying [kWh/kg cathode]	3.7 2.6-4.8	3.6 2.6-4.7
Calcining [kWh/kg cathode]	6.5 3.9-9.5	6.5 3.9-9.5
Energy Source	Natural Gas (kiln)	Natural Gas (kiln)

Table C.9: Emissions and heat input assumptions for electricity and natural gas inputs

Energy Source	Natural gas fired kiln	US Mix	NWPP	RFCM
CO _{2e} [kg/kWh]	0.257	0.5093	0.4114	0.6947
Heat Input [MJ/kWh]	4.004	6.83	5.16	8.64
NO _x [kg/kWh]	0.004	0.0004	0.0005	0.0006
SO _x [kg/kWh]	0.058	0.0007	0.0003	0.0016
Source	GREET 2016 [86]	eGrid 2014 [84]		

Table C.10: Embodied emissions for cathode materials

Input	CO _{2e} emissions [kg CO _{2e} /kg material]	Resources [MJ/kg material]	Recycled Material in Baseline Assumption	Distribution	Source
Nickel	5.76 1.6 - 9.03	83 23 - 131	44% -	Triangular	REET 2016 [86]
Cobalt Oxide	8.20 1.6 - 14.7	121 23 - 199	44% -	Triangular	REET 2016 [86]
Manganese	9.05	122	0%	Point Estimate	REET 2016 [86]
Lithium Carbonate	3.94	43	-	Point Estimate	REET 2016 [86]
Aluminum Hydroxide	0.741	10	-	Point Estimate	REET 2016 [86]
Sulfuric Acid	0.014	0.20	-	Point Estimate	REET 2016 [86]
Nitric Acid	2.04	12	-	Point Estimate	REET 2016 [86]
NaOH	2.3	33	-	Point Estimate	REET 2016 [86]
NH ₃ OH	2.76	43	-	Point Estimate	REET 2016 [86]

Table C.11: Embodied Emissions for Cell Materials (excluding cathode)

Input	CO _{2e} emissions [kg CO _{2e} /kg material]	Resources [MJ/kg material]	Recycled Material in Baseline Assumption	Distribution	Source
Steel	3.86 (1.54 - 4.69)	45 (22 - 53)	73.6%	Triangular	REET 2016 [86]
Aluminum	3.09 (2.0 - 9.27)	49 (31 - 150)	85%	Triangular	REET 2016 [86]
Copper	3.28	40	-	Point Estimate	REET 2016 [86]
Graphite	5.25	92	-	Point Estimate	REET 2016 [86]
PVDF	2.55	37	-	Point Estimate	REET 2016 [86]
LiPF ₆	13.26	188	-	Point Estimate	REET 2016 [86]
Electrolyte (EC/DC)	0.5	10	-	Point Estimate	REET 2016 [86]
Polypropylene	2.73	80	-	Point Estimate	REET 2016 [86]

Table C.12: Per ton-mile emissions for water, rail, and road transport

Method	CO _{2e} emissions CO _{2e} /ton-mile	Resources [MJ/ton-mile]	Source
Water	0.007	0.174	REET 2016 (Marine Plug-in) [86]
Rail	0.0266	0.34	
Road	0.0863	1.111	

Table C.13: Transportation Distance Assumptions (in miles) by mode for RFCM, NWPP, and US average

Material	RFCM			NWPP			US Average		
	Water	Rail	Road	Water	Rail	Road	Water	Rail	Road
Steel	10500	600	50	6000	600	50	8250	600	50
Aluminum	0	600	50	0	800	50	0	700	50
Copper	0	600	50	0	700	50	0	650	50
Graphite	10500	600	50	6000	600	50	8250	600	50
PVDF	0	500	50	0	500	50	0	500	50
LiPF ₆	0	500	50	0	500	50	0	500	50
Electrolyte	0	500	50	0	500	50	0	500	50
Polypropylene	0	500	50	0	500	50	0	500	50
Nitric Acid	0	500	50	0	500	50	0	500	50
Sulfuric Acid	0	500	50	0	500	50	0	500	50
Nickel	0	300	50	0	300	50	0	500	50
Cobalt	0	500	50	0	2500	50	0	1500	50
Manganese	0	700	50	0	2000	50	0	1350	50
Bauxite	1500	600	50	4000	600	50	2750	600	50
NaOH	0	500	50	0	500	50	0	500	50
Ammonium Hydroxide	0	500	50	0	500	50	0	500	50

Table C.14: Process inputs for pyrometallurgical Recycling. Emissions and Resource data sourced from GREET 2016.

Input	Units	Amount	CO _{2e} Emissions [kg CO2e/unit input]	Resources [MJ/unit input]
Li-ion batteries	kg	1200	Output of previous process	Output of previous process
Limestone	kg	100	0.013	0.18
Sand	kg	110	0	0
Slag*	kg	200	0	0
Coke	kg	400	3.51	36.87
Natural Gas (kiln)**	mmBtu	0.76	50.27	892
Total	Per 1200 kg batteries	-	1,456.98	15,658

*1% by weight Fe

** interview referenced in Dunn et al [83]

Table C.15: Percentage of metal content that goes to Slag and Alloy in pyrometallurgical process [1]

Component	Cu	Ni	Fe	CaO	SiO ₂	Al ₂ O ₃	Li ₂ O	Co
Slag	7.2	1.0	35.5	100	100	100	100	6.0
Alloy	92.8	99.0	64.5	0	0	0	0	94.0

Table C.16: Facility-wide parameter assumptions [2, 3]

Input	Base	Units	Optimistic	Pessimistic
Working days per year	300	Days/year	360	240
8-hour shifts per day	3	Shifts/day	3	3
Unpaid breaks per shift	1	Hours/shift	0.5	1.5
Paid breaks per shift	0.75	Hours/shift	0.5	1
Building Costs	\$3000	\$/m ²	1600	4000
Labor Rate	\$18	\$/hour	\$15	\$25
Building Useful Life	20	Years	20	20
Capital Useful Life	6	Years	6	6
Discount Rate	10%	%	10%	10%
Auxiliary Equipment Cost	10%	% of main machine cost	10%	10%
Maintenance	10%	% of main machine cost	5%	15%
Fixed Overhead	33%	% of main machine, building, aux. equip, and maintenance cost	30%	35%
Energy Cost	3%	% of material and labor cost	3%	3%
Natural gas price	2.8	Cents/kWh	2.2	3.7

Table C.17: Equipment, labor, and process rate assumptions for cathode manufacturing/ reprocessing steps [2]

Step	Equipment Cost (millions of \$)	Footprint (m ²)	Fractional use of labor	Process rate	Unplanned Downtime	Dedicated (Yes/No)
1 Receiving	3.6	900	3	6667 kg/shift	20%	Yes
2 Precursor preparation						
Mixing	0.55	200	0.67	1000 l/shift	25%	Yes
Drying	1.5 (1.2 - 1.8)	22 (20 - 25)	1	35 l/hr (29 - 44 l/hr)	25%	Yes
Mixing*	0.55	200	0.67	1000 l/shift	25%	Yes
Calcining*	1.5 (1.2 - 1.8)	22 (20 - 25)	1	20 l/hr (15 - 30 l/hr)	25%	Yes

* Steps shared by both cathode manufacturing from raw materials and reprocessing recovered cathode materials

Table C.18: Material price assumptions for cathode precursor metals and lithium carbonate. Data is based on USGS data [4]

Material	Price Assumption [\$/kg]
Nickel	\$14
Cobalt	\$12
Manganese	\$0.004
Aluminum	\$2.10
Lithium Carbonate	\$6.70 (\$6.10-\$25*)

* Not based on historical data, but instead the estimated cost of extracting lithium from seawater

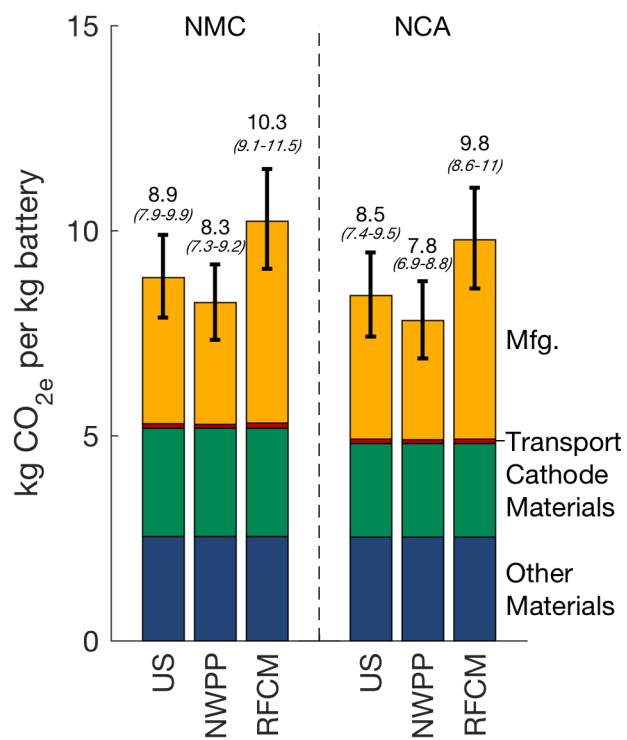


Figure C.1: kg CO_{2e} (with 95% confidence) per kg of cell emitted during the manufacturing process of NMC and NCA cylindrical cells for US average, NWPP, and RFCM average grid emissions.

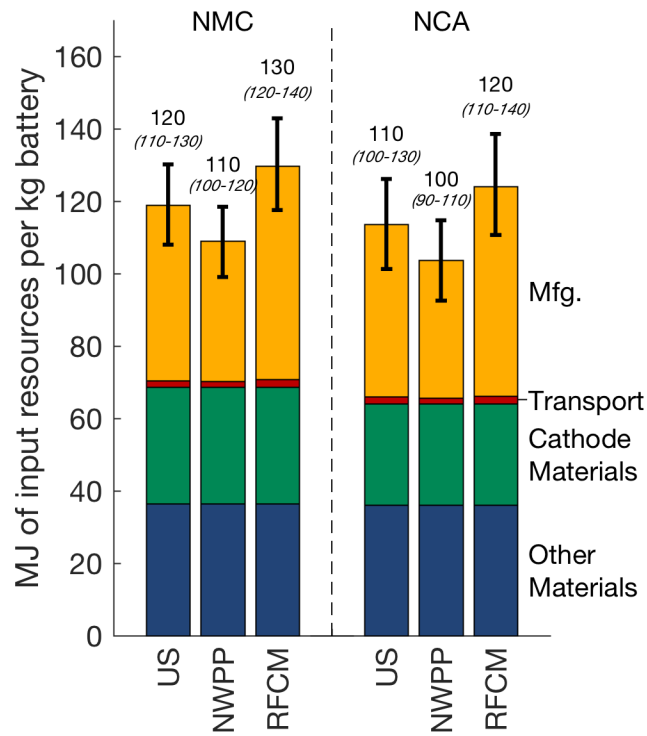


Figure C.2: MJ (with 95% CI) of input energy per kg of battery produced using a US average, NWPP, and RFCM grids

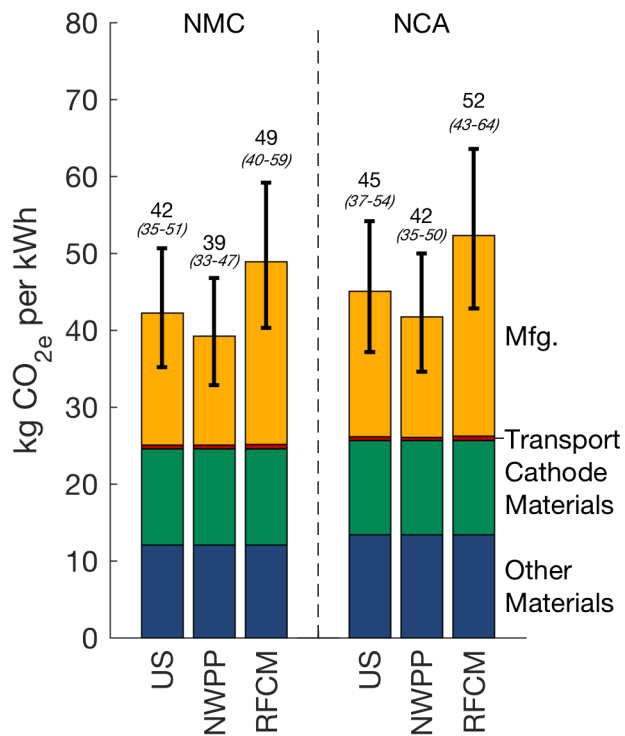


Figure C.3: kg CO_{2e} emitted per kWh of battery produced on US average, NWPP, and RFCM grids

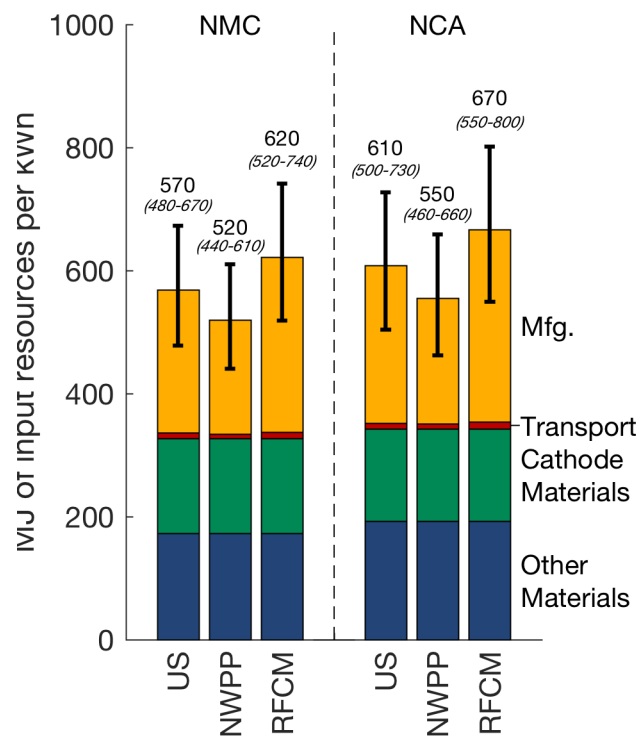


Figure C.4: MJ of input energy per kWh of battery produced on US average, NWPP, and RFCM grids

Table C.19: Comparison of greenhouse gas emissions and energy inputs to cell manufacturing between this and other studies per kWh of battery

Reference	Cathode Chemistry	Specific Energy [kWh/kg]	Greenhouse gas emissions [kg CO _{2e}] & input energy [MJ] per kg battery		
			Materials	Manufacturing	Total
Notter et al (2010) [90]	LMO	0.114	44 kg <i>750 MJ</i>	8.6 kg <i>160 MJ</i>	53 kg <i>910 MJ</i>
Zackrisson et al (2010) [91]	LFP	0.10	74 kg -	92 kg -	170 kg -
Majeau-Bettez et al (2011) [17]	NCM	0.112	140 kg <i>1200 MJ</i>	54 kg <i>710 MJ</i>	200 kg <i>1900 MJ</i>
	LFP	0.088	180 kg <i>1400 MJ</i>	69 kg <i>910 MJ</i>	250 kg <i>2300 MJ</i>
Dunn et al (2012) [77]	LMO	0.13	37 kg <i>560 MJ</i>	2.1 kg <i>21 MJ</i>	39 kg <i>580 MJ</i>
EPA (2013) [92]	Average	0.15	80 kg <i>1200 MJ</i>	33 kg <i>610 MJ</i>	110 kg <i>1800 MJ</i>
EPA (2013) <i>cells only</i> [92]	Average	0.09	69 kg <i>160 MJ</i>	0.59 kg <i>9.4 MJ</i>	69 kg <i>1000 MJ</i>
Ellingsen et al (2014) [93]	NCM	0.11	65 kg -	110 kg -	170 kg -
Ellingsen et al (2014) <i>cells only</i> [93]	NCM	0.17	53 kg -	110 kg -	160 kg -
Kim et al (2016) [94]	LMO/NCM	0.08	76 kg -	65 kg -	140 kg -
Kim et al (2016) <i>cells only</i> [94]	LMO/NCM	0.14	27 kg -	63 kg -	90 kg -
<i>This study</i> (US average power mix, 95% confidence intervals)	NMC	0.21	25 kg (21-29 kg) <i>330 MJ</i> <i>280-380 MJ</i>	17 kg (13-22 kg) <i>230 MJ</i> <i>180-300 MJ</i>	42 kg (35-51 kg) <i>570 MJ</i> <i>480-680 MJ</i>
			26 kg (21-31 kg) <i>340 MJ</i> <i>(280-400 MJ)</i>	19 kg (14-24 kg) <i>260 MJ</i> <i>(200-320 MJ)</i>	45 kg (37-54 kg) <i>610 MJ</i> <i>(500-730 MJ)</i>
	NCA	0.19			

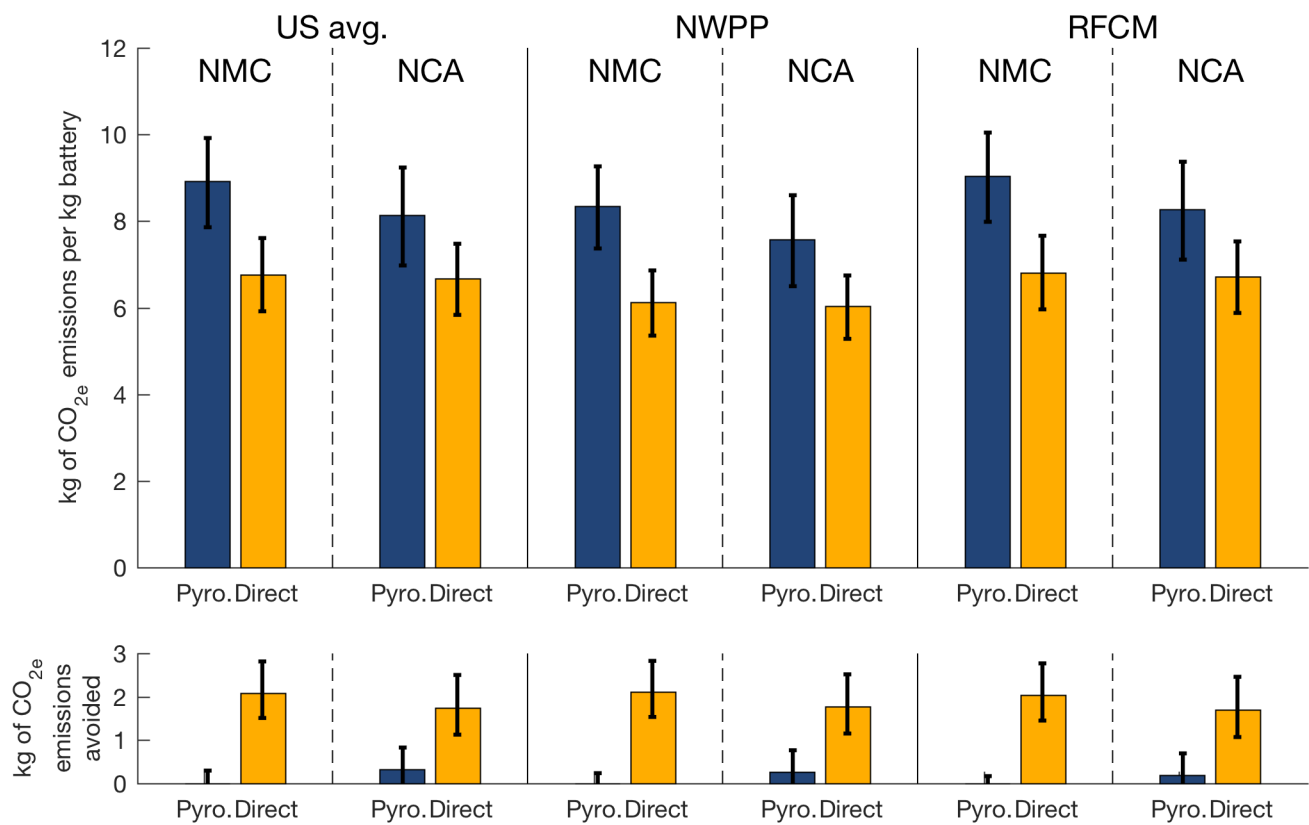


Figure C.5: Top: CO_{2e} emissions per kg of battery for battery manufacturing and pyrometallurgical recycling (blue) and for battery manufacturing and direct recycling (yellow) less the emissions offsets for product outputs for NCA and NMC cells on US average, NWPP, and RFCM grids. Bottom: Net CO_{2e} emissions avoided using a pyrometallurgical or direct recycling process. For NMC batteries, pyrometallurgical recycling has a median environmental cost (no CO_{2e} emissions avoided). For NCA cells, the emissions offsets of a pyrometallurgical process are not significantly different from zero.

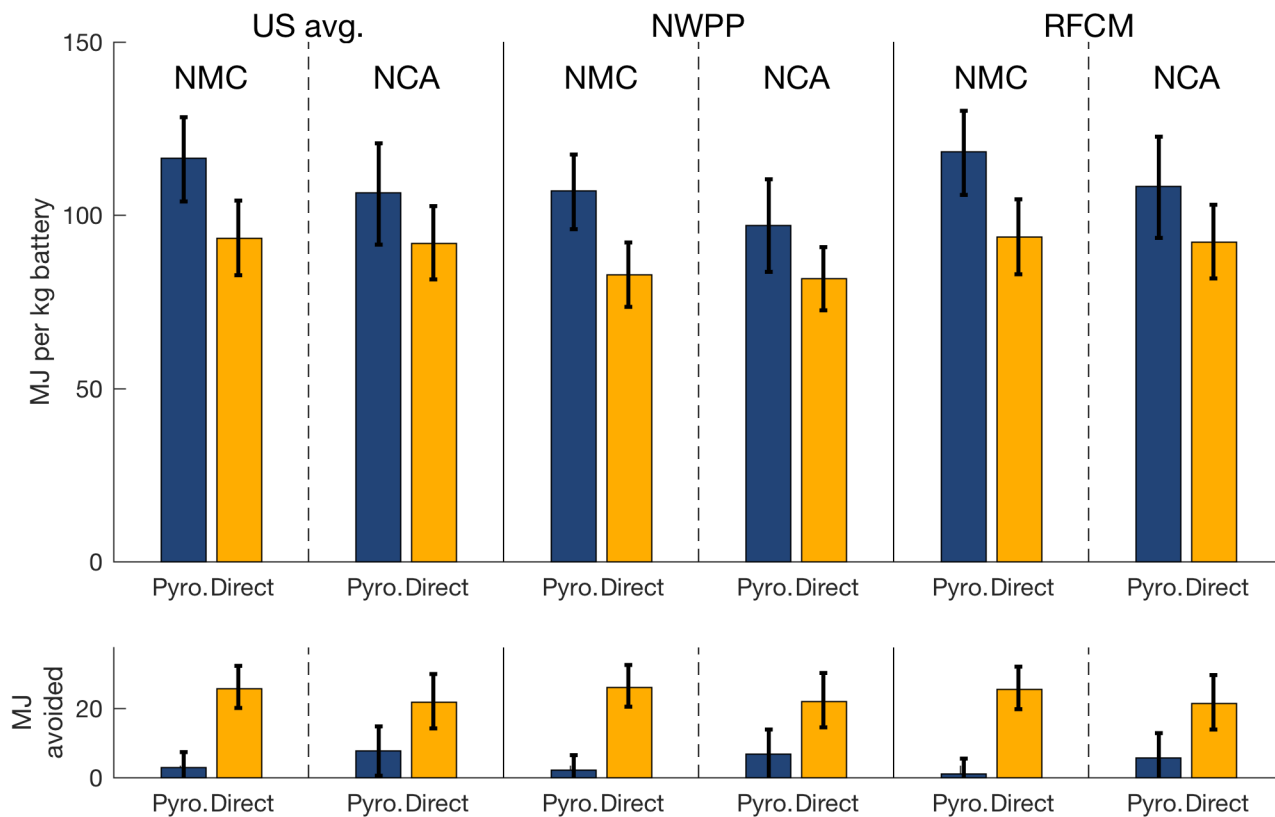


Figure C.6: Top: MJ of input energy per kg of battery for battery manufacturing and pyrometallurgical recycling (blue) and for battery manufacturing and direct recycling (yellow) less the emissions offsets for product outputs for NCA and NMC cells on US average, NWPP, and RFCM grids. Bottom: Net energy savings from using a pyrometallurgical or direct recycling process. For both chemistries, the median energy savings from pyrometallurgical recycling is positive, but not significantly different from zero.

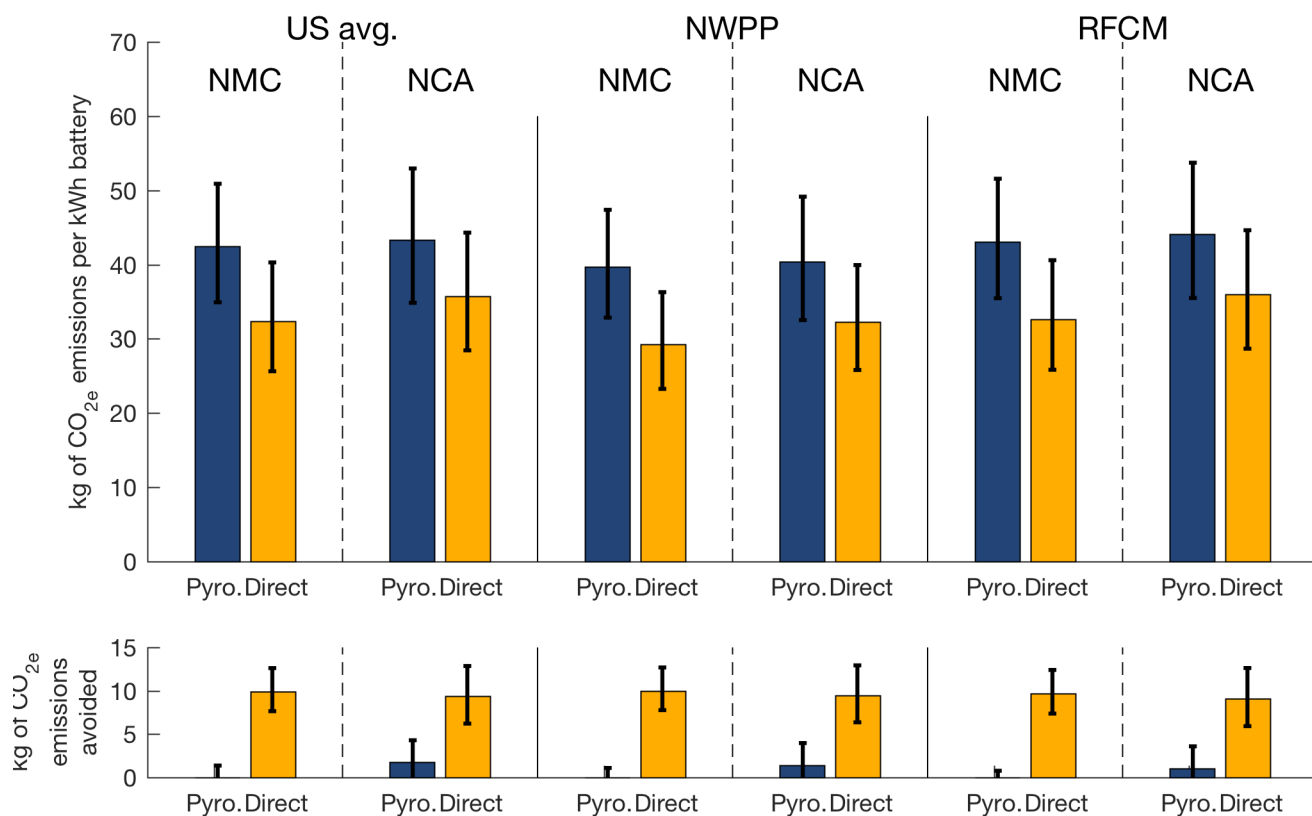


Figure C.7: Top: CO_{2e} emissions per kWh of battery for battery manufacturing and pyrometallurgical recycling (blue) and for battery manufacturing and direct recycling (yellow) less the emissions offsets for product outputs for NCA and NMC cells on US average, NWPP, and RFCM grids. Bottom: Net CO_{2e} emissions avoided using a pyrometallurgical or direct recycling process. For NMC batteries, pyrometallurgical recycling has a median environmental cost (no CO_{2e} emissions avoided). For NCA cells, the savings of a pyrometallurgical process are not significantly different from zero.

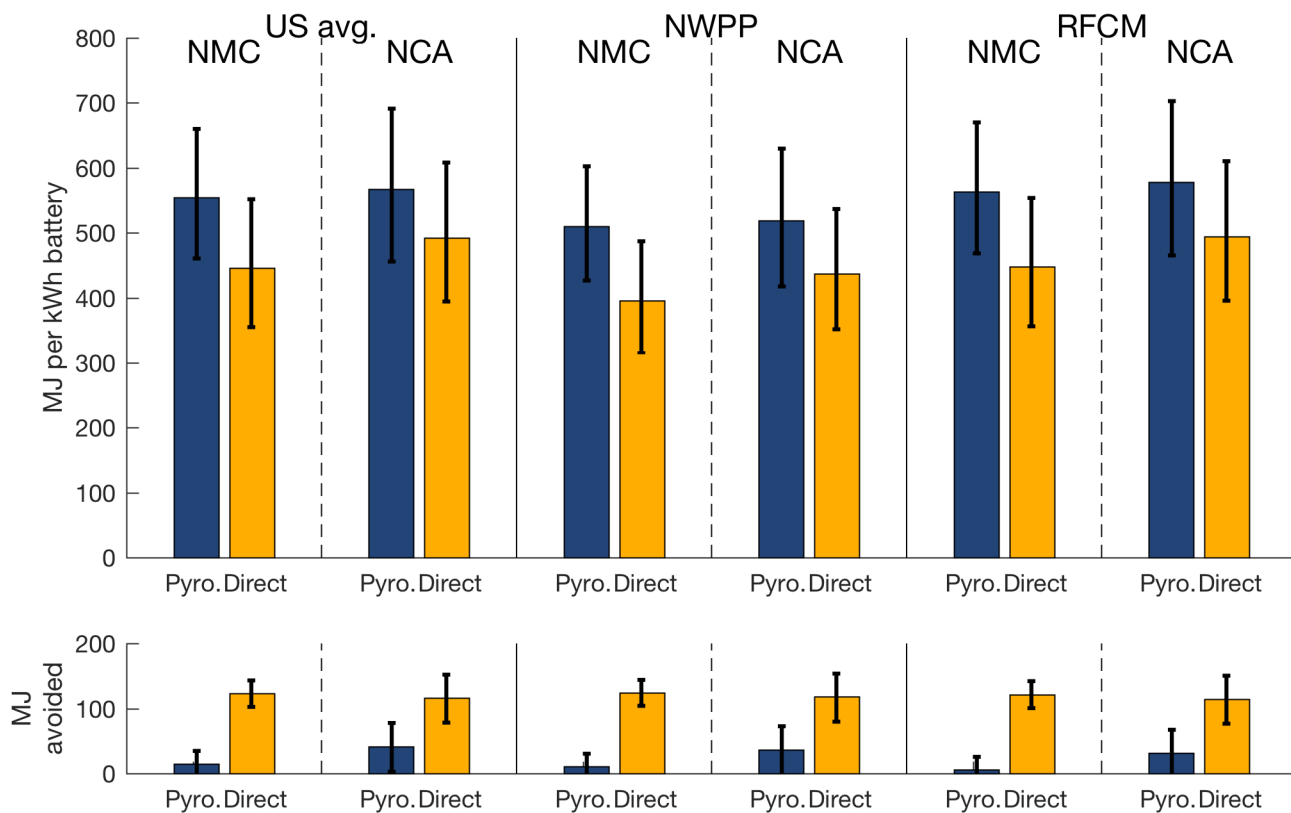


Figure C.8: Top: MJ of input energy per kg of battery for battery manufacturing and pyrometallurgical recycling (blue) and for battery manufacturing and direct recycling (yellow) less the emissions offsets for product outputs for NCA and NMC cells on US average, NWPP, and RFCM grids. Bottom: Net energy savings from using a pyrometallurgical or direct recycling process. For both chemistries, the median energy savings from pyrometallurgical recycling is positive, but not significantly different from zero.

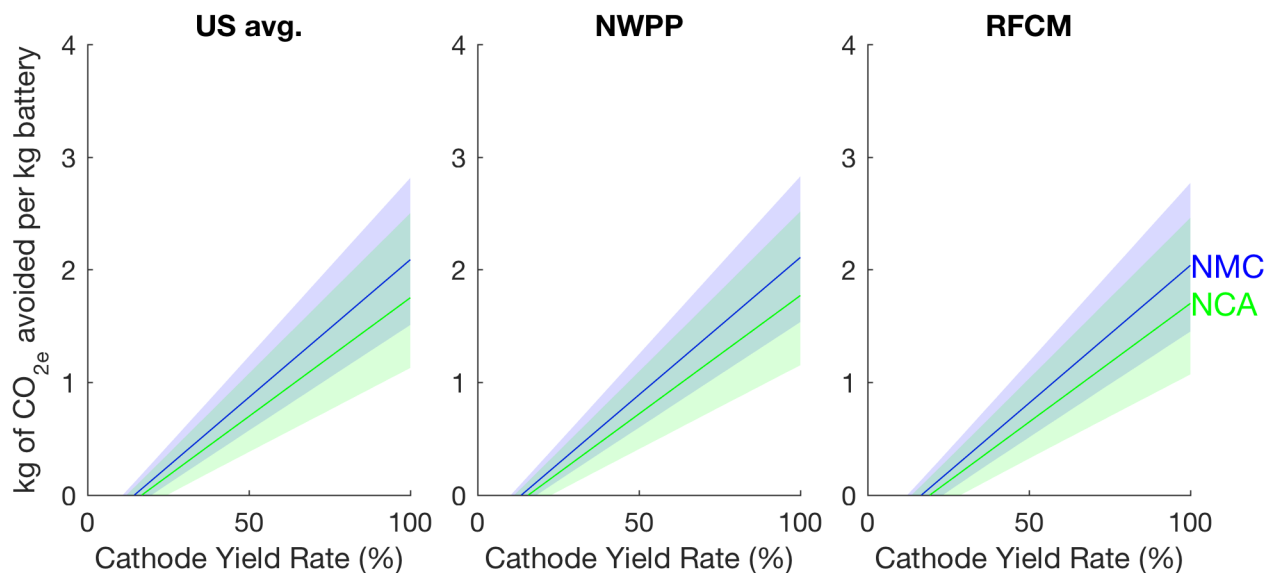


Figure C.9: net kg CO_{2e} avoided per kg of battery when combining manufacturing with direct cathode recycling over using no recycling method after manufacturing. Yield rates of recovered cathode material vary from 0 to 100% for both NMC and NCA chemistries.

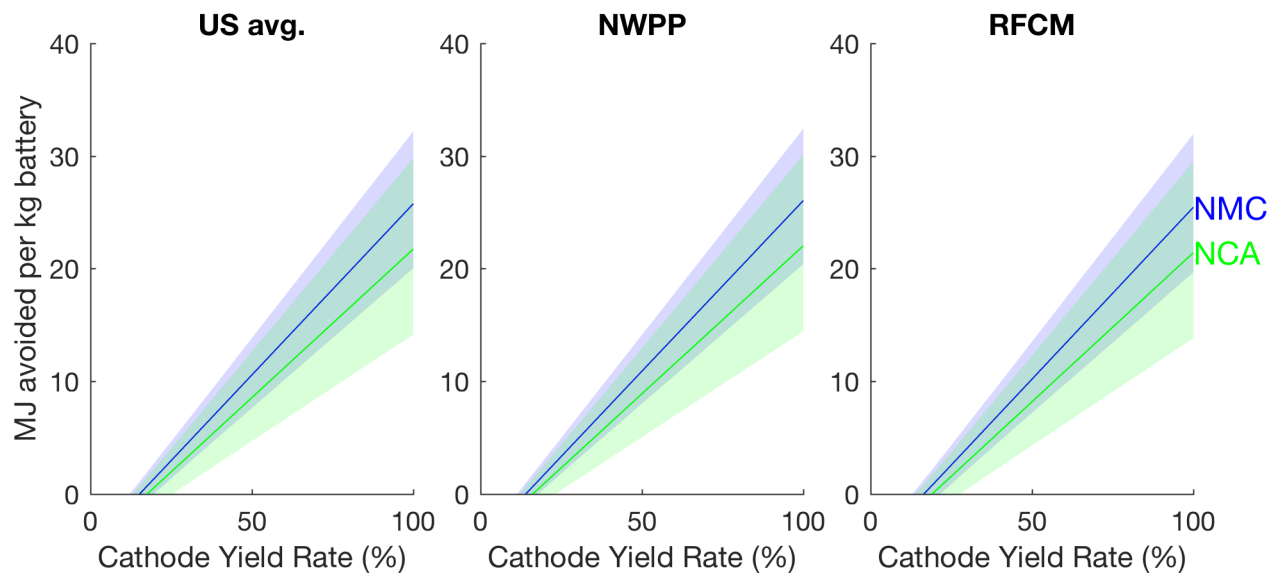


Figure C.10: MJ of energy saved by using a direct recycling process over doing nothing after cell manufacturing. Yield rates of the recovered cathode material vary from 0 to 100% for both NMC and NCA chemistries.

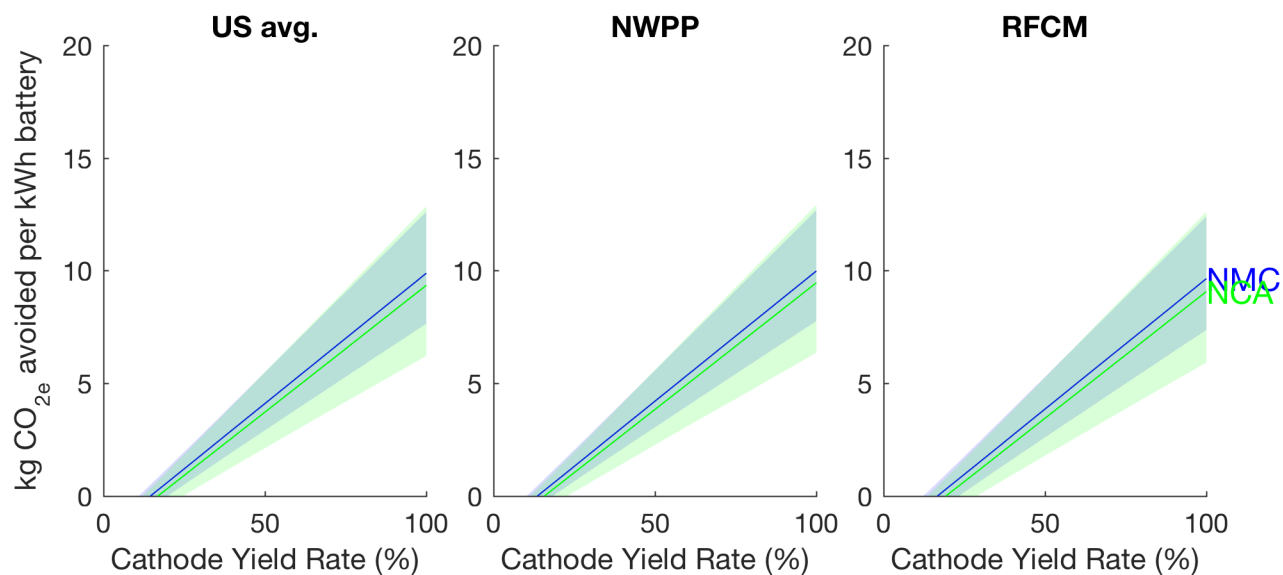


Figure C.11: net kg CO_{2e} avoided per kWh of battery by using a direct recycling process over doing nothing after cell manufacturing. Yield rates of recovered cathode material vary from 0 to 100% for both NMC and NCA chemistries.

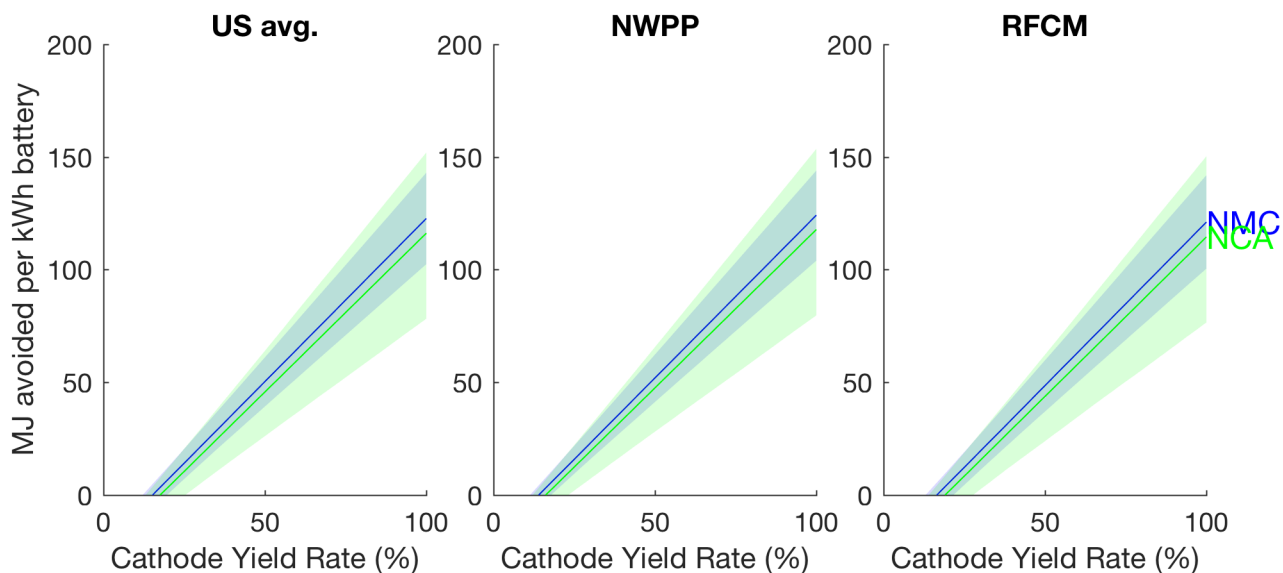


Figure C.12: MJ of energy saved by using a direct recycling process over doing nothing after cell manufacturing. Yield rates of the recovered cathode material vary from 0 to 100% for both NMC and NCA chemistries.

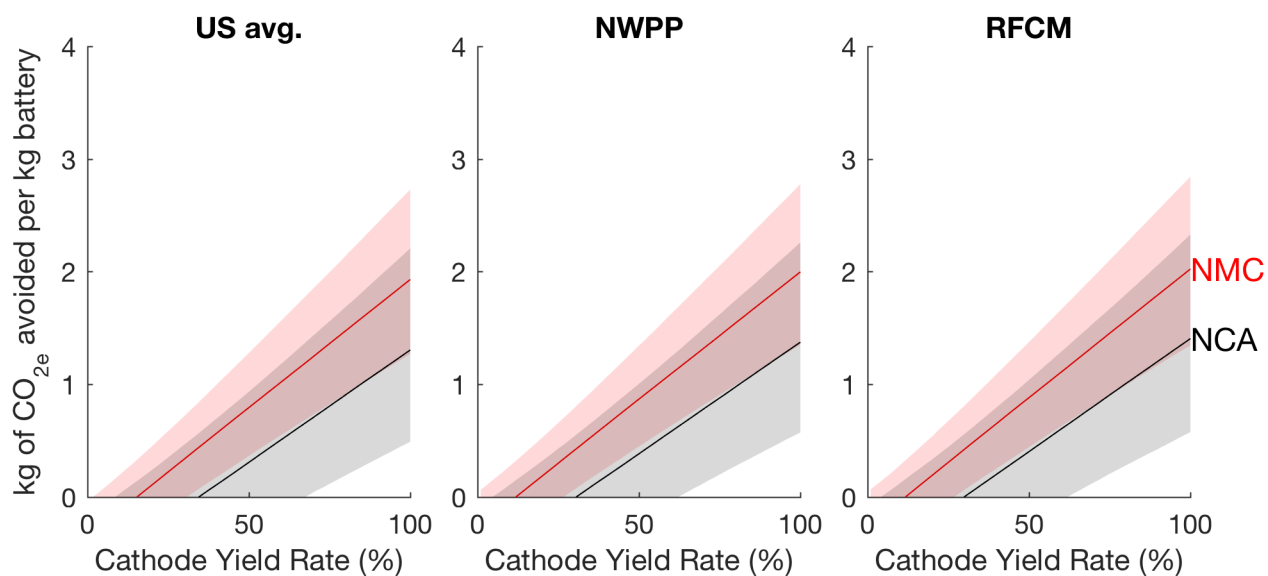


Figure C.13: kg CO_{2e} avoided per kg of battery by using a direct recycling process over a pyrometallurgical process. Yield rates of recovered cathode material vary from 0 to 100% for both NMC and NCA chemistries. Because pyrometallurgical has more environmental benefits for NCA cells than NMC cells, the yield rate for cathode material recovered during the direct recycling process must be higher for direct recycling to be more beneficial than pyrometallurgical recycling.

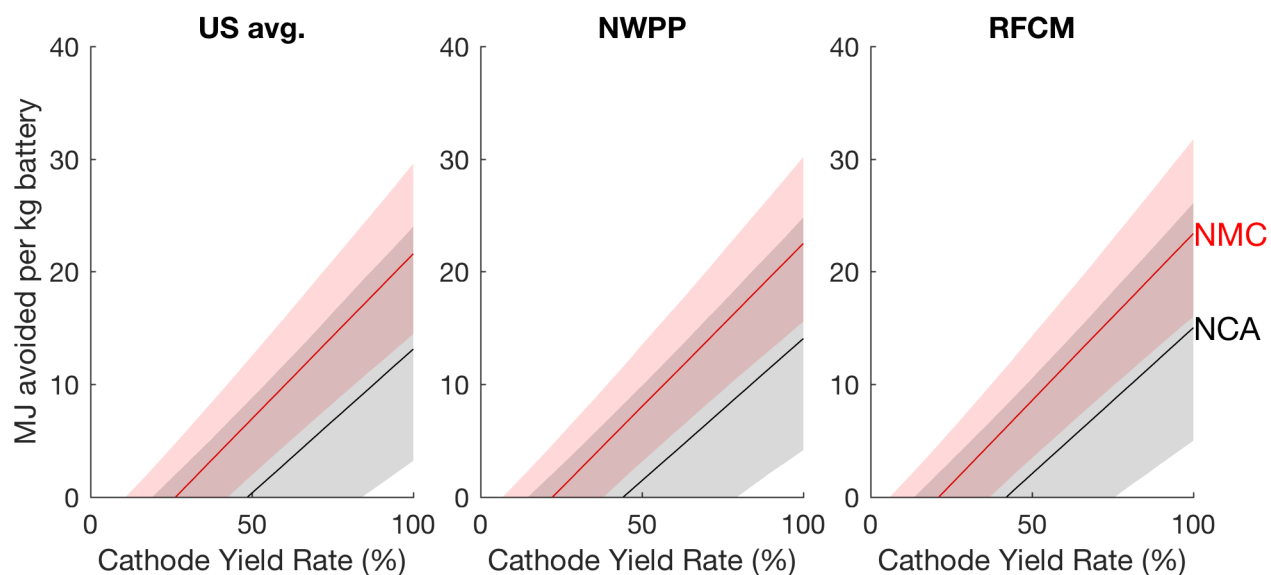


Figure C.14: MJ of input energy avoided per kg of battery by using a direct recycling process over a pyrometallurgical process. Yield rates of recovered cathode material vary from 0 to 100% for both NMC and NCA chemistries. Because pyrometallurgical has more environmental benefits for NCA cells than NMC cells, the yield rate for cathode material recovered during the direct recycling process must be higher for direct recycling to be more beneficial than pyrometallurgical recycling.

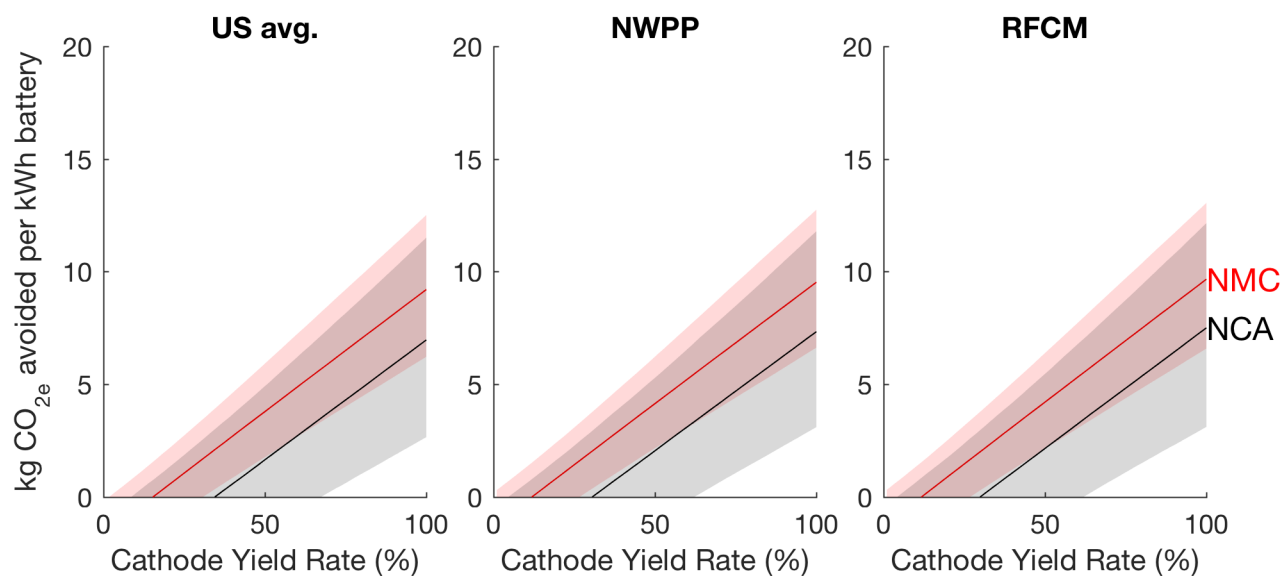


Figure C.15: kg CO_{2e} avoided per kWh of battery by using a direct recycling process over a pyrometallurgical process. Yield rates of recovered cathode material vary from 0 to 100% for both NMC and NCA chemistries. Because pyrometallurgical has more environmental benefits for NCA cells than NMC cells, the yield rate for cathode material recovered during the direct recycling process must be higher for direct recycling to be more beneficial than pyrometallurgical recycling.

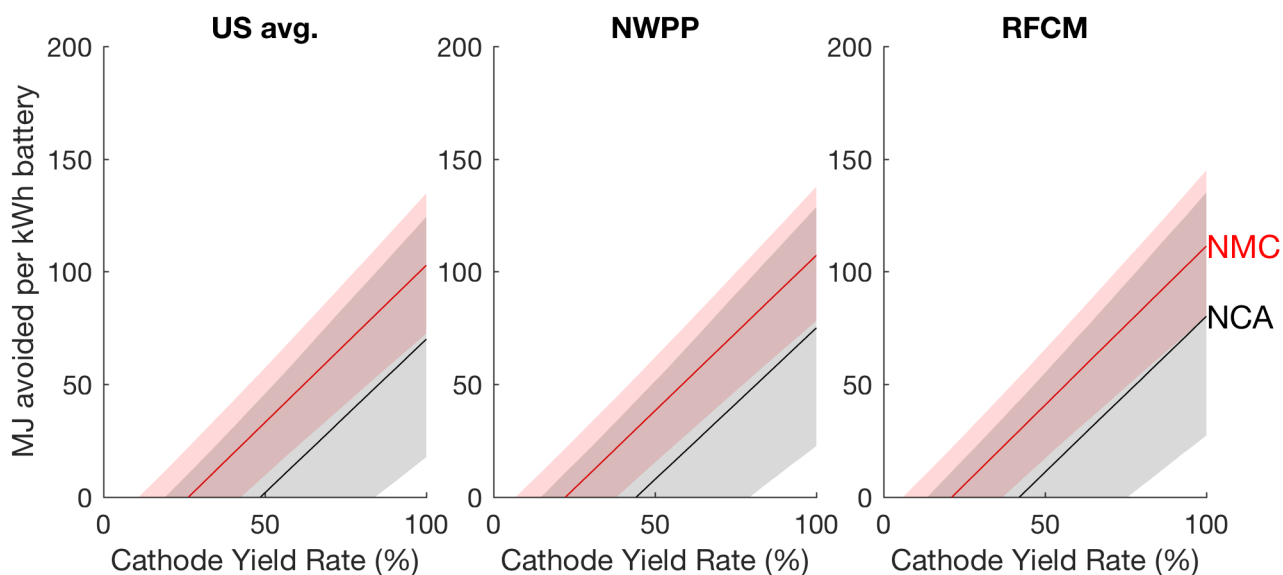


Figure C.16: MJ of energy avoided per kWh of battery by using a direct recycling process over a pyrometallurgical process. Yield rates of recovered cathode material vary from 0 to 100% for both NMC and NCA chemistries. Because pyrometallurgical has more environmental benefits for NCA cells than NMC cells, the yield rate for cathode material recovered during the direct recycling process must be higher for direct recycling to be more beneficial than pyrometallurgical recycling.

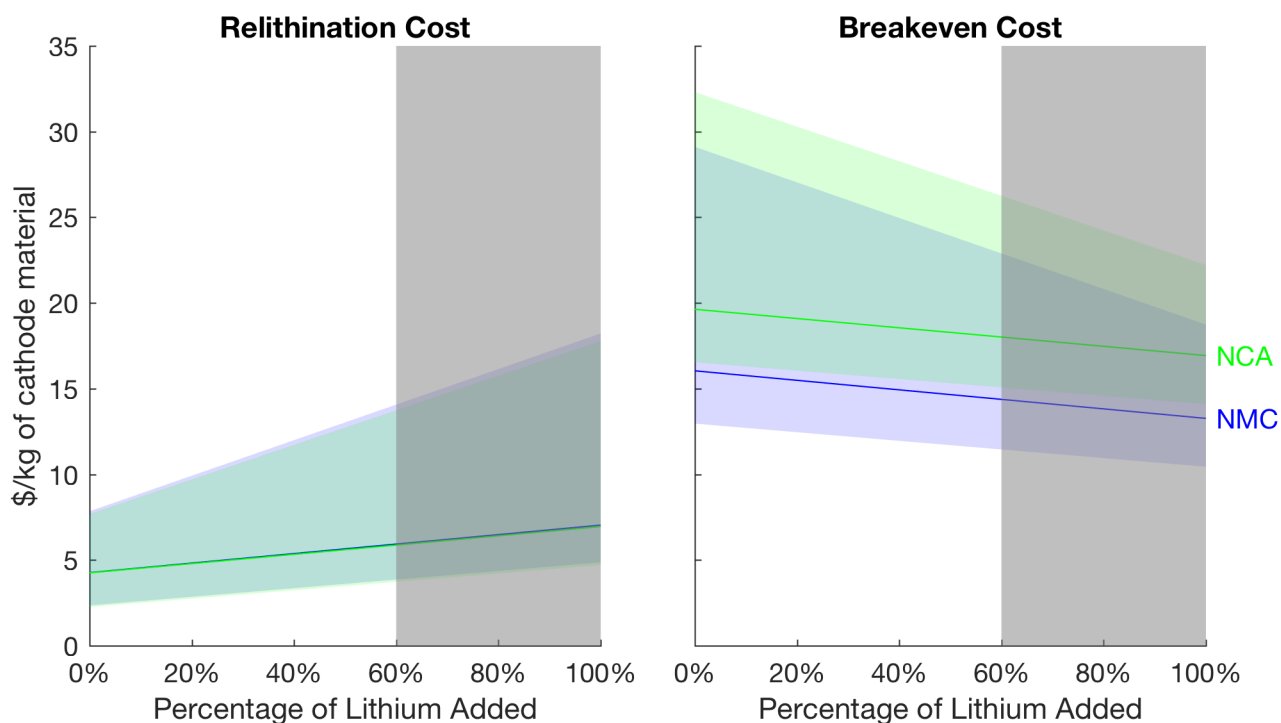


Figure C.17: Relithination costs and breakeven costs as the percentage of lithium added varies between 0 and 100%. For both cell chemistries, the lithination costs are nearly indistinguishable. In practice, no more than 60% of the lithium would need to be replaced, as the original cathode crystal structure collapses if more than 60% of the lithium is removed from the cathode (shaded in gray).

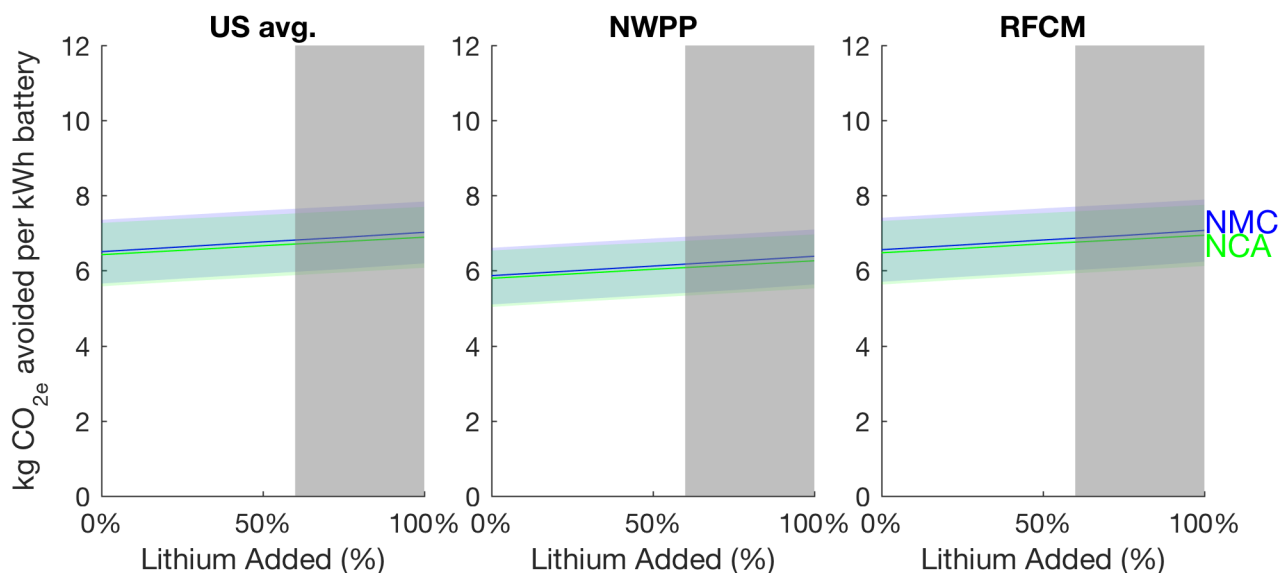


Figure C.18: kg CO_{2e} emissions per kg of battery manufactured and recycled using a direct recycling process, less the emissions offset from recycling process outputs as the lithium recovered through direct recycling varies. In practice, no more than 60% of the lithium would need to be replaced, as the original cathode crystal structure collapses if more than 60% of the lithium is removed from the cathode (shaded in gray).

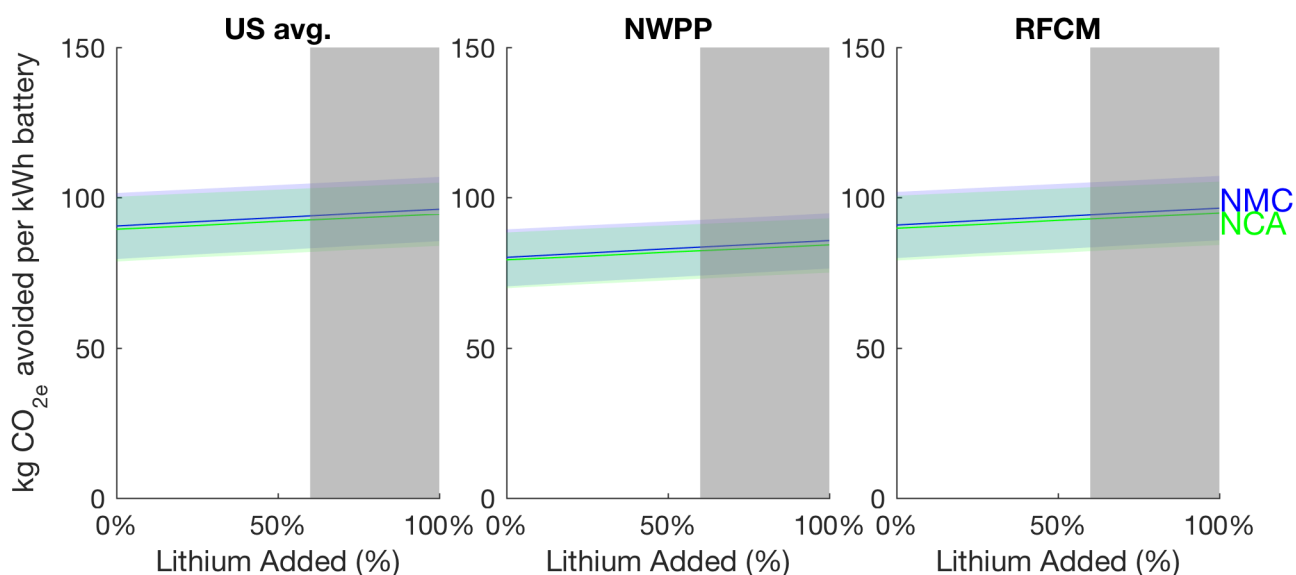


Figure C.19: MJ of energy saved per kg of battery manufactured and recycled using a direct recycling process, less the emissions offset from recycling process outputs as the lithium recovered through direct recycling varies. In practice, no more than 60% of the lithium would need to be replaced, as the original cathode crystal structure collapses if more than 60% of the lithium is removed from the cathode (shaded in gray).

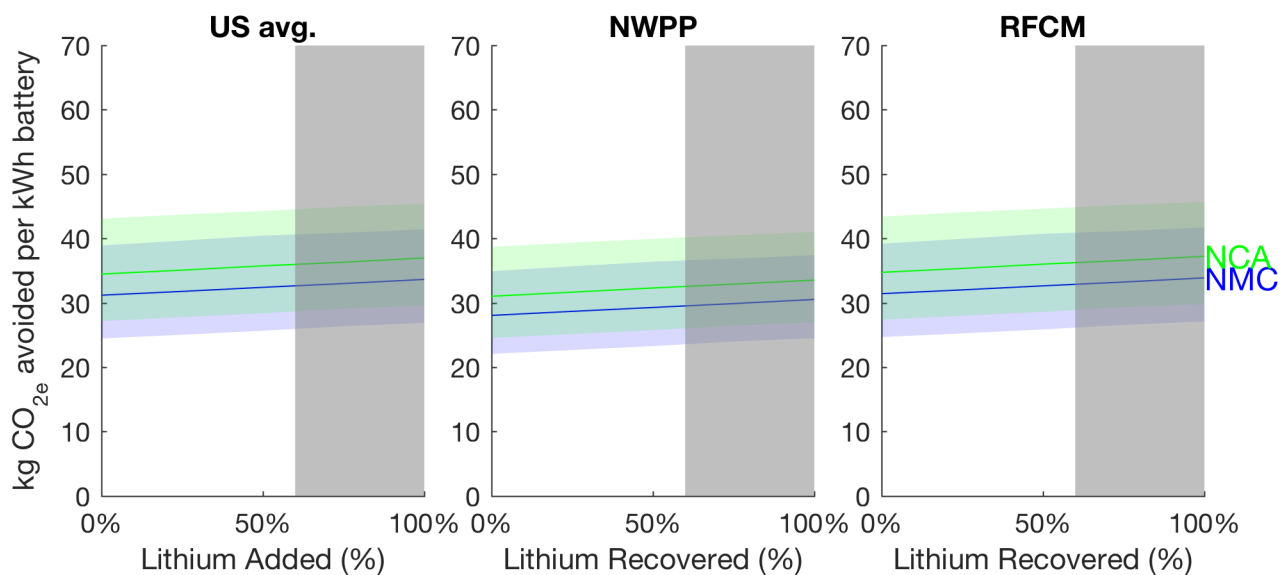


Figure C.20: kg CO_{2e} emissions per kWh of battery manufactured and recycled using a direct recycling process, less the emissions offset from recycling process outputs as the lithium recovered through direct recycling varies. In practice, no more than 60% of the lithium would need to be replaced, as the original cathode crystal structure collapses if more than 60% of the lithium is removed from the cathode (shaded in gray).

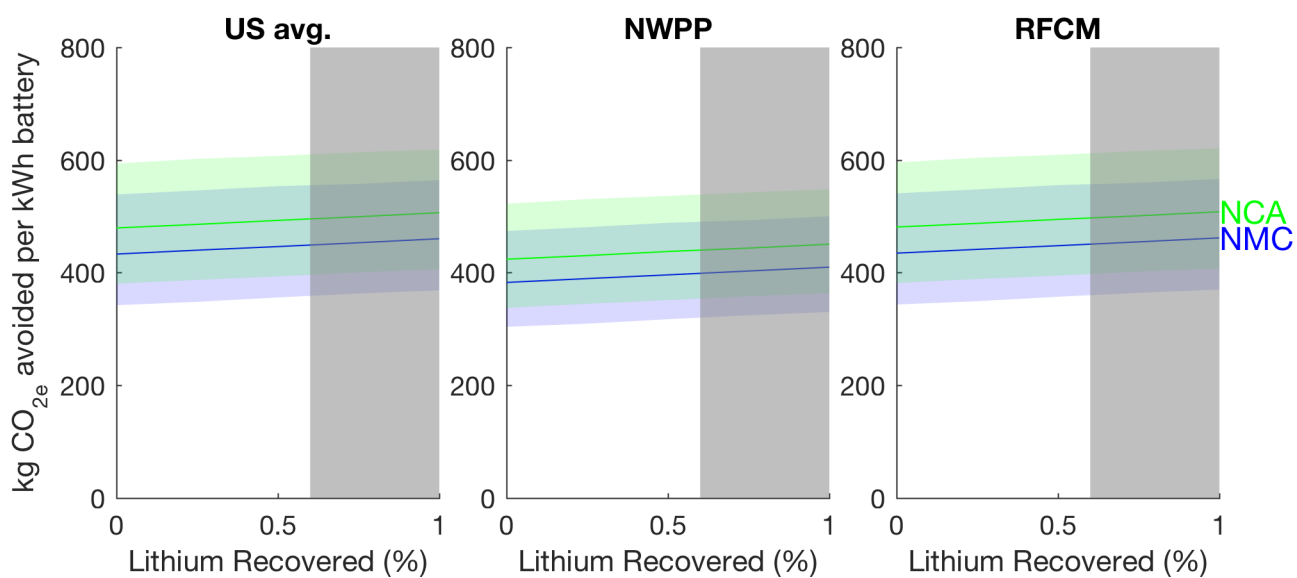


Figure C.21: MJ of energy saved per kWh of battery manufactured and recycled using a direct recycling process, less the emissions offset from recycling process outputs as the lithium recovered through direct recycling varies. In practice, no more than 60% of the lithium would need to be replaced, as the original cathode crystal structure collapses if more than 60% of the lithium is removed from the cathode (shaded in gray).

Appendix D

Survey Design Data

D.1 Market Data for Survey Levels

Attribute levels for price, vehicle electric range, vehicle warranty coverage (both percentage of the battery storage capacity guaranteed and duration of the warranty) were all based on current market data. Figure D.1 shows the MSRP and vehicle ranges for EVs available in the US in 2017. While the PHEV models have a relatively narrow band of available electric ranges, with a wide variation in price, the BEVs are essentially split into 2 clusters, with the high-end Tesla Model S and Model X offering a long electric range at a high price, and the other BEV models with both lower ranges (with the exception of the Chevrolet Bolt and Tesla Model 3) and lower MSRP.

Based on the limited number of PHEV models available with a MSRP above \$100,000, and correspondingly low sales numbers (as shown in Figure D.2 for vehicles above this price point, we capped the survey attribute price level for the PHEV survey at \$100,000.

Many manufacturers distinguish between the vehicle warranty, a powertrain warranty, and a battery warranty, with both the powertrain and battery warranties offering both longer coverage periods and longer mileage coverage than for vehicle warranties alone. The warranty terms for battery warranties are also very consistent across manufacturers and models, as shown in Table D.1. In terms of the battery performance guaranteed most manufacturers specify that some loss in storage capacity is normal, but relatively few list a specific threshold to define abnormal battery degradation levels, which would trigger battery replacements [187, 188]. The exceptions to this policy include BMW, which guarantees 70% of battery capacity over the warranty period (as stated in the owners' manual) [189] and Nissan, which guarantees that the LEAF battery should be able

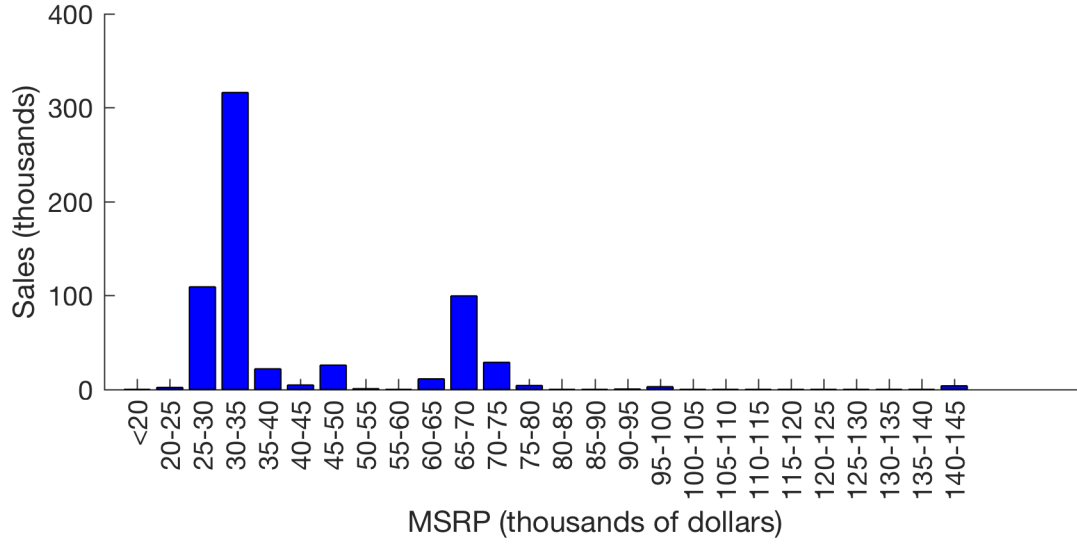


Figure D.2: Historical US sales of PHEVs by lowest model price (2010 - 2017)

Simplified model in the preference space:

$$v_j = \beta_0 p_j + \beta_1 \log(x_j^{RANGE}) + \beta_2 \log(x_j^{FINALRANGE}) + \beta_3 x_j^{WARRANTY} + \beta_4 x_j^{RECYCLED} + \beta_5 x_j^{REFURB} + \beta_6 x_j^{OG} \quad (D.4)$$

Latent class models with more classes in for PHEVs are computationally singular, but do not offer better performance:

Table D.1: Market Data - Battery Warranties

Make & Model	Type	Battery Warranty		Reference
		Years	Miles	
BMW 330e	PHEV	8	80,000	[191]
BMW 530e	PHEV	8	80,000	[192]
BMW 740e	PHEV	8	80,000	[193]
BMW i3	BEV	8	100,000	[194]
BMW i8	PHEV	8	100,000	[195]
BMW X5 xDrive40e	PHEV	8	80,000	[196]
Cadillac CT6 PHV	PHEV	8	100,000	[197]
Chevrolet Bolt	BEV	8	100,000	[198, 199]
Chevrolet Volt	PHEV	8	100,000	[199]
Chrysler Pacifica Hybrid	PHEV	10	100,000	[200]
Fiat 500e	BEV	8	-	[201]
Ford C-Max Energi	PHEV	8	100,000	[202]
Ford Fusion Energi	PHEV	8	100,000	[202, 203]
Hyundai IONIQ Electric	BEV	10	100,000	[204]
Hyundai Sonata PHV	PHEV	10	100,000	[205]
Kia Soul EV	BEV	10	100,000	[206]
Nissan LEAF	BEV	8	100,000	[190]
Tesla Model S	BEV	8	Unlimited	[188]
Tesla Model X	BEV	8	Unlimited	[188]
Toyota Prius Prime	PHEV	8	100,000	[207]
VW e-Golf	BEV	8	100,000	[208]
Volvo XC90	PHEV	8	100,000	[209]

Table D.2: Survey versions and attribute levels

Attribute	Vehicle Type		
	BEV		PHEV
	Tesla (Model S & Model X)	Other	
Price	\$55,000	\$15,000	\$15,000
	\$60,000	\$20,000	\$20,000
	\$65,000	\$25,000	\$25,000
	\$70,000	\$30,000	\$30,000
	\$75,000	\$35,000	\$35,000
	\$80,000	\$40,000	\$40,000
	\$85,000	\$45,000	\$45,000
	\$90,000		\$50,000
	\$95,000		\$55,000
	\$100,000		\$60,000
	\$105,000		\$65,000
	\$110,000		\$70,000
	\$120,000		\$80,000
	\$130,000		\$90,000
	\$140,000		\$100,000
Vehicle range with new battery	70		10
	100		20
	175		30
	250		40
	350		50
Vehicle range guarantee [†]	60%		
	70%		
	80%		
	90%		
Warranty Period [†]	7 years		
	8 years		
	9 years		
	10 years		
Battery Type	Conventional		
	Recycled		
	Refurbished		

[†]These attributes were displayed as a product of vehicle range times range guarantee, and paired with a warranty period

Table D.3: 2- and 3- Latent Class Models for BEVs in the preference space

Attribute	Class 1	Class 2	Class 1	Class 2	Class 3
Price	-0.170*** (.014)	-0.031*** (.003)	-0.162*** (.013)	0.012 *** (.004)	-0.169*** (.021)
ln(Range)	0.841 (.681)	1.151*** (.383)	1.913*** (.629)	-0.421 (.649)	2.622 *** (.804)
ln(finalrange)	1.604 ** (.669)	0.660* (.37)	1.046* (.6)	0.627 (.631)	2.035** (.863)
Warranty	0.049 (.085)	0.049 (.052)	0.068 (.076)	-0.078 (.09)	0.104 (.105)
Recycled	-0.166 (.232)	-0.019 (.131)	-0.336 (.205)	-0.007 (.232)	0.338 (.275)
Refurbished	-0.204 (.234)	-0.051 (.134)	-0.337 (.215)	0.056 (.232)	0.550 (.336)
Outside good	7.370*** (1.08)	5.813*** (.667)	9.631*** (1.012)	1.751* (.99)	12.195*** (2.091)
Class		0.622*** (.063)		-0.888*** (.082)	-0.145** (.069)
	35%	65%	44%	18%	38%
Log Likelihood	-898.64		-789.63		
AIC	1827.284		1625.256		
BIC	1904.72		1743.991		
Observations	1290		1290		
Note:			*p<0.1; **p<0.05; ***p<0.01		

Table D.4: 4 latent class model for BEVs in the preference space

Attribute	Class 1	Class 2	Class 3	Class 4
Price	-0.181*** (.027)	-0.168*** (.022)	-0.188*** (.018)	0.001 (.004)
ln(Range)	0.530 (1.296)	2.452*** (.854)	2.802*** (.712)	-0.640 (.653)
ln(finalrange)	2.606** (1.3)	2.292*** (.84)	0.772 (.651)	0.708 (.629)
Warranty	-0.137 (.174)	0.103 (.11)	0.114 (.091)	-0.009 (.087)
Recycled	-0.653 (.488)	0.401 (.281)	-0.236 (.234)	-0.038 (.231)
Refurbished	-0.751 (.466)	0.661** (.3)	-0.241 (.24)	-0.055 (.232)
Outside good	11.252*** (2.434)	11.366*** (3.325)	11.555*** (1.359)	-0.173 (.977)
Class		1.065*** (.1)	1.092*** (.103)	0.272** (.112)
	12%	35%	36%	16%
Log Likelihood	-755.11			
AIC	1572.211			
BIC	1732.245			
Observations	1290			
Note:	*p<0.1; **p<0.05; ***p<0.01			

Table D.5: 5 latent class model for BEVs in the preference space

hline Attribute	Class 1	Class 2	Class 3	Class 4	Class 5
Price	-0.316*** (.047)	-0.168*** (.022)	0.001 (.004)	-0.183*** (.024)	-0.151*** (.025)
ln(Range)	1.277 (1.391)	2.284*** (.848)	-0.652 (.645)	0.901 (1.152)	4.915*** (1.155)
ln(finalrange)	1.987 (1.246)	0.237*** (.844)	0.736 (.617)	2.219* (1.144)	-0.058 (1.011)
Warranty	-0.115 (.185)	0.103 (.11)	-0.003 (.086)	-0.070 (.151)	0.144 (.145)
Recycled	0.264 (.497)	0.423 (.282)	-0.046 (.228)	-0.436 (.425)	-0.708** (.354)
Refurbished	0.502 (.468)	0.655*** (.295)	-0.061 (.23)	-0.681 (.426)	-0.531 (.382)
Outside good	5.608** (2.655)	0.547 (361.525)	-0.100 (.957)	11.151*** (2.047)	18.974*** (2.414)
Class		0.941*** (.102)	0.197* (.113)	0.151 (.124)	0.434*** (.12)
	13%	34%	16%	16%	21%
Log Likelihood	-729.76				
AIC	1537.521				
BIC	1738.855				
Observations	1290				
Note:	*p<0.1; **p<0.05; ***p<0.01				

Table D.6: 6 latent class model for BEVs in the preference space

Attribute	Class 1	Class 2	Class 3	Class 4	Class 5	Class 6
Price	-0.183*** (.024)	-0.168*** (.022)	-0.315*** (.047)	0.002 (.004)	0.003 (.015)	-0.150*** (.025)
ln(Range)	0.851 (1.155)	2.295*** (.849)	1.191 (1.388)	-1.191* (.692)	4.900* (2.958)	4.860*** (1.143)
ln(finalrange)	2.285** (1.15)	2.362*** (.844)	2.030 (1.248)	1.261* (.666)	-4.376 (2.678)	-0.041 (1.003)
Warranty	-0.077 (.152)	0.104 (.11)	-0.117 (.185)	-0.001 (.091)	0.098 (.344)	0.139 (.144)
Recycled	-0.428 (.424)	0.423 (.282)	0.216 (.495)	-0.114 (.244)	0.143 (.798)	-0.705** (.352)
Refurbished	-0.688 (.43)	0.655** (.295)	0.460 (.467)	-0.127 (.246)	0.280 (.888)	-0.528 (.38)
Outside good	11.179*** (2.06)	5.813 (26.516)	5.331** (2.635)	-0.608 (1.027)	5.812 (3.969)	18.795*** (2.382)
Class		0.788*** (.093)	-0.141 (.123)	-0.115 (.108)	-1.873*** (.203)	0.277*** (.106)
	16%	34%	14%	14%	2%	21%
Log Likelihood	-722.35					
AIC	1538.698					
BIC	1781.33					
Observations	1290					
Note:	*p<0.1; **p<0.05; ***p<0.01					

Table D.7: 2- and 3- Latent Class Models for PHEVs in the preference space

Attribute	Class 1	Class 2	Class 1	Class 2	Class 3
Price	-0.111*** (.009)	-0.074*** (.006)	-0.122*** (.017)	-0.130*** (.012)	-0.074*** (.006)
ln(Range)	1.825** (.701)	0.998* (.557)	1.752 (1.459)	3.298*** (.919)	0.864 (.577)
ln(finalrange)	0.921 (.656)	1.785*** (.551)	0.938 (1.287)	0.388 (.853)	1.857*** (.574)
Warranty	-0.032 (.091)	0.081 (.074)	0.161 (.176)	-0.137 (.115)	0.105 (.077)
Recycled	-0.325 (.24)	-0.379* (.2)	-0.615 (.511)	-0.167 (.302)	-0.378* (.211)
Refurbished	-0.127 (.249)	-0.386* (.207)	0.212 (.428)	-0.116 (.319)	-0.405* (.216)
Outside good	5.059*** (.926)	2.856*** (.7)	6.075*** (1.872)	6.485*** (1.14)	2.383*** (.662)
Class		0.051 (.065)		0.552 (.105)	0.856 (.091)
	49%	51%	20%	34%	46%
Log Likelihood	-629.420		-599.010		
AIC	1288.840		1244.026		
BIC	1365.002		1360.808		
Observations	1185		1185		
Note:	*p<0.1; **p<0.05; ***p<0.01				

Table D.8: 4 Latent Class Models for PHEVs in the preference space

Attribute	Class 1	Class 2	Class 3	Class 4
Price	-0.207*** (.062)	-0.136*** (.013)	-0.079*** (.007)	-0.126*** (.022)
ln(Range)	-2.128 (4.311)	2.748*** (.82)	1.929*** (.687)	-3.686** (1.569)
ln(finalrange)	6.702 (4.184)	0.268 (.768)	2.012*** (.69)	5.472*** (1.67)
Warranty	0.737 (.591)	-0.116 (.105)	0.146 (.094)	0.050 (.169)
Recycled	-0.433 (1.182)	-0.276 (.278)	-0.543** (.25)	-0.285 (.466)
Refurbished	-1.827 (1.272)	-0.104 (.299)	-0.520** (.257)	0.306 (.466)
Outside good	10.960* (6.409)	4.731*** (.952)	7.000*** (.928)	-8.188*** (2.245)
Class		1.706*** (.125)	1.707*** (.124)	0.613*** (.141)
	7%	40%	40%	13%
Log Likelihood	-568.220			
AIC	1198.444			
BIC	1355.846			
Observations	1185			
<i>Note:</i>		*p<0.1; **p<0.05; ***p<0.01		

Table D.9: Latent Class Selection Criteria for PHEVs

Number of classes	Likelihood	AIC	BIC
2	-629.42	1288.84,	1365.002
3	-599.01	1244.026	1360.808
4	-568.22	1198.444	1355.846
5	-555.29	1188.592	1386.614
6	-540.01	1174.022	1412.664

Bibliography

- [1] D. Cheret and S. Santen, "Battery Recycling," US Patent 11/108 321, Jan., 2007.
- [2] R. E. Ciez and J. F. Whitacre, "Comparison between cylindrical and prismatic lithium-ion cell costs using a process based cost model," *Journal of Power Sources*, vol. 340, pp. 273–281, Feb. 2017.
- [3] C. Bloch and R. Ranganathan, "Process-Based Cost Modeling," *IEEE Transactions on Components, Hybrids, and Manufacturing Technology*, vol. 15, no. 3, pp. 288–294, Jun. 1992.
- [4] J. A. Ober, "Mineral commodity summaries 2017," USGS, Tech. Rep., 2017.
- [5] "DOE Global Energy Storage Database," US Department of Energy. [Online]. Available: http://www.energystorageexchange.org/projects/data_visualization
- [6] D. Howell, B. Cunningham, T. Duong, and P. Faguy. (2016, Jun.) Overview of the DOE VTO Advanced Battery R&D Program. [Online]. Available: http://energy.gov/sites/prod/files/2016/06/f32/es000_howell_2016_o_web.pdf
- [7] A. A. Akhil, G. Huff, A. B. Currier, B. C. Kaun, D. M. Rastler, S. B. Chen, A. L. Cotter, D. T. Bradshaw, and W. D. Gauntlett, "DOE/EPRI 2013 Electricity Storage Handbook in Collaboration with NRECA," Sandia National Laboratory, Tech. Rep., Jul. 2013.
- [8] P. A. Nelson, K. G. Gallagher, I. Bloom, and D. W. Dees, "Modeling the Performance and Cost of Lithium-Ion Batteries for Electric-Drive Vehicles," Argonne National Lab, Tech. Rep. ANL-12/55, Dec. 2012.
- [9] D. L. Wood III, J. Li, and C. Daniel, "Prospects for reducing the processing cost of lithium ion batteries," *Journal of Power Sources*, vol. 275, pp. 234–242, Nov. 2014.

- [10] A. Sakti, J. J. Michalek, E. R. H. Fuchs, and J. F. Whitacre, "A techno-economic analysis and optimization of Li-ion batteries for light-duty passenger vehicle electrification," *Journal of Power Sources*, vol. 273, no. C, pp. 966–980, Sep. 2014.
- [11] B. Nykvist and M. Nilsson, "Rapidly falling costs of battery packs for electric vehicles," *Nature Climate Change*, vol. 5, no. 4, pp. 329–332, Mar. 2015.
- [12] A. Sakti, I. M. L. Azevedo, E. R. H. Fuchs, J. J. Michalek, K. G. Gallagher, and J. F. Whitacre, "A new framework for technology forecasting: the case of Li-ion batteries for plug-in electric vehicles," *Social Science Research Network*, 2016.
- [13] K. Nakura, K. Ariyoshi, H. Yoshizawa, and T. Ohzuku, "Characterization of Lithium Insertion Electrodes and Its Verification: Prototype 18650 Batteries Consisting of LTO and LAMO," *Journal of the Electrochemical Society*, vol. 162, no. 4, pp. A622–A628, Jan. 2015.
- [14] N. S. Ong, "Manufacturing cost estimation for PCB assembly: An activity-based approach," *International Journal of Production Economics*, vol. 38, no. 2, pp. 159–172, 1995.
- [15] J. La Trobe-Bateman and D. Wild, "Design for manufacturing: use of a spreadsheet model of manufacturability to optimize product design and development," *Research in Engineering Design*, Mar. 2003.
- [16] J. M. Paulsen and J. R. Dahn, "O₂-Type Li_{2/3}[Ni_{1/3}Mn_{2/3}]O₂: A New Layered Cathode Material for Rechargeable Lithium Batteries," *Journal of the Electrochemical Society*, vol. 147, no. 7, pp. 2478–2485, 2000.
- [17] G. Majeau-Bettez, T. R. Hawkins, and A. H. Strømman, "Life Cycle Environmental Assessment of Lithium-Ion and Nickel Metal Hydride Batteries for Plug-In Hybrid and Battery Electric Vehicles," *Environmental Science and Technology*, Apr. 2011.
- [18] Electric Power Monthly. [Online]. Available: https://www.eia.gov/electricity/monthly/epm_table_grapher.cfm?t=epmt_5_3
- [19] S. I. Kohn and W. A. Hermann, "Cell cap assembly with recessed terminal and enlarged insulating gasket," US Patent 12/456,150, Nov., 2011.
- [20] A. A. Pesaran, G.-H. Kim, K. Smith, and E. C. Darcy, "Designing Safe Lithium-Ion Battery Packs Using Thermal Abuse Models," in *Lithium Mobile Power*, Dec. 2008.

- [21] R. E. Ciez and J. F. Whitacre, "The cost of lithium is unlikely to upend the price of Li-ion storage systems," *Journal of Power Sources*, vol. 320, pp. 310–313, Jul. 2016.
- [22] L. B. V. Jaffe, S. Behind-the-meter energy storage: not hypothetical anymore. [Online]. Available: <http://www.smartgridnews.com/story/behind-meter-energy-storage-not-hypothetical-anymore/2014-02-25>
- [23] J. St John. Hawaii Wants 200MW of Energy Storage for Solar, Wind Grid Challenges. [Online]. Available: <http://www.greentechmedia.com/articles/read/hawaii-wants-200mw-of-energy-storage-for-solar-wind-grid-challenges>
- [24] "Commission's inclinations on the future of hawaii's electric utilities," Public Utilities Commission of the State of Hawaii, 2014.
- [25] L. Hay Newman. (2014, May) What California's Energy Storage Requirement Really Means.
- [26] D. Frankel. (2014) Storage gets a lift from california's \$415 million for behind-the-meter generation. [Online]. Available: <http://www.smartgridnews.com/story/storage-gets-lift-california-s-415-million-behind-meter-generation/2014-06-25>
- [27] Gordon and Skinner, "Self-generation incentive program," AB-1624, California Legislature, pp. 1–5, Dec. 2014.
- [28] Power africa's beyond the grid increasing access through small-scale energy solutions. us department of energy. [Online]. Available: <http://www.energy.gov/articles/power-africa-s-beyond-grid-increasing-access-through-small-scale-energy-solutions>
- [29] D. Schnitzer, D. S. Lounsbury, J. P. Carvallo, R. Deshmukh, J. Apt, and D. M. Kammen, "Microgrids for Rural Electrification," United Nations Foundations, Tech. Rep., Feb. 2014.
- [30] J. B. Copetti and F. Chenlo, "Lead/acid batteries for photovoltaic applications. Test results and modeling," *Journal of Power Sources*, vol. 47, no. 1-2, pp. 109–118, Jan. 1994.
- [31] N. Achaibou, M. Haddadi, and A. Malek, "Modeling of Lead Acid Batteries in PV Systems," *Energy Procedia*, vol. 18, pp. 538–544, Jan. 2012.
- [32] J. F. Manwell and J. G. McGowan, "Lead Acid Battery Storage Model for Hybrid Energy Systems," *Solar Energy*, pp. 399–405, 1993.

- [33] J. J. Lander, "Further Studies on the Anodic Corrosion of Lead in H₂SO₄ Solutions," *Journal of the Electrochemical Society*, pp. 1–8, Nov. 2006.
- [34] C. Protogeropoulos, M. R.H., and B. Brinkworth, "Battery state of voltage modelling and an algorithm describing dynamic conditions for long-term storage simulation in a renewable system," *Solar Energy*, pp. 517–527, 1994.
- [35] D. Spiers and A. D. Rasinkoski, "Predicting the service lifetime of lead/acid batteries in photovoltaic systems," *Journal of Power Sources*, pp. 245–253, 1995.
- [36] S. West and P. T. Krein, "Equalization of Valve-Regulated Lead-Acid Batteries: Issues and Life Test Results," *IEEE Spectrum*, pp. 1–8, 2000.
- [37] J. Schiffer, D. U. Sauer, H. Bindner, T. Cronin, P. Lundsager, and R. Kaiser, "Model prediction for ranking lead-acid batteries according to expected lifetime in renewable energy systems and autonomous power-supply systems," *Journal of Power Sources*, vol. 168, no. 1, pp. 66–78, May 2007.
- [38] H. Binder, T. Cronin, P. Lundsager, J. F. Manwell, U. Abdulwahid, and I. Baring-Gould, "Benchmarking – Lifetime Modelling," European Commission Community Research and Development Information Service, Tech. Rep., Dec. 2013.
- [39] M. Bortolini, M. Gamberi, and A. Graziani, "Technical and economic design of photovoltaic and battery energy storage system," *Energy Conversion and Management*, vol. 86, no. C, pp. 81–92, Oct. 2014.
- [40] J. Kaldellis, D. Zafirakis, K. Kavadias, and E. Kondili, "Optimum PV-diesel hybrid systems for remote consumers of the Greek territory," *Applied Energy*, vol. 97, no. C, pp. 61–67, Sep. 2012.
- [41] E. M. Nfah, J. M. Ngundam, M. Vandenbergh, and J. Schmid, "Simulation of off-grid generation options for remote villages in Cameroon," *Renewable Energy*, vol. 33, no. 5, pp. 1064–1072, May 2008.
- [42] "Ncdc climate data: Tuscon international airport," database. [Online]. Available: http://rredc.nrel.gov/solar/old_data/nsrdb/

- [43] "National solar radiation database," database. [Online]. Available: http://rredc.nrel.gov/solar/old_data/nsrdb/
- [44] A. Pesaran and T. Markel, "Battery Requirements and Cost-Benefit Analysis for Plug-In Hybrid Vehicles (Presentation)," in *The 24th International Battery Seminar & Exhibit*, Sep. 2007, pp. 1–22.
- [45] S. B. Peterson, J. Apt, and J. F. Whitacre, "Lithium-ion battery cell degradation resulting from realistic vehicle and vehicle-to-grid utilization," *Journal of Power Sources*, vol. 195, no. 8, pp. 2385–2392, Apr. 2010.
- [46] ANR26650 M1A. [Online]. Available: <https://www.buya123products.com/goodsdetail.php?i=11>
- [47] *Panasonic NCR-18650*, Panasonic, 2014.
- [48] E. Hittinger, T. Wiley, J. Kluza, and J. Whitacre, "Evaluating the value of batteries in micro-grid electricity systems using an improved Energy Systems Model," *Energy Conversion and Management*, vol. 89, no. C, pp. 458–472, Jan. 2015.
- [49] S. Szabó, K. Bódis, T. Huld, and M. Moner-Girona, "Energy solutions in rural Africa: mapping electrification costs of distributed solar and diesel generation versus grid extension*," *Environmental Research Letters*, vol. 6, no. 3, p. 034002, Jul. 2011.
- [50] M. Anderman, "The Plug-In Hybrid and Electric Vehicle Opportunity Report," Advanced Automotive Batteries, Tech. Rep., May 2010.
- [51] R. Ciez, "Price Inquiry-SDSHobby," Personal Communication, Mar. 2015.
- [52] —, "Price Inquiry-Guangzhou Great Power Energy & Technology Co. ," Personal Communication, Mar. 2015.
- [53] —, "Price Inquiry-Shenzhen Apollo Battery Tech. Development Co. ," Personal Communication, Mar. 2015.
- [54] —, "Price Inquiry-Victpower Technology Co. ," Personal Communication, Mar. 2015.
- [55] "Quick Insights - The Economics of Residential Energy Storage," Electric Power Research Institute (EPRI), Tech. Rep., May 2015.

- [56] Retail diesel prices. [Online]. Available: <http://www.eia.gov/countries/prices/dieselwithtax.cfm>
- [57] U. Deichmann, C. Meisner, S. Murray, and D. Wheeler, "The economics of renewable energy expansion in rural Sub-Saharan Africa," *Energy Policy*, vol. 39, no. 1, pp. 215–227, Jan. 2011.
- [58] J. Huenteler, "International support for feed-in tariffs in developing countries—A review and analysis of proposed mechanisms," *Renewable and Sustainable Energy Reviews*, vol. 39, pp. 857–873, Nov. 2014.
- [59] A. Campoccia, L. Dusonchet, E. Telaretti, and G. Zizzo, "An analysis of feed-in tariffs for solar PV in six representative countries of the European Union," *Solar Energy*, vol. 107, pp. 530–542, 2014.
- [60] S. Tongsopit and C. Greacen, "An assessment of Thailand's feed-in tariff program," *Renewable Energy*, vol. 60, pp. 439–445, 2013.
- [61] Feed-in tariff: a policy tool encouraging deployment in renewable electricity technologies. [Online]. Available: <http://www.eia.gov/todayinenergy/detail.cfm?id=11471>
- [62] Feed-in tariffs and similar programs. [Online]. Available: http://www.eia.gov/electricity/policies/provider_programs.cfm
- [63] The World Bank. Putting a Price on Carbon with a Tax. [Online]. Available: http://www.worldbank.org/content/dam/Worldbank/document/Climate/background-note_carbon-tax.pdf
- [64] "Directive 2006/66/EC of the European Parliament and of the Council on batteries and accumulators and waste batteries and accumulators and repealing Directive 91/157/EEC," Sep. 2006.
- [65] Recycling Laws By State. [Online]. Available: <http://www.call2recycle.org/recycling-laws-by-state/>
- [66] *RCRA Orientation Manual 2014*, 2014.

- [67] J. Ayre. (2017, Jul.) GM Aiming For 500,000 “New Energy Vehicle” Sales Per Year By 2025. [Online]. Available: <https://cleantechnica.com/2017/07/10/gm-aiming-500000-new-energy-vehicle-sales-per-year-2025/>
- [68] T. Randall. (2016, May) Tesla’s Wild New Forecast Changes the Trajectory of an Entire Industry. [Online]. Available: <http://www.bloomberg.com/news/articles/2016-05-04/tesla-s-wild-new-forecast-changes-the-trajectory-of-an-entire-industry>
- [69] J. Xu, H. R. Thomas, R. W. Francis, K. R. Lum, J. Wang, and B. Liang, “A review of processes and technologies for the recycling of lithium-ion secondary batteries,” *Journal of Power Sources*, vol. 177, pp. 512–527, Jan. 2008.
- [70] C. Hanisch, W. Haselrieder, and A. Kwade, “Recovery of Active Materials from Spent Lithium-Ion Electrodes and Electrode Production Rejects,” in *Glocalized Solutions for Sustainability in Manufacturing*. Berlin, Heidelberg: Springer Berlin Heidelberg, 2011, pp. 85–89.
- [71] R.-C. Wang, Y.-C. Lin, and S.-H. Wu, “A novel recovery process of metal values from the cathode active materials of the lithium-ion secondary batteries,” *Hydrometallurgy*, vol. 99, no. 3-4, pp. 194–201, Nov. 2009.
- [72] S. M. Shin, N. H. Kim, J.-S. Sohn, D. H. Yang, and Y. H. Kim, “Development of a metal recovery process from Li-ion battery wastes,” *Hydrometallurgy*, vol. 79, no. 3-4, pp. 172–181, Oct. 2005.
- [73] B. Swain, J. Jeong, J.-c. Lee, G.-H. Lee, and J.-S. Sohn, “Hydrometallurgical process for recovery of cobalt from waste cathodic active material generated during manufacturing of lithium ion batteries,” *Journal of Power Sources*, vol. 167, no. 2, pp. 536–544, May 2007.
- [74] C. K. Lee and K.-I. Rhee, “Reductive leaching of cathodic active materials from lithium ion battery wastes,” *Hydrometallurgy*, vol. 68, no. 1-3, pp. 5–10, Feb. 2003.
- [75] M. Contestabile, S. Panero, and B. Scrosati, “A laboratory-scale lithium-ion battery recycling process,” *Journal of Power Sources*, vol. 92, no. 1-2, pp. 65–69, Jan. 2001.
- [76] S. Sloop, “Giga Life Cycle: Manufacture of Cells from Recycled EV Li-ion Batteries,” in *Vehicle Technologies Office Merit Review 2015*. Department of Energy Vehicle Technologies Office, Apr. 2015.

- [77] J. B. Dunn, L. Gaines, J. Sullivan, and M. Q. Wang, "Impact of Recycling on Cradle-to-Gate Energy Consumption and Greenhouse Gas Emissions of Automotive Lithium-Ion Batteries," *Environmental Science & Technology*, vol. 46, no. 22, pp. 12 704–12 710, Oct. 2012.
- [78] Z. Wang, P. Benavides, J. B. Dunn, and D. C. Cronauer, "Development of GREET Catalyst Module," Argonne National Laboratory, Tech. Rep. ANL/ESD-14/12, Sep. 2015.
- [79] M. Grützke, X. Mönnighoff, F. Horsthemke, V. Kraft, M. Winter, and S. Nowak, "Extraction of lithium-ion battery electrolytes with liquid and supercritical carbon dioxide and additional solvents," *RSC Adv.*, vol. 5, no. 54, pp. 43 209–43 217, 2015.
- [80] S. Nowak and M. Winter, "The Role of Sub- and Supercritical CO₂ as "Processing Solvent" for the Recycling and Sample Preparation of Lithium Ion Battery Electrolytes," *Molecules*, vol. 22, no. 3, p. 403, Mar. 2017.
- [81] X. Mönnighoff, A. Friesen, B. Konersmann, F. Horsthemke, M. Grützke, M. Winter, and S. Nowak, "Supercritical carbon dioxide extraction of electrolyte from spent lithium ion batteries and its characterization by gas chromatography with chemical ionization," *Journal of Power Sources*, vol. 352, pp. 56–63, Jun. 2017.
- [82] U. Zahid, J. An, U. Lee, S. P. Choi, and C. Han, "Techno-economic assessment of CO₂ liquefaction for ship transportation," *Greenhouse Gases: Science and Technology*, vol. 4, no. 6, pp. 734–749, Jun. 2014.
- [83] J. B. Dunn, L. Gaines, M. Barnes, J. L. Sullivan, and M. Wang, "Material and Energy Flows in the Materials Production, Assembly, and End-of-Life Stages of the Automotive Lithium-Ion Battery Life Cycle," Argonne National Laboratory, Argonne, IL, Tech. Rep. ANL/ESD/12-3, Sep. 2014.
- [84] O. O. C. US EPA. Emissions & Generation Resource Integrated Database. [Online]. Available: <https://www.epa.gov/energy/egrid>
- [85] "IPCC Fourth Assessment Report: Climate Change 2007," UNEP, Tech. Rep., 2007.
- [86] Argonne greet model. [Online]. Available: <https://greet.es.anl.gov/>

- [87] Transit Time, Distance calculator & Port to port distances. [Online]. Available: <https://www.searates.com/reference/portdistance/?D=706&G=15873&shipment=1&container=20st&weight=1&product=0&request=&mode=&>
- [88] World copper smelters: interactive map. [Online]. Available: <https://mrdata.usgs.gov/mineral-resources/copper-smelters.html>
- [89] J. Sullivan and L. Gaines, "A Review of Battery Life-Cycle Analysis: State of Knowledge and Critical Needs," Argonne National Lab, Tech. Rep. ANL/ESD/10-7, 2010.
- [90] D. A. Notter, M. Gauch, R. Widmer, P. Wäger, A. Stamp, R. Zah, and H.-J. Althaus, "Contribution of Li-Ion Batteries to the Environmental Impact of Electric Vehicles," *Environmental Science & Technology*, vol. 44, no. 17, pp. 6550–6556, Sep. 2010.
- [91] M. Zackrisson, L. Avellán, and J. Orlenius, "Life cycle assessment of lithium-ion batteries for plug-in hybrid electric vehicles – Critical issues," *Journal of Cleaner Production*, vol. 18, no. 15, pp. 1519–1529, Nov. 2010.
- [92] "Lithium-Ion Batteries and Nanotechnology for Electric Vehicles," US EPA, Tech. Rep. EPA 744-R-12-001, Apr. 2012.
- [93] L. A.-W. Ellingsen, G. Majeau-Bettez, B. Singh, A. K. Srivastava, L. O. Valøen, and A. H. Strømman, "Life Cycle Assessment of a Lithium-Ion Battery Vehicle Pack," *Journal of Industrial Ecology*, vol. 18, no. 1, pp. 113–124, Nov. 2013.
- [94] H. C. Kim, T. J. Wallington, R. Arsenault, C. Bae, S. Ahn, and J. Lee, "Cradle-to-Gate Emissions from a Commercial Electric Vehicle Li-Ion Battery: A Comparative Analysis," *Environmental Science & Technology*, vol. 50, no. 14, pp. 7715–7722, Jul. 2016.
- [95] L. Ciacci, E. M. Harper, N. T. Nassar, B. K. Reck, and T. E. Graedel, "Metal Dissipation and Inefficient Recycling Intensify Climate Forcing," *Environmental Science & Technology*, vol. 50, no. 20, pp. 11 394–11 402, Oct. 2016.
- [96] "Hazardous materials: Transportation of Lithium Batteries," vol. 79, no. 151, Aug. 2014.
- [97] Y. IDEMOTO and T. MATSUI, "Thermodynamic stability, crystal structure, and cathodic performance of $\text{Li}_x(\text{Mn}_{1/3}\text{Co}_{1/3}\text{Ni}_{1/3})\text{O}_2$ depend on the synthetic process and Li content," *Solid State Ionics*, vol. 179, no. 17-18, pp. 625–635, Jul. 2008.

- [98] F. Wild, J. Riseborough, and T. Wilson. (2017, Feb.) Glencore Buys Out Billionaire With \$1 Billion Congo Mining Deal. [Online]. Available: <https://www.bloomberg.com/news/articles/2017-02-13/glencore-said-to-agree-on-gertler-buyout-in-960-million-deal>
- [99] Cobalt:2010-2017 . [Online]. Available: tradingeconomics.com/commodity/cobalt
- [100] “Advancing Sustainable Materials Management: 2013 Fact Sheet,” *EPA.gov*, no. EPA530-R-15-003, pp. 1–21, Jun. 2015.
- [101] L. Gaines, “The future of automotive lithium-ion battery recycling: Charting a sustainable course,” *Sustainable Materials and Technologies*, vol. 1-2, pp. 2–7, Dec. 2014.
- [102] (2008, Jun.) Recycling and Reuse: Batteries and Accumulators: European Union Directive. [Online]. Available: https://archive.epa.gov/oswer/international/web/html/200806_tl-eu-directive-batteries-accumulators.html
- [103] A. Elshkaki, T. E. Graedel, L. Ciacci, and B. K. Reck, “Copper demand, supply, and associated energy use to 2050,” *Global Environmental Change*, vol. 39, pp. 305–315, Jul. 2016.
- [104] J. Axsen, C. Kormos, S. Goldberg, and Z. Long, “Which Types of Zero-Emissions Vehicles (ZEVs) Do Canadian Consumers Want and Why?” in *Transportation Research Board Annual Meeting*, Washington DC, 2017.
- [105] E. Gies, “Lazarus batteries,” *Nature*, vol. 526, pp. S100–S101, Oct. 2015.
- [106] E. A. Olivetti, G. Ceder, G. G. Gaustad, and X. Fu, “Lithium-Ion Battery Supply Chain Considerations: Analysis of Potential Bottlenecks in Critical Metals,” *Joule*, vol. 1, no. 2, pp. 229–243, Oct. 2017.
- [107] D. Doughty and E. P. Roth, “A General Discussion of Li Ion Battery Safety,” *The Electrochemical Society Interface*, pp. 37–44, Jun. 2012.
- [108] C. A. Lave and K. Train, “A disaggregate model of auto-type choice,” *Transportation Research Part A: General*, vol. 13, no. 1, pp. 1–9, Feb. 1979.
- [109] S. Berry, J. Levinsohn, and A. Pakes, “Automobile Prices in Market Equilibrium,” *Econometrica*, vol. 63, no. 4, p. 841, Jul. 1995.

- [110] K. S. Whitefoot and S. J. Skerlos, "Design incentives to increase vehicle size created from the U.S. footprint-based fuel economy standards," *Energy Policy*, vol. 41, pp. 402–411, Feb. 2012.
- [111] H. Allcott and N. Wozny, "Gasoline Prices, Fuel Economy, and the Energy Paradox," *Review of Economics and Statistics*, vol. 96, no. 5, pp. 779–795, Dec. 2014.
- [112] D. L. Greene, P. D. Patterson, M. Singh, and J. Li, "Feebates, rebates and gas-guzzler taxes: a study of incentives for increased fuel economy," *Energy Policy*, vol. 33, no. 6, pp. 757–775, Apr. 2005.
- [113] J. H. Boyd and R. E. Mellman, "The effect of fuel economy standards on the U.S. Automotive Market," *Transportation Research Part A: General*, vol. 14A, pp. 367–378, 1980.
- [114] S. Berry, J. Levinsohn, and A. Pakes, "Differentiated Products Demand Systems from a Combination of Micro and Macro Data: The New Car Market," *Journal of Political Economy*, vol. 112, no. 1, pp. 68–105, Feb. 2004.
- [115] K. E. Train and C. Winston, "Vehicle Choice Behavior and the Declining Market Share of U.S. Automakers," *International Economic Review*, vol. 48, no. 4, Nov. 2007.
- [116] J. Axsen and K. Kurani, "The Early U.S. Market for PHEVs: Anticipating Consumer Awareness, Recharge Potential, Design Priorities and Energy Impacts," University of California Davis Institute of Transportation Studies, Tech. Rep. UCD-ITS-RR-08-22, Aug. 2008.
- [117] J. P. Helveston, Y. Liu, E. M. Feit, E. Fuchs, E. Klampfl, and J. J. Michalek, "Will subsidies drive electric vehicle adoption? Measuring consumer preferences in the U.S. and China," *Transportation Research Part A: Policy and Practice*, vol. 73, pp. 96–112, Mar. 2015.
- [118] T. F. Golob, J. Torous, M. Bradley, D. Brownstone, S. S. Crane, and D. S. Bunch, "Commercial fleet demand for alternative-fuel vehicles in California," *Transportation Research Part A: Policy and Practice*, vol. 31, no. 3, pp. 219–233, May 1997.
- [119] P. S. McCarthy, "Market Price and Income Elasticities of New Vehicle Demands," *The Review of Economics and Statistics*, vol. 78, no. 3, p. 543, Aug. 1996.

- [120] S. Choo and P. L. Mokhtarian, "What type of vehicle do people drive? The role of attitude and lifestyle in influencing vehicle type choice," *Transportation Research Part A: Policy and Practice*, vol. 38, no. 3, pp. 201–222, Mar. 2004.
- [121] W. H. Greene, D. A. Hensher, and J. Rose, "Accounting for heterogeneity in the variance of unobserved effects in mixed logit models," *Transportation Research Part B: Methodological*, vol. 40, no. 1, pp. 75–92, Jan. 2006.
- [122] D. McFadden and K. Train, "Mixed MNL models for discrete response," *Journal of Applied Econometrics*, vol. 15, no. 5, pp. 447–470, 2000.
- [123] D. Brownstone and K. Train, "Forecasting new product penetration with flexible substitution patterns," *Journal of Econometrics*, vol. 89, pp. 109–129, 1999.
- [124] W. H. Greene and D. A. Hensher, "A latent class model for discrete choice analysis: contrasts with mixed logit," *Transportation Research Part B: Methodological*, vol. 37, no. 8, pp. 681–698, Sep. 2003.
- [125] J. Shen, "Latent class model or mixed logit model? A comparison by transport mode choice data," *Applied Economics*, vol. 41, no. 22, pp. 2915–2924, Oct. 2009.
- [126] P. Zito and G. Salvo, "Latent Class Approach to Estimate the Willingness to Pay for Transit User Information," *Journal of Transportation Technologies*, vol. 02, no. 03, pp. 193–203, 2012.
- [127] M. K. Hidrue, G. R. Parsons, W. Kempton, and M. P. Gardner, "Willingness to pay for electric vehicles and their attributes," *Resource and Energy Economics*, vol. 33, no. 3, pp. 686–705, Sep. 2011.
- [128] J. Axsen, J. Bailey, and M. A. Castro, "Preference and lifestyle heterogeneity among potential plug-in electric vehicle buyers," *Energy Economics*, vol. 50, pp. 190–201, Jul. 2015.
- [129] J. P. Helveston, E. M. Feit, and J. J. Michalek, "Pooling stated and revealed preference data in the presence of RP endogeneity," *Transportation Research Part B: Methodological*, vol. 109, pp. 70–89, Mar. 2018.

- [130] D. S. Bunch, M. Bradley, T. F. Golob, R. Kitamura, and G. P. Occhiuzzo, "Demand for clean-fuel vehicles in California: A discrete-choice stated preference pilot project," *Transportation Research Part A: Policy and Practice*, vol. 27, no. 3, pp. 237–253, May 1993.
- [131] D. Brownstone, D. S. Bunch, K. Train, and train, "Joint mixed logit models of stated and revealed preferences for alternative-fuel vehicles," *Transportation Research Part B*, vol. 34, pp. 315–338, 2000.
- [132] K. E. Train, *Discrete Choice Methods with Simulation*, 2nd ed. Cambridge: Cambridge University Press, 2009.
- [133] Q. Sun and F. Wu, "Warranty regulation and consumer demand: evidence from China's automobile market," *Journal of Regulatory Economics*, vol. 49, no. 2, pp. 152–171, Jan. 2016.
- [134] R. T. Carson and T. Groves, "Incentive and informational properties of preference questions," *Environmental and Resource Economics*, vol. 37, no. 1, pp. 181–210, May 2007.
- [135] J. Min, I. L. Azevedo, J. Michalek, and W. B. de Bruin, "Labeling energy cost on light bulbs lowers implicit discount rates," *Ecological Economics*, vol. 97, pp. 42–50, Jan. 2014.
- [136] W. Green, "Fixed and Random Effects in Nonlinear Models," Department of Economics, Stern School of Business, New York, NY, Tech. Rep. NYU Working Paper No. EC-01-01, Jan. 2001.
- [137] Compare Side-by-Side. [Online]. Available: <http://www.fueleconomy.gov/feg/Find.do?action=sbs&id=35994&id=34776&id=34775>
- [138] J. Voelcker. (2015, Jul.) UPDATED: Tesla Model S Gets New 90-kWh Battery, 'Ludicrous' Performance Mode. [Online]. Available: http://www.greencarreports.com/news/1099178_breaking-tesla-model-s-gets-new-90-kwh-battery-ludicrous-performance-mode
- [139] J. R. Croy, D. Kim, M. Balasubramanian, K. Gallagher, S.-H. Kang, and M. M. Thackeray, "Countering the Voltage Decay in High Capacity $x\text{Li}_2\text{MnO}_3 \cdot (1-x)\text{LiMO}_2$ Electrodes (M=Mn, Ni, Co) for Li^+ -Ion Batteries," *Journal of the Electrochemical Society*, vol. 159, no. 6, pp. A781–A790, Jan. 2012.

- [140] A. Hardin, "LG Chem, Argonne sign licensing deal to make, commercialize advanced battery material | Argonne National Laboratory," Jan. 2011.
- [141] T. Aoki, M. Nagata, and H. Tsukamoto, "Positive Electrode Active Material for Lithium Secondary Battery," US Patent US 5 718 989, Feb., 1998.
- [142] T. Itou, T. Saito, H. Horie, and Nissan Motor Co, Ltd, "Positive electrode material for non-aqueous electrolyte lithium ion battery and battery using the same," US Patent US 10/581,858, Apr., 2007.
- [143] *EV / HEV Safety*. Nissan Moto Co., Ltd, 2012.
- [144] Life Cycle Environmental Certificate Mercedes-Benz S-Class. [Online]. Available: http://media.daimler.com/Projects/c2c/channel/documents/2573527_rz_update_UZ_S_engl_09_2015.pdf
- [145] E. Loveday. GM Shifts 2015 Chevy Spark EV Battery Manufacturing To In-House Facility. [Online]. Available: <http://insideevs.com/gm-shifts-2015-chevy-spark-ev-battery-manufacturing-house-facility/>
- [146] Honda Fit EV Review. [Online]. Available: <http://www.pluginCars.com/honda-fit-ev>
- [147] (2012, Jul.) 2013 Honda Fit EV First Drive. [Online]. Available: <https://www.edmunds.com/honda/fit-ev/2013/>
- [148] K. Field. (2015, Nov.) Electric Bus Adoption Is Taking Off In China. [Online]. Available: <http://cleantechnica.com/2015/11/26/electric-bus-adoption-taking-off-china/>
- [149] (2014, Jul.) BMW Group and Samsung SDI expand partnership on electric drive batteries; i3, i8 and additional hybrid models. [Online]. Available: <http://www.greencarcongress.com/2014/07/20140715-bmw.html>
- [150] BMW i3 Review. [Online]. Available: <http://www.pluginCars.com/bmw-i3.html>
- [151] B. Berman. (2012, Feb.) GS Yuasa to Triple Lithium-Ion Battery Cell Production for Honda's Plug-in Vehicles. [Online]. Available: <http://www.pluginCars.com/gs-yuasa-triple-lithium-production-honda-113107.html>

- [152] G. Shenhar. (2013, Jun.) The Chevrolet Spark EV shocks us. [Online]. Available: <http://www.consumerreports.org/cro/news/2013/06/first-drive-the-chevrolet-spark-ev-shocks-us/index.htm>
- [153] J. Cole. LG Chem To Supply 200 Mile Batteries In 2016; But To Whom? [Online]. Available: <http://insideevs.com/lg-chem-supply-200-mile-battery-2016/>
- [154] *Fiat 500e First Responders Guide*, Mar. 2013.
- [155] E. Loveday. Daimler Ready to Exit Li-Tec Battery Joint Venture? | Inside EVs. [Online]. Available: <http://insideevs.com/daimler-ready-to-exit-li-tec-battery-joint-venture/>
- [156] 2016 Focus Electric | View Focus Electric Highlights . [Online]. Available: <http://www.ford.com/cars/focus/trim/electric/>
- [157] A. Ingram. (2010, Jun.) Ford Announces Battery Supplier For 2012 Focus Electric. [Online]. Available: http://www.greencarreports.com/news/1047189_ford-announces-battery-supplier-for-2012-focus-electric
- [158] E. Loveday. Full Details Released on 2015 Kia Soul EV's "Advanced Battery" | Inside EVs. [Online]. Available: <http://insideevs.com/full-details-released-on-2015-kia-soul-evs-advanced-battery/>
- [159] (2014, Feb.) Green Car Congress: Kia using SK Innovation NCM Li-ion cells in Soul EV. [Online]. Available: <http://www.greencarcongress.com/2014/02/20140224-kia.html>
- [160] Mercedes B-Class Electric Drive. [Online]. Available: <http://www.plugincars.com/mercedes-b-class-e-cell>
- [161] "2012 Mitsubishi i-MiEV," U.S Department of Energy Energy Efficiency and Renewable Energy, Tech. Rep., Jun. 2014.
- [162] T. Schafer, "Batterietechnologie: Trends, Entwicklungen, Anwendungen," in *energiemetropole-leipzig.de*, 2009.
- [163] Model X. [Online]. Available: <https://www.teslamotors.com/modelx>
- [164] (2012, Aug.) Green Car Congress: Toyota RAV4 EV key for meeting California ZEV requirements; Tesla powertrain uses Model S components. [Online]. Available: <http://www.greencarcongress.com/2012/08/rav4ev-20120803.html>

- [165] M. Rovito. (2015, Jan.) 2015 VW e-Golf ushers in an era of interchangeable drive-trains for every Volkswagen model. [Online]. Available: <https://chargedevs.com/features/the-2015-vw-e-golf-ushers-in-an-era-of-interchangeable-drivetrains-for-every-volkswagen-model/>
- [166] S. Blanco. (2011, Sep.) Toyota Plug-in Prius priced at 32,000 * *and Prius V to start at 26,400**. [Online]. Available: <http://www.autoblog.com/2011/09/16/toyota-plug-in-prius-priced-at-32-000-prius-v-starts-at-26-40/>
- [167] B. Stertz, "Powerful battery in Audi electric car with cell modules from LG and Samsung," Aug. 2015.
- [168] (2015, Nov.) First drive: US spec Audi A3 Sportback e-tron plug-in hybrid; 83-86 MPGe with 16-17 mile EV range. [Online]. Available: <http://www.greencarcongress.com/2015/11/20151103-a3.html>
- [169] D. Sherman. (2014, May) All About the Batteries, Baby: 2015 BMW i8 Battery Pack Dictated Its Entire Design. [Online]. Available: <http://blog.caranddriver.com/all-about-the-batteries-baby-2015-bmw-i8-battery-pack-dictated-its-entire-design/>
- [170] M. Kane. (2015, Mar.) Samsung SDI To Supply Lithium-Ion Battery Packs For BMW X5 eDrive Plug-In Hybrid. [Online]. Available: <http://insideevs.com/samsung-sdi-supply-lithium-ion-battery-packs-bmw-x5-edrive-plug-hybrid/>
- [171] (2014, Feb.) Test Drive: BMW X5 eDrive Plug-In Hybrid Prototype. [Online]. Available: <http://insideevs.com/test-drive-bmw-x5-edrive-plug-in-hybrid-prototype/>
- [172] E. Loveday. Cadillac ELR Gets Priced at \$75,995 | Inside EVs. [Online]. Available: <http://insideevs.com/cadilla-elr-gets-priced-at-75995/>
- [173] Chevrolet Volt Battery.
- [174] E. Loveday. (2012, Feb.) Panasonic Selected to Electrify Ford Fusion Energi, C-Max Energi Plug-in Hybrids. [Online]. Available: <http://www.plugin cars.com/panasonic-selected-electrify-ford-fusion-energi-c-max-energi-plug-hybrids-113414.html>
- [175] 2016 Ford C-MAX | View Full Engine Specifications. [Online]. Available: <http://www.ford.com/cars/cmax/specifications/engine/>

- [176] 2016 Fusion Sedan | Engine Specs . [Online]. Available: <http://www.ford.com/cars/fusion/specifications/engine/>
- [177] (2015, Jun.) Hyundai Sonata PHEV may be a game (and mind) changer. [Online]. Available: <http://www.autoblog.com/2015/06/17/hyundai-sonata-phev-game-mind-changer/>
- [178] M. Kane. (2015, Jun.) Hyundai Sonata PHEV First Drive. [Online]. Available: <http://insideevs.com/hyundai-sonata-phev-first-drive/>
- [179] K. Reynolds. (2015, May) 2016 Hyundai Sonata Hybrid, Plug-In - First Drive Review. [Online]. Available: <http://www.motortrend.com/news/2016-hyundai-sonata-hybrid-first-drive-review/>
- [180] K. C. Colwell. (2014, Oct.) 2015 Porsche Cayenne S E-Hybrid - First Drive Review. [Online]. Available: <http://www.caranddriver.com/reviews/2015-porsche-cayenne-s-e-hybrid-first-drive-review>
- [181] "From battery cell to electric motor Bosch paving the way to electromobility," Bosch, Nov. 2011.
- [182] Automotive(Electric Vehicle) Prismatic Battery Cells | Samsung SDI. [Online]. Available: <http://www.samsungsdi.com/automotive-battery/battery-cells>
- [183] K. Smith, M. Earleywine, E. Wood, J. Neubauer, and A. Pesaran, "Comparison of Plug-In Hybrid Electric Vehicle Battery Life Across Geographies and Drive Cycles," in *SAE World Congress and Exhibition*, Apr. 2012.
- [184] "Panasonic Group to Supply Lithium-ion Batteries for Toyota Prius Plug-in Hybrid | Headquarters News | Panasonic Newsroom Global," Nov. 2011.
- [185] S. Edelstein. (2015, May) 2016 Volvo XC90 T8: First Plug-In Hybrid With 240-Volt Charging Cord. [Online]. Available: http://www.greencarreports.com/news/1098399_2016-volvo-t8-first-plug-in-hybrid-with-built-in-240-volt-charging
- [186] (2015, May) First drive: Volvo XC90 T8 Drive-E Twin Engine PHEV sets a high bar for full-size luxury SUV plug-ins in US. [Online]. Available: <http://www.greencarcongress.com/2015/05/20150517-xc90.html>
- [187] *2017 Ford Focus Electric Owner's Manual*, Oct. 2016.

- [188] (2017, Feb.) Tesla Vehicle Warranty. [Online]. Available: <https://www.tesla.com/support/vehicle-warranty>
- [189] T. Moloughney. (2017, Apr.) BMW i3 Long Term Battery Capacity Report: Better Than Expected. [Online]. Available: <http://www.bmwblog.com/2017/04/24/bmw-i3-long-term-battery-capacity-report-better-expected/>
- [190] 2017 Nissan LEAF Electric Car Battery. [Online]. Available: <https://www.nissanusa.com/electric-cars/leaf/charging-range/battery>
- [191] BMW 330e iPerformance - Features & Specifications - BMW USA. [Online]. Available: <https://www.bmwusa.com/vehicles/3-series/sedan/330e-iperformance.html>
- [192] BMW 530e iPerformance - Features & Specifications - BMW USA. [Online]. Available: <https://www.bmwusa.com/vehicles/5-series/sedan/530e-iperformance.html>
- [193] BMW 740e xDrive iPerformance - Features & Specifications - BMW USA. [Online]. Available: <https://www.bmwusa.com/vehicles/7-series/sedan/740e-xdrive-iperformance.html>
- [194] BMW i3 - Features & Specifications - BMW USA. [Online]. Available: <https://www.bmwusa.com/vehicles/bmwi/bmw-i3/bmw-i3-features-and-specs.html>
- [195] BMW i8 - Features & Specifications - BMW USA. [Online]. Available: https://www.bmwusa.com/vehicles/bmwi/bmw-i8/bmw-i8-features-and-specs.html?from=/Standard/Content/Vehicles/2017/i8/BMWi8/Features{_}and{_}Specs.aspx{\&}return=/Standard/Content/Vehicles/2017/i8/BMWi8/Features{_}and{_}Specs.aspx
- [196] BMW X5 xDrive40e - Features & Specifications - BMW USA. [Online]. Available: <https://www.bmwusa.com/vehicles/x-models/x5/x5-xdrive40e.html>
- [197] Cadillac | 2018 CT6 Plug-In - Build Your Own. [Online]. Available: <http://www.cadillac.com/plug-in-hybrids/ct6-plug-in/build-and-price/features/trim/?section=Highlights{\&}section=Dimensions{\&}section=Warranty{\&}styleOne=390680>
- [198] 2018 Bolt EV: Electric Car | Electric Vehicle | Chevrolet. [Online]. Available: www.chevrolet.com/index/vehicles/2018/cars/bolt-ev/overview.html
- [199] Complete Care: Warranty, Maintenance & More | Chevrolet. [Online]. Available: www.chevrolet.com/index/experience-chevrolet/complete-care.html

- [200] Official Mopar Site | Current Model Year Coverage. [Online]. Available: <https://www.mopar.com/chrysler/en-us/care/current-model-year-coverage.html>
- [201] 2017 FIAT 500e - Electric Car. [Online]. Available: <https://www.fiatusa.com/500e.html>
- [202] *2018 Model Year Ford Hybrid Car and Electric Vehicle Warranty Guide*, Sep. 2017.
- [203] 2017 Ford Fusion Energi | U.S. News & World Report. [Online]. Available: [/cars-trucks/ford/fusion-energi](https://www.usnews.com/cars-trucks/ford/fusion-energi)
- [204] 2017 Hyundai Ioniq Electric - Features & Specs | Hyundai. [Online]. Available: <https://www.hyundaiusa.com/ioniq-electric/specifications.aspx>
- [205] 2017 Sonata Hybrid - Specs & Trim | Hyundai. [Online]. Available: <https://www.hyundaiusa.com/sonata-hybrid/specifications.aspx>
- [206] 2017 Kia Soul-EV | Compare Related Vehicles | Kia. [Online]. Available: <https://www.kia.com/us/en/vehicle/soul-ev/2017/compare>
- [207] 2017 Prius Prime. [Online]. Available: <https://www.toyota.com/priusprime/ebrochure>
- [208] 2016 E-Golf Press Kit. [Online]. Available: <https://media.vw.com/press-kits/2016-e-golf-press-kit>
- [209] T8 Hybrid Battery Warranty. [Online]. Available: http://volvo.custhelp.com/app/answers/detail/a/{_}id/9590/~/t8-hybrid-battery-warranty